The Heparan Sulfate Proteoglycan Perlecan Regulates Axonal and Synaptic Stability

by

Ellen Jane Guss

A.B. Neuroscience (Cellular)
Colgate University, 2013

Submitted to the Department of Biology
in partial fulfillment of the requirements for the degree of

Doctor of Philosophy in Biology

at the

MASSACHUSETTS INSTITUTE OF TECHNOLOGY

June 2023

Author . . . . . .
Ellen Jane Guss
Department of Biology
February 23, 2023

Certified by. . . . . .
J. Troy Littleton
Menicon Professor of Neuroscience
Thesis Supervisor

Accepted by . . . . . .
Mary Gehring
Associate Professor of Biology
Member, Whitehead Institute
Director, Biology Graduate Committee

The Heparan Sulfate Proteoglycan Perlecan Regulates Axonal and Synaptic Stability

by

Ellen Jane Guss

Submitted to the Department of Biology on February 23, 2023
in partial fulfillment of the requirements for the degree of
Doctor of Philosophy in Biology

Abstract

Heparan sulfate proteoglycans (HSPGs) form essential components of the extracellular matrix (ECM) and basement membrane (BM) and have both structural and signaling roles. Perlecan is a secreted ECM-localized HSPG that contributes to tissue integrity and cell-cell communication. In this thesis, I identify a role for *Drosophila* Perlecan in the maintenance of larval motoneuron axonal and synaptic stability. In Chapter 1, I discuss known roles for Perlecan and other HSPGs in animal development, with a focus on their functions within the nervous system. In Chapter 2, I describe how loss of *Drosophila* Perlecan causes alterations in the axonal cytoskeleton and breakage of axons, followed by synaptic retraction of neuromuscular junctions. These phenotypes are not prevented by blocking Wallerian degeneration and are independent of Perlecan's role in Wingless signaling. Overexpression of Perlecan in motoneurons cannot rescue synaptic retraction phenotypes. Similarly, removing Perlecan specifically from neurons, glia, muscle, fat body, or hemocytes does not cause synaptic retraction, indicating the protein is secreted from multiple cell types and functions non-cell autonomously. Within the peripheral nervous system, Perlecan predominantly localizes to the neural lamella, a specialized ECM surrounding nerve bundles. Loss of Perlecan disrupts neural lamella structure, with reduced ECM thickness observed for the co-localized Viking protein, a *Drosophila* type IV Collagen homolog. In addition, Viking shows abnormal accumulation and aggregation at sites along the neural lamella that are associated with axonal breakage and exit from their usual boundary within the nerve bundle. Entire nerve bundles degenerate in a temporally coordinated manner across individual hemi-segments during the late stages of larval development. These observations indicate disruption of neural lamella ECM function triggers axonal destabilization and synaptic retraction of motoneurons, revealing a role for Perlecan in axonal and synaptic integrity during nervous system development.

Thesis Supervisor: J. Troy Littleton
Title: Menicon Professor of Neuroscience

Acknowledgments

Thank you to Troy for always having the next scientific suggestion ready, for never hesitating to provide help when requested, and for passing along a love of all things *Drosophila*. Thank you to Adam, Joey, and Steve for excellent advice and challenging questions. Many thanks to Yulia, Karen, and Chad for your experimental contributions to this thesis. Thank you to all of my previous scientific mentors and peers, including Mark, Susan, Brittany, Mike, Maura, and Damhnait for your encouragement, wisdom, and scientific passion. Thanks are also due to Elizabeth, Chad, Karen, Nicole, Mónica, and Andrés for being my fellow graduate student support network and friends in the Littleton lab.

Thank you to so many friends: Talya, Teresa, Shruthi, Dia, Laurel, Elizabeth, Karen, Coco, Rebecca, Dani, Halley, Sam, Cassidy, Jennifer, Kami, Alex, and Ali. Some of you have also been scientific peers and mentors to me and all of you have been inspiring, supportive, motivational, fun, and wise.

Thanks to my family and Dylan's family: Mom, Dad, Grandma, Grandpa, Grams, aunts, uncles, and cousins, Sam, Gillian, Stephanie, and Jon for letting me talk excitedly about flies and brains and only occasionally pestering me about my career plans. A million thanks to Dylan, Kirkland, Tuckington, and baby girl Guss: without you, it certainly would not have been possible.

Contents

Chapter 3. Conclusions and future directions

List of Figures

Chapter 1

Heparan sulfate proteoglycans in nervous system development and maturation

1.1 Introduction

Heparan sulfate proteoglycans (HSPGs) are a highly conserved family of membrane-associated and secreted glycoproteins. HPSGs are characterized by a core protein on which up to five heparan sulfate (HS) sugar chains are attached. These sugar chains feature repeating glucuronic acid and N-acetyl-glucosamine units which are enzymatically modified throughout the length of the chain following their synthesis (Bishop et al., 2007; Condomitti and de Wit, 2018; Dreyfuss et al., 2009; Sarrazin et al., 2011). As components of extracellular matrices (ECMs) and basement membranes (BMs) (with the exception of the hematopoietic HSPG serglycin ((Sarrazin et al., 2011)), these proteins participate in numerous cellular activities and are critical for proper cell development, migration, structure, and communication (Bishop et al., 2007; Condomitti and de Wit, 2018; Dreyfuss et al., 2009; Sarrazin et al., 2011).

HSPG sugar chains and core proteins are able to bind to a host of signaling molecules, from growth factors (most notably members of the fibroblast growth factor (FGF) family) to morphogens and chemokines. In addition, HSPGs are able to communicate directly with the intracellular space by binding to transmembrane Integrins or binding components of the cytoskeleton (Bishop et al., 2007; Dreyfuss et al., 2009; Sarrazin et al., 2011). By forming well-organized ECMs, these proteins also provide structural support to underlying cells and facilitate cell migration and adhesion (Bishop et al., 2007; Condomitti and de Wit, 2018; Sarrazin et al., 2011).

This chapter will provide an overview of BMs and HSPGs, then introduce the known roles of HSPGs in nervous system (NS) development and maturation, with particular emphasis on Perlecan. Perlecan is the HSPG with the largest core mass, performing essential signaling and structural roles for numerous tissues throughout the body, including the NS (Arikawa-Hirasawa et al., 1999; Bishop et al., 2007; Bix and Iozzo, 2008; Condomitti and de Wit, 2018; Costell et al., 2002, 1999; Díaz-Torres et al., 2021; Dreyfuss et al., 2009; Poulain and Yost, 2015; Sarrazin et al., 2011; You et al., 2014). Given HSPGs are evolutionary conserved proteins, the following sections will cover the role of HSPGs in NS development in vertebrates and invertebrates. Roles in *Caenorhabditis elegans* and *Drosophila melanogaster* development will be discussed in separate sub-chapters given the extensive research performed in each of these organisms to define the roles of HSPGs. This chapter will also introduce the *Drosophila* larval NS and neuromuscular junction (NMJ), and highlight several known genes and pathways that impact neurodegeneration

and synaptic retraction at NMJs. Numerous articles and reviews about HSPG functions are available for multiple contexts, given their widespread roles in tissue and cellular development and function (Bishop et al., 2007; Condomitti and de Wit, 2018; Dreyfuss et al., 2009; Poulain and Yost, 2015; Sarrazin et al., 2011). Note that some invertebrate and vertebrate homologs of Perlecan are known by other names (e.g. Heparan Sulfate Proteoglycan 2). In this section, Perlecan will be used to refer to all homologs.

1.1.1 Basement membrane and heparan sulfate proteoglycans

BMs are specialized ECMs which are deposited on the basal surface of epithelial and endothelial cells, muscle, Schwann cells, other peripheral nervous system (PNS) tissues and cells, and fat (Erickson and Couchman, 2000; Khalilgharibi and Mao, 2021; Martin et al., 1988; Martin and Timpl, 1987; Ramos-Lewis and Page-McCaw, 2019; Stork et al., 2008; Yurchenco, 2011). Four requisite molecules are incorporated into BMs during development in vertebrates and invertebrates: Laminin, Collagen IV, Nidogen, and Perlecan (Hynes, 2009; Kruegel and Miosge, 2010; Timpl and Brown, 1996; Yurchenco, 2011). Additional proteins contribute to the form and function of the BM, including Integrin receptors which bridge the extra- to intracellular gap, matrix metalloproteases which enzymatically cleave BM components and contribute to their turnover, and sequestered cell-cell signaling molecules (Bittern et al., 2021; Hunter et al., 2020; Hynes, 2009; Ramos-Lewis and Page-McCaw, 2019; Whitelock et al., 2008; Yurchenco, 2011). Cells can autonomously generate and secrete components of their own BMs or the protein components of these matrices can be assembled and packaged in other cell types and transported to nascent BMs throughout the organism (Isabella and Horne-Badovinac, 2015; Matsubayashi et al., 2017; Pastor-Pareja and Xu, 2011; Ramos-Lewis and Page-McCaw, 2019).

Laminin is composed of three subunits to form a large, heterotrimeric glycoprotein (Kruegel and Miosge, 2010; Ramos-Lewis and Page-McCaw, 2019; Urbano et al., 2009). Multiple Laminin molecules can be deposited in various orientations to form complex matrices that are directly anchored to cell membranes via Integrins and other transmembrane proteins (Hamill et al., 2009; Töpfer et al., 2022; Yurchenco, 2011). Laminin is deposited first to form the BM and is required for BM formation, consistent with its role in directly binding cell surface proteins (Matsubayashi et al., 2017; Urbano et al., 2009).

Collagen IV is another heterotrimeric protein which forms its own matrixed network of molecules to contribute to the developing BM (Khalilgharibi and Mao, 2021; Kruegel and Miosge, 2010; Yurchenco, 2011). The Laminin and Collagen networks are linked by the glycoprotein Nidogen (Kruegel and Miosge, 2010; Töpfer et al., 2022; Yurchenco, 2011). In contrast to Laminin, Collagen IV is required later in BM development; BMs can form in the absence of Collagen but their structure and integrity are compromised during maturation (Matsubayashi et al., 2017; Pastor-Pareja and Xu, 2011; Pöschl et al., 2004). Atomic force measurements and analysis of organ shape during development has revealed a role for Collagen IV in establishing BM stiffness (Crest et al., 2017; Khalilgharibi and Mao, 2021; Pastor-Pareja and Xu, 2011; Pöschl et al., 2004; Ramos-Lewis and Page-McCaw, 2019; Töpfer et al., 2022). This role is made possible by sulfilimine crosslinking between Collagen subunits, a process which increases stability of individual Collagen proteins and their networks (McCall et al., 2014; Ramos-Lewis and Page-McCaw, 2019; Vanacore et al., 2009).

The HSPG Perlecan is the final ubiquitous BM component. Like Nidogen, Perlecan serves to link together the BM and binds to Integrins, the Laminin and Collagen IV networks, and Nidogen (Matsubayashi et al., 2017; Pastor-Pareja and Xu, 2011; Pöschl et al., 2004; Töpfer et al., 2022; Yurchenco, 2011). Like Collagen IV, Perlecan is required later in BM development (Costell et al., 1999; Matsubayashi et al., 2017; Pastor-Pareja and Xu, 2011; Pöschl et al., 2004; Töpfer et al., 2022). Atomic force measurements and osmotic stress experiments have indicated that Perlecan acts in opposition to Collagen IV by providing BMs with malleability (Crest et al., 2017; Khalilgharibi and Mao, 2021; Pastor-Pareja and Xu, 2011; Ramos-Lewis and Page-McCaw, 2019; Töpfer et al., 2022). Perlecan is a large protein with five domains and numerous extracellular motifs which can bind various growth factors (Bishop et al., 2007; Farach-Carson et al., 2014; Noonan et al., 1991; Whitelock et al., 2008). The long, modified HS chains attached to the protein also bind to growth factors and other molecules (Dreyfuss et al., 2009; Farach-Carson et al., 2014; Poulain and Yost, 2015; Sarrazin et al., 2011; Whitelock et al., 2008). Together Laminin, Collagen IV, Nidogen, Perlecan, and the supporting cast of BM proteins form well-organized BMs which facilitate cell signaling, grow with developing tissues and organs, and protect cells and tissues from immune insults and other dangers.

While not all HSPGs are ubiquitous to the BM like Perlecan, nearly all HSPGs localize to ECMs and BMs, where they are able to readily contribute to cell-cell signaling, communication,

adhesion, and cell structure (Dreyfuss et al., 2009; Sarrazin et al., 2011). HSPGs exist in a small number of subfamilies: transmembrane HSPGs (e.g. Syndecan), glycophosphatiylinositol (GPI)-linked HSPGs (e.g. Glypican), secreted HSPGs (e.g. Agrin and Perlecan), and the intracellular hematopoietic HSPG Serglycin (Bishop et al., 2007; Dreyfuss et al., 2009; Sarrazin et al., 2011). Vertebrates and invertebrates both possess members of each subfamily, but vertebrates encode more individual members of each family (Condomitti and de Wit, 2018). The long HS chains are attached to serine residues within the core protein via a tetrasaccharide linker followed by sequential addition of glucuronic acid and N-acetyl-glucosamine (Bishop et al., 2007; Dreyfuss et al., 2009; Sarrazin et al., 2011). These sugars are then modified by a series of enzymes which deacetylate, sulfate, and epimerize various residues. Short stretches of the HS chains are heavily modified, followed by longer stretches of unmodified sugars, providing regions of affinity for various binding partners (Bishop et al., 2007; Dreyfuss et al., 2009; Poulain and Yost, 2015; Sarrazin et al., 2011). The core proteins of HSPGs also interact with HSPG binding partners (Bishop et al., 2007; Dreyfuss et al., 2009; Gubbiotti et al., 2017; Sarrazin et al., 2011; Whitelock et al., 2008).

HSPGs contribute to growth factor and chemokine signaling, cell-cell adhesion and motility, and ECM structure in a variety of capacities. HSPGs on the cell surface or within the ECM may bind growth factor ligands, receptors, or both, and sequester or cluster these binding partners to facilitate signaling at low concentrations. HSPGs can present signaling ligands and receptors to nearby cells to facilitate cell-cell signaling and crosstalk (Bishop et al., 2007; Dreyfuss et al., 2009; Sarrazin et al., 2011). Binding of chemokines by HSPGs can allow for presentation of the chemokines to nearby cells or can protect chemokines from degradation (Bishop et al., 2007; Sarrazin et al., 2011). Cleavage of HS chains sequestering growth factors or morphogens allows for the release and active function of the morphogen (Bishop et al., 2007). HSPGs can also communicate with the cytoskeleton. Secreted HSPGs like Perlecan accomplish this signaling via ECM receptors like Integrins, but transmembrane HSPGs like Syndecan can directly bind cytoskeletal components to influence cell shape and motility (Bishop et al., 2007; Yurchenco, 2011). This conserved family of proteins contributes to vertebrate and invertebrate development and maturation on numerous fronts (Bishop et al., 2007; Sarrazin et al., 2011; Warren et al., 2015), both physically as components of ECMs and BMs and as participators in a variety of signaling pathways.

1.2 Perlecan in tissue development outside of the nervous system

Before discussing the NS at length, it is important to highlight the critical role that Perlecan plays in the development of many tissues and organs. This section will place a particular emphasis on vertebrate development and disease in the absence of Perlecan.

Complete loss of Perlecan in mouse or human is embryonic lethal (Costell et al., 1999; Farach-Carson et al., 2014). Although the protein is not necessary for embryo implantation, Perlecan is enriched at both embryonic-uterine and placental-uterine boundaries, suggesting it is involved in development at very early timepoints (Costell et al., 1999; Farach-Carson et al., 2014). During embryonic development, mice and other vertebrates without Perlecan experience widespread developmental abnormalities, with major defects in heart, brain (as discussed in depth in the next section), cartilage, muscle, bone, and blood vessels (Arikawa-Hirasawa et al., 1999; Costell et al., 1999; Farach-Carson et al., 2014; Zoeller et al., 2009). Consistent with its dual roles in maintaining a functional ECM and localizing signaling molecules, defects in the absence of Perlecan have been attributed in some cases to a failure in localizing signaling molecules like vascular endothelial growth factor (VEGF) or FGF family members (angiogenesis, cartilage development) and in other cases to defects in maintaining organized ECM and cell-cell attachments, particularly in the face of increased mechanical stress on tissues (brain, heart) (Arikawa-Hirasawa et al., 1999; Costell et al., 1999; Farach-Carson et al., 2014; Zoeller et al., 2009).

Perlecan interacts with multiple signaling pathways to control proper bone development. During bone development, some cartilage progenitor cells differentiate to form bone (Lowe et al., 2014; Martinez et al., 2018). In the absence of Perlecan, these progenitors differentiate too quickly, resulting in misshapen bones with disorganized cell layers (Lowe et al., 2014; Martinez et al., 2018). This excess differentiation was sensitive to Bone Morphogenic Protein 2 (BMP2) levels, suggesting that Perlecan may sequester BMP2 or its receptor during normal development in order to properly regulate differentiation timing (Lowe et al., 2014). The misshapen bones formed in the absence of Perlecan are also weak and brittle, responding poorly to mechanical loading (Lowe et al., 2014; Martinez et al., 2018; Wang et al., 2014). This phenotype is the result of impaired calcium (Ca^{2+}) signaling in the absence of Perlecan. Perlecan binds to the voltage-gated calcium channel (VGCC) subunit $\alpha_2\delta_1$ within bone and mechanically opens the VGCC in response to

mechanical load on the bone. Without Perlecan, this Ca^{2+} signaling is substantially reduced and bone response to loading is subsequently impaired (Martinez et al., 2018; Pei et al., 2020; Reyes Fernandez et al., 2022).

During vertebrate heart development, Perlecan within the BM acts as structural support for the growing and pumping organ. Embryonic mice without Perlecan at E9.5 have no cardiac defects. By E10.5, control hearts are still morphologically normal, but the hearts of embryonic mice without Perlecan leak blood (Costell et al., 1999; Sasse et al., 2008). Dye injections into control and mutant hearts confirm progressive loss of structural heart integrity in the absence of Perlecan: dextran injected into heart ventricles of E10.5 *perlecan*$^{-/-}$ mice leaks into the space around the heart, while E9.5 hearts had no leakage (Sasse et al., 2008). Ultrastructural visualization of heart BM shows thin and disorganized BM, confirming that Perlecan is necessary to form BM that can support the mechanical stress of repeated heart pumping (Boland et al., 2021; Costell et al., 1999). Similar to its role in embryonic heart development, Perlecan is necessary for heart recovery and normal function after myocardial infarction (heart attack) and reduced (but not absent) Perlecan still compromises BM integrity and maturity, leading to heart instability and aortic rupture in mouse adolescents (Nonaka et al., 2021; Trinh et al., 2022).

Partial loss of Perlecan function in humans results in several autosomal recessive genetic diseases: dyssegmental dysplasia, Silverman-Handmaker type (DSSH) and Schwartz-Jampel syndrome (SJS) (Farach-Carson et al., 2014; Gubbiotti et al., 2017). DSSH is considerably more severe, with functionally null mutations in *perlecan* that result in severe disruptions in cartilage formation and subsequent lethality (Arikawa-Hirasawa et al., 2001a, 2001b; Farach-Carson et al., 2014; Gubbiotti et al., 2017). Less severe hypomorphic mutations in *perlecan* result in SJS, which is characterized by glial, motoneuron (MN), and muscle defects, resulting in myotonia and corresponding MN hyperexcitability. Some disruptions in bone and cartilage formation and function are still evident in these patients (Arikawa-Hirasawa et al., 2002a; Bangratz et al., 2012; Farach-Carson et al., 2014; Gubbiotti et al., 2017; Martinez et al., 2018; Nicole et al., 2000).

This literature makes it clear that Perlecan is critically involved in organism development, and that its role in ensuring proper development and maintenance of various tissues utilizes both its ability to bind a vast array of signaling molecules and its structural role in maintaining the architecture of ECM and BM.

1.3 HSPGs in vertebrate nervous system development and maturation

1.3.1 Agrin

At the vertebrate NMJ, cholinergic MNs form synapses on muscle fibers. As the MN growth cone forms a specialized NMJ synapse, acetylcholine receptors (AChRs) gather and stabilize in the postsynaptic membrane opposite to the presynapse (Sanes and Lichtman, 1999). In the 1970s, experiments in the McMahan laboratory determined that mature pre- and postsynaptic NMJs were incredibly stable, able to reform in their original location following ablation and regrowth of either MNs or muscles as long as the extracellular material between the partners was left intact (Sanes et al., 1978). These data indicated that a secreted organizing protein within the ECM-like environment of the synaptic cleft was likely specifying the location of the synapse and driving organization of both pre- and postsynaptic components. The secreted heparan sulfate proteoglycan Agrin was purified and identified in 1987 as a candidate organizer for NMJ development (Nitkin et al., 1987). Perhaps the most well-known HPSG in NS development, a specific splicing variant of Agrin is secreted by the presynaptic MN and binds to a muscle-specific kinase (MuSK) and LDL receptor related protein 4 (Lrp4) receptor complex on the muscle surface (DeChiara et al., 1996; Kim et al., 2008; Ruggiu et al., 2009). Upon binding of Agrin by these receptors, the cytosolic protein Rapsyn is recruited within muscle and activates a signaling cascade which leads to clustering of AChRs opposite presynaptic structures (Apel et al., 1997; Gautam et al., 1995; Sanes and Lichtman, 1999).

Agrin is responsible not only for the specific localization of postsynaptic structures, but also their stability. AChRs in Agrin-dependent clusters have a half-life approximately 10 times longer than AChRs in extrasynaptic muscle or in denervated muscle fibers (Bezakova et al., 2001; Hall and Sanes, 1993; Sanes and Lichtman, 1999). Thus, the HSPG Agrin is important not only for synaptic specification but also structural stability and maintenance of the postsynaptic architecture of the vertebrate NMJ.

1.3.2 Other HPSGs

HSPGs other than Agrin are involved in many aspects of the development of the vertebrate NS, from initial patterning to axon guidance to synapse development and maturation (Condomitti and de Wit, 2018; Poulain and Yost, 2015). GPI-linked Glypicans and transmembrane Syndecans are both important for the development and maturation of synapses in the central nervous system (CNS) of vertebrates.

In mouse hippocampus, Syndecan-2 controls differentiation and specialization of both pre- and postsynaptic compartments. In the postsynaptic compartment, phosphorylation of dendritic spine-localized Syndecan-2 by EphB2 results in recruitment of intracellular Syndecan-2 binding partners and subsequent morphological maturation of dendritic spines (Condomitti and de Wit, 2018; Ethell et al., 2001; Ethell and Yamaguchi, 1999). Syndecan-2 controls presynaptic maturation in the hippocampus via its extracellular domain, which binds FGF22 and presents the ligand to receptors on the presynaptic cell. This FGF signaling allows for presynaptic maturation (Condomitti and de Wit, 2018; Hu et al., 2016).

Glypicans regulate pre- and postsynaptic maturation depending upon which cell presents the HSPG. When made and anchored to presynaptic membranes, Glypican-4 promotes excitatory pre- and postsynaptic development (Condomitti and de Wit, 2018; de Wit et al., 2013; Ko et al., 2015; Siddiqui et al., 2013). When made by astrocytes in close contact with hippocampal neurons, Glypican-4 and Glypican-6 drive postsynaptic maturation (Allen et al., 2012; Condomitti and de Wit, 2018; Farhy-Tselnicker et al., 2017). Human case studies and genome-wide association studies have implicated reduced function of Glypicans and HSPG sulfation enzymes in autism spectrum disorder and intellectual disability (Condomitti and de Wit, 2018).

Functional roles for HSPGs in early NS development are often associated with defects in FGF signaling (Poulain and Yost, 2015). HS chains bind to FGF ligands and receptors (FGFR), acting as co-receptors for ligand binding and lowering the concentration of ligand and receptor required to initiate signaling (Bishop et al., 2007; Sarrazin et al., 2011). HS chains are intimately associated with these ligand-receptor pairs. The crystal structure of FGF-FGFR reveals multiple hydrogen bonds linking highly sulfated HS chains with the ligand and receptor to facilitate a favorable binding orientation (Bishop et al., 2007; Schlessinger et al., 2000). FGF signaling is critical for posterior NS patterning in vertebrates and invertebrates (Pasini et al., 2012; Pownall and Isaacs, 2010). Conditional knockout of the enzyme EXT1—responsible for adding glucuronic acid to HSPG sugar chains—results in loss of FGF8 signaling at the midbrain-hindbrain boundary

and major defects in brain patterning and axon guidance in mice (Chen et al., 2009; Inatani et al., 2003; Poulain and Yost, 2015). Loss of individual HSPGs, including a number of Glypicans and Syndecans, can also result in patterning and gross morphological defects due to disrupted FGF, Wnt, or PKC signaling (Poulain and Yost, 2015).

1.3.3 Perlecan

Perlecan specifically plays roles in vertebrate NS cell migration, genesis and proliferation, and synapse development (Poulain and Yost, 2015). *Perlecan*$^{-/-}$ mouse embryos initially develop normal BMs surrounding the brain. Within a few days, however, brain-associated BM thins and becomes patchy, allowing neuronal cells to migrate past the border of the BM (Costell et al., 1999). In some cases, this misplaced migration is so severe that the embryos develop exencephaly, despite normal neural tube closure earlier in embryonic development (Costell et al., 1999).

In cases of *perlecan*$^{-/-}$ brain development where exencephaly does not occur, proliferation defects are observed. In *perlecan*$^{-/-}$ brains, neural progenitors fail to maintain cell cycle exit rates, resulting in a decline of corticogenesis over time (Girós et al., 2007). In adult mice lacking Perlecan in all tissues except cartilage, neurogenesis is impaired due to cell cycle disruption (Kerever et al., 2014). It is likely that both of these cell proliferation defects are the result of impaired FGF2 signaling in the absence of Perlecan (Girós et al., 2007; Kerever et al., 2014; Mashayekhi et al., 2011).

At the vertebrate NMJ of embryonic mice lacking Perlecan, synaptic connections form normally, but acetylcholinesterase (AChE) fails to properly cluster in the basal lamina (Arikawa-Hirasawa et al., 2002b). Work with *Xenopus* proteins established that a Perlecan-Dystroglycan complex is able to directly bind AChE, confirming that Perlecan participates in proper functioning of this synapse by localizing AChE to allow for appropriate termination of the muscle contraction signal (Peng et al., 1999).

These data indicate that Perlecan is involved in many aspects of vertebrate NS development, maturation, and maintenance, both by participating in cell-cell signaling and by contributing structurally to the proper maintenance of the vertebrate basal lamina.

1.4 HSPGS in invertebrate nervous system development – *Caenorhabditis elegans*

1.4.1 Other HPSGs

In the nematode *C. elegans*, the role of HSPGs in neuron and neuroblast migration and axon guidance is well-established. During *C. elegans* embryonic and larval development, the neuronal progenitor Q neuroblasts migrate along the anterior-posterior axis of the animal and subsequently differentiate into multiple neurons, including AVM, AQR and PQR sensory neurons (Middelkoop and Korswagen, 2018). The *C. elegans* C5-epimerase is required for the proper positioning of the AQR and PQR neurons; in its absence, 15-25% of AQR and PQR neurons do not properly localize to the anterior and posterior tips of the animal, respectively (Sundararajan et al., 2015). Analysis of individual HSPGs revealed that the *C. elegans* Syndecan is required for AQR and PQR migration, suggesting that epimerization is necessary for Syndecan HS sugars specifically (Sundararajan et al., 2015). In this role, Syndecan is required cell-autonomously and may be interacting with Wnt signaling to control migration (Sundararajan et al., 2015; Wang et al., 2013). Additional studies have established a role for Syndecan in Q neuroblast migration prior to differentiation as well (Rhiner et al., 2005). *C. elegans* Glypicans, Syndecan, and HS sulfation enzymes are required to establish normal migration and positioning of the AVM, ALM, and HSN neuron cell bodies. HSPGs interact with Wnt ligands and receptors to control the migration of these neurons (Saied-Santiago et al., 2017). Hypomorphic alleles of the enzymes which synthesize and elongate HSPG sugar chains also resulted in defects in *C. elegans* neuronal migration events (Blanchette et al., 2017).

Syndecan, one *C. elegans* Glypican, and the enzymes which modify their HS chains are involved in axon guidance. While Syndecan and several HS modifying enzymes coordinate with Slit/Robo signaling (see below for more details) to ensure proper midline crossing of *C. elegans* nerves (Kinnunen, 2014; Rhiner et al., 2005), the Glypican encoded by the gene *lon-2* coordinates with Netrin signaling to drive appropriate axonal extension down the ventral axis of nematode larvae (Blanchette et al., 2015; Kinnunen, 2014). Syndecan is also involved in the regeneration of axons after damage (Edwards and Hammarlund, 2014). Recent evidence has established that Syndecan is necessary at the *C. elegans* synapse. At cholinergic *C. elegans* synapses, the

extracellular domain of Syndecan physically interacts with a neuronally secreted organizing molecule. The intracellular domain of Syndecan then activates a downstream signaling cascade in order to recruit AChRs, much like vertebrate Agrin (Zhou et al., 2021).

1.4.2 Perlecan

Perlecan in *C. elegans* is involved in neuron migration, dendritogenesis, and synaptic development. The secreted HSPG acts with Syndecan and Glypicans in regulating the anterior migration of the HSN neuron (Saied-Santiago et al., 2017). Perlecan is also important for the formation of dendrite branches of the sensory neuron PVD in *C. elegans*. BM-localized Perlecan binds to a network of muscle, skin and neuron-derived receptors and ligands to control dendritic branching (Celestrin et al., 2018; Liang et al., 2015; Zou et al., 2016).

Perlecan also plays a structural role in synaptic bouton formation in *C. elegans*. During development of the DD, VD, and AS motoneurons, boutons are regularly spaced along the dorsal and ventral edge of the animal (Qin et al., 2014). In *emb-9* (Collagen IV) and *gon-1* (matrix metalloprotease ADAMTS9) mutants, ectopic synaptic boutons form away from the dorsal and ventral edges of the nematode. This phenotype is suppressed by the loss of Perlecan, suggesting that Collagen IV and ADAMTS9 function to restrict synaptic bouton growth, while Perlecan promotes growth (Qin et al., 2014). Matrix metalloproteases like ADAMTS9 are ECM and BM-localized molecules that enzymatically cleave components of the BM and contribute to BM protein turnover and BM stiffness and structure (Khalilgharibi and Mao, 2021; Ramos-Lewis and Page-McCaw, 2019). These data are consistent with the structural role of Perlecan in other contexts and species, where the protein often acts in opposition to Collagen IV to establish appropriate BM malleability to accommodate cell and tissue growth during development (Crest et al., 2017; Khalilgharibi and Mao, 2021; Pastor-Pareja and Xu, 2011; Ramos-Lewis and Page-McCaw, 2019; Töpfer et al., 2022).

1.5 HSPGS in invertebrate nervous system development – *Drosophila melanogaster*

1.5.1 *Drosophila* ventral nerve cord and larval neuromuscular junction

The *Drosophila melanogaster* larval NMJ has served as a model glutamatergic synapse for decades. Easily accessible for imaging and with a wealth of genetic tools, the *Drosophila* larval NMJ has provided numerous breakthroughs about neuronal and synaptic biology (Andlauer and Sigrist, 2012; Collins and DiAntonio, 2007; Harris and Littleton, 2015; Kanca et al., 2017; Owald and Sigrist, 2009; Şentürk and Bellen, 2018). Approximately 35 MNs form stereotyped connections with 30 body wall muscles in each larval hemisegment. Most of these neurons are glutamatergic and fall into two categories: tonic type Ib and phasic type Is (Aponte-Santiago et al., 2020; Hoang and Chiba, 2001; Kohsaka et al., 2012; Pérez-Moreno and O'Kane, 2019). The remaining neuromodulatory neurons are referred to as type II and type III. All of these MNs have cell bodies in the larval ventral nerve cord (VNC); they send axonal projections out of the VNC in six individual nerves which innervate muscle groups based on medial/lateral and dorsal/ventral location within the hemisegment (Hoang and Chiba, 2001; Kohsaka et al., 2012; Pérez-Moreno and O'Kane, 2019). Upon exiting the VNC, all six nerve branches initially travel together in one nerve bundle in each hemisegment, before specific axons exit the main branch to innervate their target muscles along the way (Matzat et al., 2015; Pérez-Moreno and O'Kane, 2019). The VNC and axon bundles are surrounded by a continuous layer of specialized ECM called the neural lamella (NL) (Edwards et al., 1993; Skeath et al., 2017; Stork et al., 2008). In between the NL and the neural tissue are protective layers of glia which act as the *Drosophila* blood-brain barrier (BBB) (Edwards et al., 1993; Hunter et al., 2020; Matzat et al., 2015; Meyer et al., 2014; Skeath et al., 2017; Stork et al., 2008).

The NL is the *Drosophila* PNS BM and is comprised mainly of the four conserved components of BMs discussed above: Laminin, Nidogen, Perlecan, and the *Drosophila* Collagen IV homolog Viking (Vkg) (Carson et al., 1993; Erickson and Couchman, 2000; Hassell et al., 1980; Martin et al., 1988; Martin and Timpl, 1987; Mouw et al., 2014; Noonan et al., 1991; Skeath et al., 2017; Stork et al., 2008). During NL development, like development of other BMs, Laminin is deposited first, followed by Vkg and Perlecan, which are delivered to nascent BMs to promote their maturation (Matsubayashi et al., 2017; Pöschl et al., 2004). Together with Nidogen, these proteins form a tight protective matrix which allows the developing VNC and projecting axons to

both resist mechanical stress during their growth and to receive appropriate signaling molecules throughout development (Isabella and Horne-Badovinac, 2015; Khalilgharibi and Mao, 2021; Matsubayashi et al., 2017; Ramos-Lewis and Page-McCaw, 2019; Stork et al., 2008; Töpfer et al., 2022; Yurchenco, 2011). In their roles as drivers of NL and BM maturation, Vkg and Perlecan often act in opposition to one another, with Vkg promoting membrane stiffness to provide tissue support and Perlecan promoting its malleability to allow flexibility during growth and movement (Khalilgharibi and Mao, 2021; Pastor-Pareja and Xu, 2011; Ramos-Lewis and Page-McCaw, 2019; Skeath et al., 2017; Töpfer et al., 2022). Although both proteins are required to maintain the proper shape of developing organs and tissues, they have been shown in multiple systems to be dispensable for initial formation of BMs, consistent with their delivery after Laminin to the *Drosophila* NL (Costell et al., 1999; Olofsson and Page, 2005; Pastor-Pareja and Xu, 2011; Pöschl et al., 2004; Skeath et al., 2017).

1.5.1.1 *Drosophila* NMJ retraction and Wallerian degeneration

Formation and maintenance of the presynaptic cytoskeleton is critical for maintaining *Drosophila* larval NMJ synapses. The first proteins whose loss results in synaptic retraction were identified in 2002; Eaton and colleagues determined that loss in MNs of several individual components of the microtubule-associated dynactin complex results in progressive loss of NMJ synapses. This retraction proceeds distinctively, with initial loss of presynaptic material leaving behind postsynaptic "footprints" (Eaton et al., 2002). A number of additional microtubule-associated proteins have been shown to be necessary for synaptic stability as well: loss of *Drosophila* LIM Kinase1, Stathmin, and the giant Ankyrin Ank2 all result in synapse retraction (Eaton and Davis, 2005; Graf et al., 2011; Koch et al., 2008; Pielage et al., 2008). These retraction events appear to be due to general cytoskeletal disruption, rather than breakdown of a specific trafficking or turnover process (Eaton et al., 2002).

The spectrin cytoskeleton is also important for synaptic maintenance. Loss of presynaptic α- or β-Spectrin both result in synaptic retraction (Pielage et al., 2005). This presynaptic role for these cytoskeletal components is independent of their role postsynaptically at this synapse; in *Drosophila* larval muscles, the spectrin cytoskeleton regulates spacing of individual synaptic release sites (active zones) and receptor fields (Blunk et al., 2014; Pielage et al., 2006). The actin

cytoskeleton also plays a role in presynaptic stability; loss of the Actin capping protein Hts (the *Drosophila* Adducin homolog) causes synapses to retract (Pielage et al., 2011).

Work to understand the molecular pathway by which disruption of the cytoskeleton leads to synaptic retraction identified increased JNK-Fos signaling as protective in the face of α-Spectrin loss (Massaro et al., 2009). Components of the Wallerian degeneration signaling pathway were also able to rescue synapse loss in this paradigm (Massaro et al., 2009).

Wallerian degeneration is a well-characterized, conserved pathway for axonal degeneration following injury (Coleman and Höke, 2020; Conforti et al., 2014; DiAntonio, 2019; Llobet Rosell and Neukomm, 2019; Luo and O'Leary, 2005; Waller, 1850; Wang et al., 2012). Following damage to an individual larval motor axon, the *Drosophila* nicotinamide mononucleotide adenylyltransferase Nmnat (dNmnat) is depleted, resulting in upregulation of *Drosophila* Sarm (dSarm) (Fang et al., 2012; Gerdts et al., 2013; Llobet Rosell et al., 2022; Osterloh et al., 2012; Sambashivan and Freeman, 2021; Sasaki et al., 2016). dSarm then triggers axonal degeneration, though the exact molecular pathways are still unknown: characteristically, cytoskeletal disruptions occur first, resulting in diminished or absent transport. Axons and downstream synapses then undergo fragmentation and are lost (Coleman and Höke, 2020; Lincoln et al., 2015; Lincoln and Keller, 2016; Wang et al., 2012).

Drosophila larval neurons are also destabilized during the process of metamorphosis to establish the adult NS (Boulanger et al., 2012; Broadie and Bate, 1991; Liu et al., 2010; Watts et al., 2003). In contrast to Wallerian degeneration and synaptic retraction that occur when the cytoskeleton is disrupted as an initial trigger, dismantling of postsynaptic NMJ material occurs first during the process of metamorphosis (Boulanger et al., 2012; Liu et al., 2010). In addition, although the presynaptic cytoskeleton is lost during pupal remodeling, microtubule tracks first thicken during the process of metamorphosis. This thickening is in contrast to degeneration described previously, during which microtubules first thin (Boulanger et al., 2012; Coleman and Höke, 2020; Lincoln et al., 2015; Lincoln and Keller, 2016; Wang et al., 2012). During pupation, loss of the dynactin complex delays presynaptic dissolution, in contrast to inappropriate retraction during larval stages which can be triggered by loss of components of this complex (Eaton et al., 2002; Liu et al., 2010).

In summary, the process of forming, maintaining, and dismantling the *Drosophila* larval NMJ and other NS material involves a complex molecular interplay, from NL to local cytoskeleton.

1.5.2 Other HSPGs

Given the numerous cell types and signaling pathways involved in forming and maintaining the *Drosophila* larval NS, many HSPGs have been shown to regulate multiple aspects of this development. While the NS is forming in the *Drosophila* embryo, growing axons must either exit from the side of the VNC where their cell bodies originate (ipsilateral), or they must cross the embryonic midline and travel contralaterally to reach their targets. The proteins which prevent ipsilateral crossing and repeated contralateral crossing are the ligand Slit and its receptors in the Robo family (Rajagopalan et al., 2000; Rusch and Van Vactor, 2000; Simpson et al., 2000). Like *C. elegans*, HSPGs interact with Slit/Robo signaling in *Drosophila* to ensure proper axon guidance. The HPSGs Syndecan and Dallylike (a *Drosophila* Glypican homolog) both participate in axon guidance at the midline by helping to establish a Slit axon repulsion gradient and by regulating formation of ipsilateral axon tracts, respectively (Johnson et al., 2004; Smart et al., 2011; Steigemann et al., 2004).

Drosophila Syndecan and Dallylike are also important for NMJ synapse formation. Syndecan is made postsynaptically and promotes proper growth of synapses; in its absence, NMJs have reduced synaptic bouton number (Nguyen et al., 2016). Syndecan and Dallylike are both able to bind the receptor protein tyrosine phosphatase LAR, which localizes to synaptic boutons at the *Drosophila* NMJ (Johnson et al., 2006). While Syndecan-LAR binding promotes synaptic growth, Dallylike antagonizes LAR in its role to promote proper active zone size and spacing (Kaufmann et al., 2002). In the absence of Dallylike, synaptic active zone number is increased and the size of individual active zones is significantly smaller than controls (Johnson et al., 2006).

1.5.3 Perlecan

The *Drosophila* homolog of Perlecan was first discovered in a genetic screen in 1992 (Datta and Kankel, 1992). The screen sought to identify genes which disrupted formation and proliferation of the larval optic lobes in the *Drosophila* CNS, with the goal of uncovering larval

lethal mutations that play a role in adult eye development. The gene encoding the *Drosophila* Perlecan homolog was named *terribly reduced optic lobes* (*trol*) given the strong neuroblast proliferation defects observed (Datta and Kankel, 1992).

Following the identification of *trol*, extensive studies have examined how the encoded protein regulates neuroblast proliferation. Genetic interaction analysis first determined that *trol* interacts with *even-skipped*, a gene which controls segment fate and NS development in *Drosophila*, *anachronism*, a proliferation inhibitor secreted by glia, and *string*, a known cell cycle regulator, to ensure proper optic lobe development (Datta, 1995; Park et al., 1998, 2003a; Voigt et al., 2002). Additional work confirmed that Perlecan protein is present in the embryonic CNS and that the protein can interact with multiple signaling pathways to regulate proliferation, including FGF, Hedgehog, the *Drosophila* TGFβ homolog Decapentaplegic, and the *Drosophila* Wnt homolog Wingless (Friedrich et al., 2000; Lindner et al., 2007; Park et al., 2003b).

Additional roles for *Drosophila* Perlecan in NS development have also been described. Much like other HSPGs in *Drosophila* and other species, Perlecan is important for axon guidance during midline crossing and axon outgrowth (Cho et al., 2012). In this context, Perlecan interacts with the transmembrane axon guidance cue Semaphorin in order to ensure repulsion of axons from the midline (Cho et al., 2012).

In the developing *Drosophila* NS, Perlecan functions with the matrix metalloprotease AdamTS-A to ensure proper positioning of neurons (Skeath et al., 2017). In the absence of either protein, the larval CNS becomes disorganized, with misplaced neural tissue bulging out of its usual boundaries. In this role, Perlecan acts in opposition to Collagen IV and β-Integrin to help shape the NL surrounding the brain and VNC (Skeath et al., 2017).

Perlecan also has a known role in driving proper development of the *Drosophila* larval NMJ. In this context, Perlecan is secreted from larval body wall muscles and is found in the extracellular space surrounding the subsynaptic reticulum, specialized infoldings of the muscle plasma membrane around synaptic boutons, where it sequesters Wingless (Wg) and regulates its diffusion to ensure proper pre- and postsynaptic development (Kamimura et al., 2013). In the absence of Perlecan, increased presynaptic Wg signaling results in over-proliferation of "satellite" boutons (small boutons budding off of a main bouton) while decreased postsynaptic Wg signaling results in both satellite and ghost boutons (boutons with presynaptic and no postsynaptic material) (Kamimura et al., 2013).

This introduction highlighted a subset of the roles Perlecan plays during development and maturation of several tissues, including the NS. Given the importance of the protein in regulating signaling and structure in ECMs and BMs, additional roles for Perlecan will surely be uncovered in the future, both within the NS and in other tissues. In Chapter 2, I describe my studies of Perlecan's role within the *Drosophila* larval PNS, focusing initially on abdominal NMJs, a model glutamatergic synapse that the Littleton lab has used to uncover basic mechanisms for synaptic transmission and active zone assembly and function. I discovered that synaptic boutons at the NMJ undergo retraction during later stages of larval development. Although I initially focused on a putative physical or signaling role for Perlecan at the NMJ itself in maintaining synaptic stability, I found that loss of Perlecan disrupted the NL ECM that surrounds larval nerves. This disruption causes secondary defects in the axonal microtubule cytoskeleton, with axonal breakage observed that precedes NMJ retraction. These data indicate Perlecan acts within the NL to regulate its structure and properties such that axons maintain their structural integrity throughout development. Loss of Perlecan damages the ECM surrounding larval nerves, causing axon damage and breakage, followed by retraction of larval MN NMJ synapses.

References

Allen, N.J., Bennett, M.L., Foo, L.C., Wang, G.X., Chakraborty, C., Smith, S.J., Barres, B.A., 2012. Astrocyte glypicans 4 and 6 promote formation of excitatory synapses via GluA1 AMPA receptors. Nature 486, 410–414. doi:10.1038/nature11059

Andlauer, T.F.M., Sigrist, S.J., 2012. Quantitative analysis of Drosophila larval neuromuscular junction morphology. Cold Spring Harb. Protoc. 2012, 490–493. doi:10.1101/pdb.prot068601

Apel, E.D., Glass, D.J., Moscoso, L.M., Yancopoulos, G.D., Sanes, J.R., 1997. Rapsyn is required for MuSK signaling and recruits synaptic components to a MuSK-containing scaffold. Neuron 18, 623–635. doi:10.1016/s0896-6273(00)80303-7

Aponte-Santiago, N.A., Ormerod, K.G., Akbergenova, Y., Littleton, J.T., 2020. Synaptic plasticity induced by differential manipulation of tonic and phasic motoneurons in drosophila. J. Neurosci. 40, 6270–6288. doi:10.1523/JNEUROSCI.0925-20.2020

Arikawa-Hirasawa, E., Le, A.H., Nishino, I., Nonaka, I., Ho, N.C., Francomano, C.A., Govindraj, P., Hassell, J.R., Devaney, J.M., Spranger, J., Stevenson, R.E., Iannaccone, S., Dalakas, M.C., Yamada, Y., 2002a. Structural and functional mutations of the perlecan gene cause Schwartz-Jampel syndrome, with myotonic myopathy and chondrodysplasia. Am. J. Hum. Genet. 70, 1368–1375. doi:10.1086/340390

Arikawa-Hirasawa, E., Rossi, S.G., Rotundo, R.L., Yamada, Y., 2002b. Absence of acetylcholinesterase at the neuromuscular junctions of perlecan-null mice. Nat. Neurosci. 5, 119–123. doi:10.1038/nn801

Arikawa-Hirasawa, E., Watanabe, H., Takami, H., Hassell, J.R., Yamada, Y., 1999. Perlecan is essential for cartilage and cephalic development. Nat. Genet. 23, 354–358. doi:10.1038/15537

Arikawa-Hirasawa, E., Wilcox, W.R., Le, A.H., Silverman, N., Govindraj, P., Hassell, J.R., Yamada, Y., 2001a. Dyssegmental dysplasia, Silverman-Handmaker type, is caused by functional null mutations of the perlecan gene. Nat. Genet. 27, 431–434. doi:10.1038/86941

Arikawa-Hirasawa, E., Wilcox, W.R., Yamada, Y., 2001b. Dyssegmental dysplasia, Silverman-Handmaker type: unexpected role of perlecan in cartilage development. Am. J. Med. Genet. 106, 254–257. doi:10.1002/ajmg.10229

Bangratz, M., Sarrazin, N., Devaux, J., Zambroni, D., Echaniz-Laguna, A., René, F., Boërio, D., Davoine, C.-S., Fontaine, B., Feltri, M.L., Benoit, E., Nicole, S., 2012. A mouse model of Schwartz-Jampel syndrome reveals myelinating Schwann cell dysfunction with persistent axonal depolarization in vitro and distal peripheral nerve hyperexcitability when perlecan is lacking. Am. J. Pathol. 180, 2040–2055. doi:10.1016/j.ajpath.2012.01.035

Bezakova, G., Rabben, I., Sefland, I., Fumagalli, G., Lømo, T., 2001. Neural agrin controls acetylcholine receptor stability in skeletal muscle fibers. Proc. Natl. Acad. Sci. USA 98, 9924–9929. doi:10.1073/pnas.171539698

Bishop, J.R., Schuksz, M., Esko, J.D., 2007. Heparan sulphate proteoglycans fine-tune mammalian physiology. Nature 446, 1030–1037. doi:10.1038/nature05817

Bittern, J., Pogodalla, N., Ohm, H., Brüser, L., Kottmeier, R., Schirmeier, S., Klämbt, C., 2021. Neuron-glia interaction in the Drosophila nervous system. Dev. Neurobiol. 81, 438–452. doi:10.1002/dneu.22737

Bix, G., Iozzo, R.V., 2008. Novel interactions of perlecan: unraveling perlecan's role in angiogenesis. Microsc. Res. Tech. 71, 339–348. doi:10.1002/jemt.20562
Blanchette, C.R., Perrat, P.N., Thackeray, A., Bénard, C.Y., 2015. Glypican Is a Modulator of Netrin-Mediated Axon Guidance. PLoS Biol. 13, e1002183. doi:10.1371/journal.pbio.1002183
Blanchette, C.R., Thackeray, A., Perrat, P.N., Hekimi, S., Bénard, C.Y., 2017. Functional Requirements for Heparan Sulfate Biosynthesis in Morphogenesis and Nervous System Development in C. elegans. PLoS Genet. 13, e1006525. doi:10.1371/journal.pgen.1006525
Blunk, A.D., Akbergenova, Y., Cho, R.W., Lee, J., Walldorf, U., Xu, K., Zhong, G., Zhuang, X., Littleton, J.T., 2014. Postsynaptic actin regulates active zone spacing and glutamate receptor apposition at the Drosophila neuromuscular junction. Mol. Cell. Neurosci. 61, 241–254. doi:10.1016/j.mcn.2014.07.005
Boland, E., Quondamatteo, F., Van Agtmael, T., 2021. The role of basement membranes in cardiac biology and disease. Biosci. Rep. 41. doi:10.1042/BSR20204185
Boulanger, A., Farge, M., Ramanoudjame, C., Wharton, K., Dura, J.-M., 2012. Drosophila motor neuron retraction during metamorphosis is mediated by inputs from TGF-β/BMP signaling and orphan nuclear receptors. PLoS One 7, e40255. doi:10.1371/journal.pone.0040255
Broadie, K.S., Bate, M., 1991. The development of adult muscles in Drosophila: ablation of identified muscle precursor cells. Development 113, 103–118. doi:10.1242/dev.113.1.103
Carson, D.D., Tang, J.P., Julian, J., 1993. Heparan sulfate proteoglycan (perlecan) expression by mouse embryos during acquisition of attachment competence. Dev. Biol. 155, 97–106. doi:10.1006/dbio.1993.1010
Celestrin, K., Díaz-Balzac, C.A., Tang, L.T.H., Ackley, B.D., Bülow, H.E., 2018. Four specific immunoglobulin domains in UNC-52/Perlecan function with NID-1/Nidogen during dendrite morphogenesis in Caenorhabditis elegans. Development 145. doi:10.1242/dev.158881
Chen, Y., Mohammadi, M., Flanagan, J.G., 2009. Graded levels of FGF protein span the midbrain and can instruct graded induction and repression of neural mapping labels. Neuron 62, 773–780. doi:10.1016/j.neuron.2009.05.023
Cho, J.Y., Chak, K., Andreone, B.J., Wooley, J.R., Kolodkin, A.L., 2012. The extracellular matrix proteoglycan perlecan facilitates transmembrane semaphorin-mediated repulsive guidance. Genes Dev. 26, 2222–2235. doi:10.1101/gad.193136.112
Coleman, M.P., Höke, A., 2020. Programmed axon degeneration: from mouse to mechanism to medicine. Nat. Rev. Neurosci. 21, 183–196. doi:10.1038/s41583-020-0269-3
Collins, C.A., DiAntonio, A., 2007. Synaptic development: insights from Drosophila. Curr. Opin. Neurobiol. 17, 35–42. doi:10.1016/j.conb.2007.01.001
Condomitti, G., de Wit, J., 2018. Heparan sulfate proteoglycans as emerging players in synaptic specificity. Front. Mol. Neurosci. 11, 14. doi:10.3389/fnmol.2018.00014
Conforti, L., Gilley, J., Coleman, M.P., 2014. Wallerian degeneration: an emerging axon death pathway linking injury and disease. Nat. Rev. Neurosci. 15, 394–409. doi:10.1038/nrn3680
Costell, M., Carmona, R., Gustafsson, E., González-Iriarte, M., Fässler, R., Muñoz-Chápuli, R., 2002. Hyperplastic conotruncal endocardial cushions and transposition of great arteries in perlecan-null mice. Circ. Res. 91, 158–164. doi:10.1161/01.res.0000026056.81424.da

Costell, M., Gustafsson, E., Aszódi, A., Mörgelin, M., Bloch, W., Hunziker, E., Addicks, K., Timpl, R., Fässler, R., 1999. Perlecan maintains the integrity of cartilage and some basement membranes. J. Cell Biol. 147, 1109–1122. doi:10.1083/jcb.147.5.1109

Crest, J., Diz-Muñoz, A., Chen, D.-Y., Fletcher, D.A., Bilder, D., 2017. Organ sculpting by patterned extracellular matrix stiffness. Elife 6. doi:10.7554/eLife.24958

Datta, S., 1995. Control of proliferation activation in quiescent neuroblasts of the Drosophila central nervous system. Development 121, 1173–1182. doi:10.1242/dev.121.4.1173

Datta, S., Kankel, D.R., 1992. l(1)trol and l(1)devl, loci affecting the development of the adult central nervous system in Drosophila melanogaster. Genetics 130, 523–537.

de Wit, J., O'Sullivan, M.L., Savas, J.N., Condomitti, G., Caccese, M.C., Vennekens, K.M., Yates, J.R., Ghosh, A., 2013. Unbiased discovery of glypican as a receptor for LRRTM4 in regulating excitatory synapse development. Neuron 79, 696–711. doi:10.1016/j.neuron.2013.06.049

DeChiara, T.M., Bowen, D.C., Valenzuela, D.M., Simmons, M.V., Poueymirou, W.T., Thomas, S., Kinetz, E., Compton, D.L., Rojas, E., Park, J.S., Smith, C., DiStefano, P.S., Glass, D.J., Burden, S.J., Yancopoulos, G.D., 1996. The receptor tyrosine kinase MuSK is required for neuromuscular junction formation in vivo. Cell 85, 501–512. doi:10.1016/s0092-8674(00)81251-9

DiAntonio, A., 2019. Axon degeneration: mechanistic insights lead to therapeutic opportunities for the prevention and treatment of peripheral neuropathy. Pain 160 Suppl 1, S17–S22. doi:10.1097/j.pain.0000000000001528

Díaz-Torres, A., Rosales-Nieves, A.E., Pearson, J.R., Santa-Cruz Mateos, C., Marín-Menguiano, M., Marshall, O.J., Brand, A.H., González-Reyes, A., 2021. Stem cell niche organization in the Drosophila ovary requires the ECM component Perlecan. Curr. Biol. 31, 1744–1753.e5. doi:10.1016/j.cub.2021.01.071

Dreyfuss, J.L., Regatieri, C.V., Jarrouge, T.R., Cavalheiro, R.P., Sampaio, L.O., Nader, H.B., 2009. Heparan sulfate proteoglycans: structure, protein interactions and cell signaling. An. Acad. Bras. Cienc. 81, 409–429. doi:10.1590/s0001-37652009000300007

Eaton, B.A., Davis, G.W., 2005. LIM Kinase1 controls synaptic stability downstream of the type II BMP receptor. Neuron 47, 695–708. doi:10.1016/j.neuron.2005.08.010

Eaton, B.A., Fetter, R.D., Davis, G.W., 2002. Dynactin is necessary for synapse stabilization. Neuron 34, 729–741. doi:10.1016/s0896-6273(02)00721-3

Edwards, J.S., Swales, L.S., Bate, M., 1993. The differentiation between neuroglia and connective tissue sheath in insect ganglia revisited: the neural lamella and perineurial sheath cells are absent in a mesodermless mutant of Drosophila. J. Comp. Neurol. 333, 301–308. doi:10.1002/cne.903330214

Edwards, T.J., Hammarlund, M., 2014. Syndecan promotes axon regeneration by stabilizing growth cone migration. Cell Rep. 8, 272–283. doi:10.1016/j.celrep.2014.06.008

Erickson, A.C., Couchman, J.R., 2000. Still more complexity in mammalian basement membranes. J. Histochem. Cytochem. 48, 1291–1306. doi:10.1177/002215540004801001

Ethell, I.M., Irie, F., Kalo, M.S., Couchman, J.R., Pasquale, E.B., Yamaguchi, Y., 2001. EphB/syndecan-2 signaling in dendritic spine morphogenesis. Neuron 31, 1001–1013. doi:10.1016/s0896-6273(01)00440-8

Ethell, I.M., Yamaguchi, Y., 1999. Cell surface heparan sulfate proteoglycan syndecan-2 induces the maturation of dendritic spines in rat hippocampal neurons. J. Cell Biol. 144, 575–586.

doi:10.1083/jcb.144.3.575
Fang, Y., Soares, L., Teng, X., Geary, M., Bonini, N.M., 2012. A novel Drosophila model of nerve injury reveals an essential role of Nmnat in maintaining axonal integrity. Curr. Biol. 22, 590–595. doi:10.1016/j.cub.2012.01.065
Farach-Carson, M.C., Warren, C.R., Harrington, D.A., Carson, D.D., 2014. Border patrol: insights into the unique role of perlecan/heparan sulfate proteoglycan 2 at cell and tissue borders. Matrix Biol 34, 64–79. doi:10.1016/j.matbio.2013.08.004
Farhy-Tselnicker, I., van Casteren, A.C.M., Lee, A., Chang, V.T., Aricescu, A.R., Allen, N.J., 2017. Astrocyte-Secreted Glypican 4 Regulates Release of Neuronal Pentraxin 1 from Axons to Induce Functional Synapse Formation. Neuron 96, 428–445.e13. doi:10.1016/j.neuron.2017.09.053
Friedrich, M.V., Schneider, M., Timpl, R., Baumgartner, S., 2000. Perlecan domain V of Drosophila melanogaster. Sequence, recombinant analysis and tissue expression. Eur. J. Biochem. 267, 3149–3159. doi:10.1046/j.1432-1327.2000.01337.x
Gautam, M., Noakes, P.G., Mudd, J., Nichol, M., Chu, G.C., Sanes, J.R., Merlie, J.P., 1995. Failure of postsynaptic specialization to develop at neuromuscular junctions of rapsyn-deficient mice. Nature 377, 232–236. doi:10.1038/377232a0
Gerdts, J., Summers, D.W., Sasaki, Y., DiAntonio, A., Milbrandt, J., 2013. Sarm1-mediated axon degeneration requires both SAM and TIR interactions. J. Neurosci. 33, 13569–13580. doi:10.1523/JNEUROSCI.1197-13.2013
Girós, A., Morante, J., Gil-Sanz, C., Fairén, A., Costell, M., 2007. Perlecan controls neurogenesis in the developing telencephalon. BMC Dev. Biol. 7, 29. doi:10.1186/1471-213X-7-29
Graf, E.R., Heerssen, H.M., Wright, C.M., Davis, G.W., DiAntonio, A., 2011. Stathmin is required for stability of the Drosophila neuromuscular junction. J. Neurosci. 31, 15026–15034. doi:10.1523/JNEUROSCI.2024-11.2011
Gubbiotti, M.A., Neill, T., Iozzo, R.V., 2017. A current view of perlecan in physiology and pathology: A mosaic of functions. Matrix Biol 57–58, 285–298. doi:10.1016/j.matbio.2016.09.003
Hall, Z.W., Sanes, J.R., 1993. Synaptic structure and development: the neuromuscular junction. Cell 72 Suppl, 99–121. doi:10.1016/s0092-8674(05)80031-5
Hamill, K.J., Kligys, K., Hopkinson, S.B., Jones, J.C.R., 2009. Laminin deposition in the extracellular matrix: a complex picture emerges. J. Cell Sci. 122, 4409–4417. doi:10.1242/jcs.041095
Harris, K.P., Littleton, J.T., 2015. Transmission, development, and plasticity of synapses. Genetics 201, 345–375. doi:10.1534/genetics.115.176529
Hassell, J.R., Robey, P.G., Barrach, H.J., Wilczek, J., Rennard, S.I., Martin, G.R., 1980. Isolation of a heparan sulfate-containing proteoglycan from basement membrane. Proc. Natl. Acad. Sci. USA 77, 4494–4498. doi:10.1073/pnas.77.8.4494
Hoang, B., Chiba, A., 2001. Single-cell analysis of Drosophila larval neuromuscular synapses. Dev. Biol. 229, 55–70. doi:10.1006/dbio.2000.9983
Hu, H.-T., Umemori, H., Hsueh, Y.-P., 2016. Postsynaptic SDC2 induces transsynaptic signaling via FGF22 for bidirectional synaptic formation. Sci. Rep. 6, 33592. doi:10.1038/srep33592
Hunter, A.C., Petley-Ragan, L.M., Das, M., Auld, V.J., 2020. Basigin Associates with Integrin in Order to Regulate Perineurial Glia and Drosophila Nervous System Morphology. J.

Neurosci. 40, 3360–3373. doi:10.1523/JNEUROSCI.1397-19.2020
Hynes, R.O., 2009. The extracellular matrix: not just pretty fibrils. Science 326, 1216–1219. doi:10.1126/science.1176009
Inatani, M., Irie, F., Plump, A.S., Tessier-Lavigne, M., Yamaguchi, Y., 2003. Mammalian brain morphogenesis and midline axon guidance require heparan sulfate. Science 302, 1044–1046. doi:10.1126/science.1090497
Isabella, A.J., Horne-Badovinac, S., 2015. Building from the Ground up: Basement Membranes in Drosophila Development. Curr Top Membr 76, 305–336. doi:10.1016/bs.ctm.2015.07.001
Johnson, K.G., Ghose, A., Epstein, E., Lincecum, J., O'Connor, M.B., Van Vactor, D., 2004. Axonal heparan sulfate proteoglycans regulate the distribution and efficiency of the repellent slit during midline axon guidance. Curr. Biol. 14, 499–504. doi:10.1016/j.cub.2004.02.005
Johnson, K.G., Tenney, A.P., Ghose, A., Duckworth, A.M., Higashi, M.E., Parfitt, K., Marcu, O., Heslip, T.R., Marsh, J.L., Schwarz, T.L., Flanagan, J.G., Van Vactor, D., 2006. The HSPGs Syndecan and Dallylike bind the receptor phosphatase LAR and exert distinct effects on synaptic development. Neuron 49, 517–531. doi:10.1016/j.neuron.2006.01.026
Kamimura, K., Ueno, K., Nakagawa, J., Hamada, R., Saitoe, M., Maeda, N., 2013. Perlecan regulates bidirectional Wnt signaling at the Drosophila neuromuscular junction. J. Cell Biol. 200, 219–233. doi:10.1083/jcb.201207036
Kanca, O., Bellen, H.J., Schnorrer, F., 2017. Gene tagging strategies to assess protein expression, localization, and function in drosophila. Genetics 207, 389–412. doi:10.1534/genetics.117.199968
Kaufmann, N., DeProto, J., Ranjan, R., Wan, H., Van Vactor, D., 2002. Drosophila liprin-alpha and the receptor phosphatase Dlar control synapse morphogenesis. Neuron 34, 27–38. doi:10.1016/s0896-6273(02)00643-8
Kerever, A., Mercier, F., Nonaka, R., de Vega, S., Oda, Y., Zalc, B., Okada, Y., Hattori, N., Yamada, Y., Arikawa-Hirasawa, E., 2014. Perlecan is required for FGF-2 signaling in the neural stem cell niche. Stem Cell Res. 12, 492–505. doi:10.1016/j.scr.2013.12.009
Khalilgharibi, N., Mao, Y., 2021. To form and function: on the role of basement membrane mechanics in tissue development, homeostasis and disease. Open Biol 11, 200360. doi:10.1098/rsob.200360
Kim, N., Stiegler, A.L., Cameron, T.O., Hallock, P.T., Gomez, A.M., Huang, J.H., Hubbard, S.R., Dustin, M.L., Burden, S.J., 2008. Lrp4 is a receptor for Agrin and forms a complex with MuSK. Cell 135, 334–342. doi:10.1016/j.cell.2008.10.002
Kinnunen, T.K., 2014. Combinatorial roles of heparan sulfate proteoglycans and heparan sulfates in Caenorhabditis elegans neural development. PLoS One 9, e102919. doi:10.1371/journal.pone.0102919
Ko, J.S., Pramanik, G., Um, J.W., Shim, J.S., Lee, D., Kim, K.H., Chung, G.-Y., Condomitti, G., Kim, H.M., Kim, H., de Wit, J., Park, K.-S., Tabuchi, K., Ko, J., 2015. PTPσ functions as a presynaptic receptor for the glypican-4/LRRTM4 complex and is essential for excitatory synaptic transmission. Proc. Natl. Acad. Sci. USA 112, 1874–1879. doi:10.1073/pnas.1410138112
Koch, I., Schwarz, H., Beuchle, D., Goellner, B., Langegger, M., Aberle, H., 2008. Drosophila ankyrin 2 is required for synaptic stability. Neuron 58, 210–222. doi:10.1016/j.neuron.2008.03.019

Kohsaka, H., Okusawa, S., Itakura, Y., Fushiki, A., Nose, A., 2012. Development of larval motor circuits in Drosophila. Dev. Growth Differ. 54, 408–419. doi:10.1111/j.1440-169X.2012.01347.x

Kruegel, J., Miosge, N., 2010. Basement membrane components are key players in specialized extracellular matrices. Cell Mol. Life Sci. 67, 2879–2895. doi:10.1007/s00018-010-0367-x

Liang, X., Dong, X., Moerman, D.G., Shen, K., Wang, X., 2015. Sarcomeres Pattern Proprioceptive Sensory Dendritic Endings through UNC-52/Perlecan in C. elegans. Dev. Cell 33, 388–400. doi:10.1016/j.devcel.2015.03.010

Lincoln, B.L., Alabsi, S.H., Frendo, N., Freund, R., Keller, L.C., 2015. Drosophila neuronal injury follows a temporal sequence of cellular events leading to degeneration at the neuromuscular junction. J. Exp. Neurosci. 9, 1–9. doi:10.4137/JEN.S25516

Lincoln, B.L., Keller, L.C., 2016. Drosophila neuronal injury model allows for temporal dissection of neurodegenerative events. Neural Regen. Res. 11, 416–417. doi:10.4103/1673-5374.179046

Lindner, J.R., Hillman, P.R., Barrett, A.L., Jackson, M.C., Perry, T.L., Park, Y., Datta, S., 2007. The Drosophila Perlecan gene trol regulates multiple signaling pathways in different developmental contexts. BMC Dev. Biol. 7, 121. doi:10.1186/1471-213X-7-121

Liu, Z., Chen, Y., Wang, D., Wang, S., Zhang, Y.Q., 2010. Distinct presynaptic and postsynaptic dismantling processes of Drosophila neuromuscular junctions during metamorphosis. J. Neurosci. 30, 11624–11634. doi:10.1523/JNEUROSCI.0410-10.2010

Llobet Rosell, A., Neukomm, L.J., 2019. Axon death signalling in Wallerian degeneration among species and in disease. Open Biol 9, 190118. doi:10.1098/rsob.190118

Llobet Rosell, A., Paglione, M., Gilley, J., Kocia, M., Perillo, G., Gasparrini, M., Cialabrini, L., Raffaelli, N., Angeletti, C., Orsomando, G., Wu, P.-H., Coleman, M.P., Loreto, A., Neukomm, L.J., 2022. The NAD+ precursor NMN activates dSarm to trigger axon degeneration in Drosophila. Elife 11. doi:10.7554/eLife.80245

Lowe, D.A., Lepori-Bui, N., Fomin, P.V., Sloofman, L.G., Zhou, X., Farach-Carson, M.C., Wang, L., Kirn-Safran, C.B., 2014. Deficiency in perlecan/HSPG2 during bone development enhances osteogenesis and decreases quality of adult bone in mice. Calcif. Tissue Int. 95, 29–38. doi:10.1007/s00223-014-9859-2

Luo, L., O'Leary, D.D.M., 2005. Axon retraction and degeneration in development and disease. Annu. Rev. Neurosci. 28, 127–156. doi:10.1146/annurev.neuro.28.061604.135632

Martin, G.R., Timpl, R., 1987. Laminin and other basement membrane components. Annu. Rev. Cell Biol. 3, 57–85. doi:10.1146/annurev.cb.03.110187.000421

Martin, G.R., Timpl, R., Kühn, K., 1988. Basement membrane proteins: molecular structure and function. Adv. Protein Chem. 39, 1–50. doi:10.1016/s0065-3233(08)60374-5

Martinez, J.R., Dhawan, A., Farach-Carson, M.C., 2018. Modular proteoglycan perlecan/hspg2: mutations, phenotypes, and functions. Genes (Basel) 9. doi:10.3390/genes9110556

Mashayekhi, F., Sadeghi, M., Rajaei, F., 2011. Induction of perlecan expression and neural cell proliferation by FGF-2 in the developing cerebral cortex: an in vivo study. J. Mol. Neurosci. 45, 87–93. doi:10.1007/s12031-010-9393-2

Massaro, C.M., Pielage, J., Davis, G.W., 2009. Molecular mechanisms that enhance synapse stability despite persistent disruption of the spectrin/ankyrin/microtubule cytoskeleton. J. Cell Biol. 187, 101–117. doi:10.1083/jcb.200903166

Matsubayashi, Y., Louani, A., Dragu, A., Sánchez-Sánchez, B.J., Serna-Morales, E., Yolland, L.,

Gyoergy, A., Vizcay, G., Fleck, R.A., Heddleston, J.M., Chew, T.-L., Siekhaus, D.E., Stramer, B.M., 2017. A moving source of matrix components is essential for de novo basement membrane formation. Curr. Biol. 27, 3526–3534.e4. doi:10.1016/j.cub.2017.10.001

Matzat, T., Sieglitz, F., Kottmeier, R., Babatz, F., Engelen, D., Klämbt, C., 2015. Axonal wrapping in the Drosophila PNS is controlled by glia-derived neuregulin homolog Vein. Development 142, 1336–1345. doi:10.1242/dev.116616

McCall, A.S., Cummings, C.F., Bhave, G., Vanacore, R., Page-McCaw, A., Hudson, B.G., 2014. Bromine is an essential trace element for assembly of collagen IV scaffolds in tissue development and architecture. Cell 157, 1380–1392. doi:10.1016/j.cell.2014.05.009

Meyer, S., Schmidt, I., Klämbt, C., 2014. Glia ECM interactions are required to shape the Drosophila nervous system. Mech. Dev. 133, 105–116. doi:10.1016/j.mod.2014.05.003

Middelkoop, T.C., Korswagen, H.C., 2018. Development and migration of the C. elegans Q neuroblasts and their descendants, in: WormBook: The Online Review of C. Elegans Biology. Pasadena (CA).

Mouw, J.K., Ou, G., Weaver, V.M., 2014. Extracellular matrix assembly: a multiscale deconstruction. Nat. Rev. Mol. Cell Biol. 15, 771–785. doi:10.1038/nrm3902

Nguyen, M.U., Kwong, J., Chang, J., Gillet, V.G., Lee, R.M., Johnson, K.G., 2016. The extracellular and cytoplasmic domains of syndecan cooperate postsynaptically to promote synapse growth at the drosophila neuromuscular junction. PLoS One 11, e0151621. doi:10.1371/journal.pone.0151621

Nicole, S., Davoine, C.S., Topaloglu, H., Cattolico, L., Barral, D., Beighton, P., Hamida, C.B., Hammouda, H., Cruaud, C., White, P.S., Samson, D., Urtizberea, J.A., Lehmann-Horn, F., Weissenbach, J., Hentati, F., Fontaine, B., 2000. Perlecan, the major proteoglycan of basement membranes, is altered in patients with Schwartz-Jampel syndrome (chondrodystrophic myotonia). Nat. Genet. 26, 480–483. doi:10.1038/82638

Nitkin, R.M., Smith, M.A., Magill, C., Fallon, J.R., Yao, Y.M., Wallace, B.G., McMahan, U.J., 1987. Identification of agrin, a synaptic organizing protein from Torpedo electric organ. J. Cell Biol. 105, 2471–2478. doi:10.1083/jcb.105.6.2471

Nonaka, R., Iesaki, T., Kerever, A., Arikawa-Hirasawa, E., 2021. Increased Risk of Aortic Dissection with Perlecan Deficiency. Int. J. Mol. Sci. 23. doi:10.3390/ijms23010315

Noonan, D.M., Fulle, A., Valente, P., Cai, S., Horigan, E., Sasaki, M., Yamada, Y., Hassell, J.R., 1991. The complete sequence of perlecan, a basement membrane heparan sulfate proteoglycan, reveals extensive similarity with laminin A chain, low density lipoprotein-receptor, and the neural cell adhesion molecule. J. Biol. Chem. 266, 22939–22947. doi:10.1016/S0021-9258(18)54445-8

Olofsson, B., Page, D.T., 2005. Condensation of the central nervous system in embryonic Drosophila is inhibited by blocking hemocyte migration or neural activity. Dev. Biol. 279, 233–243. doi:10.1016/j.ydbio.2004.12.020

Osterloh, J.M., Yang, J., Rooney, T.M., Fox, A.N., Adalbert, R., Powell, E.H., Sheehan, A.E., Avery, M.A., Hackett, R., Logan, M.A., MacDonald, J.M., Ziegenfuss, J.S., Milde, S., Hou, Y.-J., Nathan, C., Ding, A., Brown, R.H., Conforti, L., Coleman, M., Tessier-Lavigne, M., Züchner, S., Freeman, M.R., 2012. dSarm/Sarm1 is required for activation of an injury-induced axon death pathway. Science 337, 481–484. doi:10.1126/science.1223899

Owald, D., Sigrist, S.J., 2009. Assembling the presynaptic active zone. Curr. Opin. Neurobiol.

19, 311–318. doi:10.1016/j.conb.2009.03.003
Park, Y., Fujioka, M., Jaynes, J.B., Datta, S., 1998. Drosophila homeobox geneeve enhancestrol, an activator of neuroblast proliferation in the larval CNS. Dev. Genet. 23, 247–257. doi:10.1002/(SICI)1520-6408(1998)23:3<247::AID-DVG9>3.0.CO;2-I
Park, Y., Ng, C., Datta, S., 2003a. Induction of string rescues the neuroblast proliferation defect in trol mutant animals. Genesis 36, 187–195. doi:10.1002/gene.10216
Park, Y., Rangel, C., Reynolds, M.M., Caldwell, M.C., Johns, M., Nayak, M., Welsh, C.J.R., McDermott, S., Datta, S., 2003b. Drosophila perlecan modulates FGF and hedgehog signals to activate neural stem cell division. Dev. Biol. 253, 247–257. doi:10.1016/s0012-1606(02)00019-2
Pasini, A., Manenti, R., Rothbächer, U., Lemaire, P., 2012. Antagonizing retinoic acid and FGF/MAPK pathways control posterior body patterning in the invertebrate chordate Ciona intestinalis. PLoS One 7, e46193. doi:10.1371/journal.pone.0046193
Pastor-Pareja, J.C., Xu, T., 2011. Shaping cells and organs in Drosophila by opposing roles of fat body-secreted Collagen IV and perlecan. Dev. Cell 21, 245–256. doi:10.1016/j.devcel.2011.06.026
Pei, S., Parthasarathy, S., Parajuli, A., Martinez, J., Lv, M., Jiang, S., Wu, D., Wei, S., Lu, X.L., Farach-Carson, M.C., Kirn-Safran, C.B., Wang, L., 2020. Perlecan/Hspg2 deficiency impairs bone's calcium signaling and associated transcriptome in response to mechanical loading. Bone 131, 115078. doi:10.1016/j.bone.2019.115078
Peng, H.B., Xie, H., Rossi, S.G., Rotundo, R.L., 1999. Acetylcholinesterase clustering at the neuromuscular junction involves perlecan and dystroglycan. J. Cell Biol. 145, 911–921. doi:10.1083/jcb.145.4.911
Pérez-Moreno, J.J., O'Kane, C.J., 2019. GAL4 drivers specific for type ib and type is motor neurons in drosophila. G3 (Bethesda) 9, 453–462. doi:10.1534/g3.118.200809
Pielage, J., Bulat, V., Zuchero, J.B., Fetter, R.D., Davis, G.W., 2011. Hts/Adducin controls synaptic elaboration and elimination. Neuron 69, 1114–1131. doi:10.1016/j.neuron.2011.02.007
Pielage, J., Cheng, L., Fetter, R.D., Carlton, P.M., Sedat, J.W., Davis, G.W., 2008. A presynaptic giant ankyrin stabilizes the NMJ through regulation of presynaptic microtubules and transsynaptic cell adhesion. Neuron 58, 195–209. doi:10.1016/j.neuron.2008.02.017
Pielage, J., Fetter, R.D., Davis, G.W., 2005. Presynaptic spectrin is essential for synapse stabilization. Curr. Biol. 15, 918–928. doi:10.1016/j.cub.2005.04.030
Pielage, J., Fetter, R.D., Davis, G.W., 2006. A postsynaptic spectrin scaffold defines active zone size, spacing, and efficacy at the Drosophila neuromuscular junction. J. Cell Biol. 175, 491–503. doi:10.1083/jcb.200607036
Pöschl, E., Schlötzer-Schrehardt, U., Brachvogel, B., Saito, K., Ninomiya, Y., Mayer, U., 2004. Collagen IV is essential for basement membrane stability but dispensable for initiation of its assembly during early development. Development 131, 1619–1628. doi:10.1242/dev.01037
Poulain, F.E., Yost, H.J., 2015. Heparan sulfate proteoglycans: a sugar code for vertebrate development? Development 142, 3456–3467. doi:10.1242/dev.098178
Pownall, M.E., Isaacs, H.V., 2010. FGF Signalling and Posterior Neural Patterning, in: FGF Signalling in Vertebrate Development. Morgan & Claypool Life Sciences, San Rafael (CA).
Qin, J., Liang, J., Ding, M., 2014. Perlecan antagonizes collagen IV and ADAMTS9/GON-1 in

restricting the growth of presynaptic boutons. J. Neurosci. 34, 10311–10324. doi:10.1523/JNEUROSCI.5128-13.2014
Rajagopalan, S., Vivancos, V., Nicolas, E., Dickson, B.J., 2000. Selecting a longitudinal pathway: Robo receptors specify the lateral position of axons in the Drosophila CNS. Cell 103, 1033–1045. doi:10.1016/s0092-8674(00)00207-5
Ramos-Lewis, W., Page-McCaw, A., 2019. Basement membrane mechanics shape development: Lessons from the fly. Matrix Biol 75–76, 72–81. doi:10.1016/j.matbio.2018.04.004
Reyes Fernandez, P.C., Wright, C.S., Masterson, A.N., Yi, X., Tellman, T.V., Bonteanu, A., Rust, K., Noonan, M.L., White, K.E., Lewis, K.J., Sankar, U., Hum, J.M., Bix, G., Wu, D., Robling, A.G., Sardar, R., Farach-Carson, M.C., Thompson, W.R., 2022. Gabapentin Disrupts Binding of Perlecan to the α2δ1 Voltage Sensitive Calcium Channel Subunit and Impairs Skeletal Mechanosensation. Biomolecules 12. doi:10.3390/biom12121857
Rhiner, C., Gysi, S., Fröhli, E., Hengartner, M.O., Hajnal, A., 2005. Syndecan regulates cell migration and axon guidance in C. elegans. Development 132, 4621–4633. doi:10.1242/dev.02042
Ruggiu, M., Herbst, R., Kim, N., Jevsek, M., Fak, J.J., Mann, M.A., Fischbach, G., Burden, S.J., Darnell, R.B., 2009. Rescuing Z+ agrin splicing in Nova null mice restores synapse formation and unmasks a physiologic defect in motor neuron firing. Proc. Natl. Acad. Sci. USA 106, 3513–3518. doi:10.1073/pnas.0813112106
Rusch, J., Van Vactor, D., 2000. New Roundabouts send axons into the Fas lane. Neuron 28, 637–640. doi:10.1016/s0896-6273(00)00143-4
Saied-Santiago, K., Townley, R.A., Attonito, J.D., da Cunha, D.S., Díaz-Balzac, C.A., Tecle, E., Bülow, H.E., 2017. Coordination of Heparan Sulfate Proteoglycans with Wnt Signaling To Control Cellular Migrations and Positioning in Caenorhabditis elegans. Genetics 206, 1951–1967. doi:10.1534/genetics.116.198739
Sambashivan, S., Freeman, M.R., 2021. SARM1 signaling mechanisms in the injured nervous system. Curr. Opin. Neurobiol. 69, 247–255. doi:10.1016/j.conb.2021.05.004
Sanes, J.R., Lichtman, J.W., 1999. Development of the vertebrate neuromuscular junction. Annu. Rev. Neurosci. 22, 389–442. doi:10.1146/annurev.neuro.22.1.389
Sanes, J.R., Marshall, L.M., McMahan, U.J., 1978. Reinnervation of muscle fiber basal lamina after removal of myofibers. Differentiation of regenerating axons at original synaptic sites. J. Cell Biol. 78, 176–198. doi:10.1083/jcb.78.1.176
Sarrazin, S., Lamanna, W.C., Esko, J.D., 2011. Heparan sulfate proteoglycans. Cold Spring Harb. Perspect. Biol. 3. doi:10.1101/cshperspect.a004952
Sasaki, Y., Nakagawa, T., Mao, X., DiAntonio, A., Milbrandt, J., 2016. NMNAT1 inhibits axon degeneration via blockade of SARM1-mediated NAD+ depletion. Elife 5. doi:10.7554/eLife.19749
Sasse, P., Malan, D., Fleischmann, M., Roell, W., Gustafsson, E., Bostani, T., Fan, Y., Kolbe, T., Breitbach, M., Addicks, K., Welz, A., Brem, G., Hescheler, J., Aszodi, A., Costell, M., Bloch, W., Fleischmann, B.K., 2008. Perlecan is critical for heart stability. Cardiovasc. Res. 80, 435–444. doi:10.1093/cvr/cvn225
Schlessinger, J., Plotnikov, A.N., Ibrahimi, O.A., Eliseenkova, A.V., Yeh, B.K., Yayon, A., Linhardt, R.J., Mohammadi, M., 2000. Crystal structure of a ternary FGF-FGFR-heparin complex reveals a dual role for heparin in FGFR binding and dimerization. Mol. Cell 6, 743–750. doi:10.1016/s1097-2765(00)00073-3
Şentürk, M., Bellen, H.J., 2018. Genetic strategies to tackle neurological diseases in fruit flies.

Curr. Opin. Neurobiol. 50, 24–32. doi:10.1016/j.conb.2017.10.017
Siddiqui, T.J., Tari, P.K., Connor, S.A., Zhang, P., Dobie, F.A., She, K., Kawabe, H., Wang, Y.T., Brose, N., Craig, A.M., 2013. An LRRTM4-HSPG complex mediates excitatory synapse development on dentate gyrus granule cells. Neuron 79, 680–695. doi:10.1016/j.neuron.2013.06.029
Simpson, J.H., Bland, K.S., Fetter, R.D., Goodman, C.S., 2000. Short-range and long-range guidance by Slit and its Robo receptors: a combinatorial code of Robo receptors controls lateral position. Cell 103, 1019–1032. doi:10.1016/s0092-8674(00)00206-3
Skeath, J.B., Wilson, B.A., Romero, S.E., Snee, M.J., Zhu, Y., Lacin, H., 2017. The extracellular metalloprotease AdamTS-A anchors neural lineages in place within and preserves the architecture of the central nervous system. Development 144, 3102–3113. doi:10.1242/dev.145854
Smart, A.D., Course, M.M., Rawson, J., Selleck, S., Van Vactor, D., Johnson, K.G., 2011. Heparan sulfate proteoglycan specificity during axon pathway formation in the Drosophila embryo. Dev. Neurobiol. 71, 608–618. doi:10.1002/dneu.20854
Steigemann, P., Molitor, A., Fellert, S., Jäckle, H., Vorbrüggen, G., 2004. Heparan sulfate proteoglycan syndecan promotes axonal and myotube guidance by slit/robo signaling. Curr. Biol. 14, 225–230. doi:10.1016/j.cub.2004.01.006
Stork, T., Engelen, D., Krudewig, A., Silies, M., Bainton, R.J., Klämbt, C., 2008. Organization and function of the blood-brain barrier in Drosophila. J. Neurosci. 28, 587–597. doi:10.1523/JNEUROSCI.4367-07.2008
Sundararajan, L., Norris, M.L., Lundquist, E.A., 2015. SDN-1/Syndecan Acts in Parallel to the Transmembrane Molecule MIG-13 to Promote Anterior Neuroblast Migration. G3 (Bethesda) 5, 1567–1574. doi:10.1534/g3.115.018770
Timpl, R., Brown, J.C., 1996. Supramolecular assembly of basement membranes. Bioessays 18, 123–132. doi:10.1002/bies.950180208
Töpfer, U., Guerra Santillán, K.Y., Fischer-Friedrich, E., Dahmann, C., 2022. Distinct contributions of ECM proteins to basement membrane mechanical properties in Drosophila. Development 149. doi:10.1242/dev.200456
Trinh, K., Julovi, S.M., Rogers, N.M., 2022. The role of matrix proteins in cardiac pathology. Int. J. Mol. Sci. 23. doi:10.3390/ijms23031338
Urbano, J.M., Torgler, C.N., Molnar, C., Tepass, U., López-Varea, A., Brown, N.H., de Celis, J.F., Martín-Bermudo, M.D., 2009. Drosophila laminins act as key regulators of basement membrane assembly and morphogenesis. Development 136, 4165–4176. doi:10.1242/dev.044263
Vanacore, R., Ham, A.-J.L., Voehler, M., Sanders, C.R., Conrads, T.P., Veenstra, T.D., Sharpless, K.B., Dawson, P.E., Hudson, B.G., 2009. A sulfilimine bond identified in collagen IV. Science 325, 1230–1234. doi:10.1126/science.1176811
Voigt, A., Pflanz, R., Schäfer, U., Jäckle, H., 2002. Perlecan participates in proliferation activation of quiescent Drosophila neuroblasts. Dev. Dyn. 224, 403–412. doi:10.1002/dvdy.10120
Waller, A., 1850. Experiments on the section of the glossopharyngeal and hypoglossal nerves of the frog, and observations of the alterations produced thereby in the structure of their primitive fibres. Philosophical Transactions of the Royal Society of London 140, 423–429. doi:10.1098/rstl.1850.0021
Wang, B., Lai, X., Price, C., Thompson, W.R., Li, W., Quabili, T.R., Tseng, W.-J., Liu, X.S.,

Zhang, H., Pan, J., Kirn-Safran, C.B., Farach-Carson, M.C., Wang, L., 2014. Perlecan-containing pericellular matrix regulates solute transport and mechanosensing within the osteocyte lacunar-canalicular system. J. Bone Miner. Res. 29, 878–891. doi:10.1002/jbmr.2105

Wang, J.T., Medress, Z.A., Barres, B.A., 2012. Axon degeneration: molecular mechanisms of a self-destruction pathway. J. Cell Biol. 196, 7–18. doi:10.1083/jcb.201108111

Wang, X., Zhou, F., Lv, S., Yi, P., Zhu, Z., Yang, Y., Feng, G., Li, W., Ou, G., 2013. Transmembrane protein MIG-13 links the Wnt signaling and Hox genes to the cell polarity in neuronal migration. Proc. Natl. Acad. Sci. USA 110, 11175–11180. doi:10.1073/pnas.1301849110

Warren, C.R., Kassir, E., Spurlin, J., Martinez, J., Putnam, N.H., Farach-Carson, M.C., 2015. Evolution of the perlecan/HSPG2 gene and its activation in regenerating Nematostella vectensis. PLoS One 10, e0124578. doi:10.1371/journal.pone.0124578

Watts, R.J., Hoopfer, E.D., Luo, L., 2003. Axon pruning during Drosophila metamorphosis: evidence for local degeneration and requirement of the ubiquitin-proteasome system. Neuron 38, 871–885. doi:10.1016/s0896-6273(03)00295-2

Whitelock, J.M., Melrose, J., Iozzo, R.V., 2008. Diverse cell signaling events modulated by perlecan. Biochemistry 47, 11174–11183. doi:10.1021/bi8013938

You, J., Zhang, Y., Li, Z., Lou, Z., Jin, L., Lin, X., 2014. Drosophila perlecan regulates intestinal stem cell activity via cell-matrix attachment. Stem Cell Rep. 2, 761–769. doi:10.1016/j.stemcr.2014.04.007

Yurchenco, P.D., 2011. Basement membranes: cell scaffoldings and signaling platforms. Cold Spring Harb. Perspect. Biol. 3, a004911. doi:10.1101/cshperspect.a004911

Zhou, X., Vachon, C., Cizeron, M., Romatif, O., Bülow, H.E., Jospin, M., Bessereau, J.-L., 2021. The HSPG syndecan is a core organizer of cholinergic synapses. J. Cell Biol. 220. doi:10.1083/jcb.202011144

Zoeller, J.J., Whitelock, J.M., Iozzo, R.V., 2009. Perlecan regulates developmental angiogenesis by modulating the VEGF-VEGFR2 axis. Matrix Biol 28, 284–291. doi:10.1016/j.matbio.2009.04.010

Zou, W., Shen, A., Dong, X., Tugizova, M., Xiang, Y.K., Shen, K., 2016. A multi-protein receptor-ligand complex underlies combinatorial dendrite guidance choices in C. elegans. Elife 5. doi:10.7554/eLife.18345

Ellen Guss performed most of the work in this chapter. Karen Cunningham and Chad Sauvola performed the Apex proximity labeling screen. Yulia Akbergenova performed the live intravital imaging and the anti-Futsch, UAS-*myrRFP*, and UAS-*10xGFP* axon imaging.

Chapter 2

Loss of the extracellular matrix protein Perlecan disrupts axonal and synaptic stability during *Drosophila* development

2.1 Introduction

Neurons require regulated polarization and transport of synaptic material to maintain their distinctive shape and electrical properties. Indeed, disruption of axonal transport is linked to numerous neurodevelopmental and neurodegenerative disorders (Cheng et al., 2022; De Vos et al., 2008; DiAntonio, 2019; Fernandopulle et al., 2021; Krench and Littleton, 2013; Luo and O'Leary, 2005; Mariano et al., 2018; Neukomm and Freeman, 2014). Neuronal development depends upon multiple transmembrane and secreted proteins that facilitate intercellular communication and interactions with the extracellular environment. The heparan sulfate proteoglycans (HSPGs), including the transmembrane Syndecans, the glycosylphosphatidylinositol (GPI)-linked Glypicans and the secreted Agrin and Perlecan proteins (Bernfield et al., 1999; Häcker et al., 2005; Kamimura and Maeda, 2021; Lin, 2004; Sarrazin et al., 2011), play multiple roles in neuronal development. These include regulating neuronal migration and axon guidance, controlling diffusion of secreted signaling ligands, forming extracellular matrix (ECM) barriers that maintain cell boundaries, and clustering synaptic transmembrane and secreted proteins (Arikawa-Hirasawa et al., 2002; Cho et al., 2012; Fox and Zinn, 2005; Johnson et al., 2006; Kamimura et al., 2013; Kamimura and Maeda, 2021; Kinnunen, 2014; Nitkin et al., 1987; Sanes et al., 1978). HSPGs encode core proteins with multiple extracellular motifs that are heavily modified by covalently attached heparan sulfate sugar chains which undergo their own enzymatic modifications (Bishop et al., 2007). Perlecan has the largest core mass of all HSPGs and is a conserved component of the ECM and basement membranes (BMs) with Laminin, Nidogen and type IV Collagen (Carson et al., 1993; Erickson and Couchman, 2000; Hassell et al., 1980; Martin et al., 1988; Martin and Timpl, 1987; Mouw et al., 2014; Noonan et al., 1991). The ECM plays essential structural and signaling roles in multiple contexts by maintaining tissue integrity and restricting diffusion of secreted signaling ligands (Aviezer et al., 1994; Lindner et al., 2007; Park et al., 2003; Schaefer and Schaefer, 2010). In this study, we identified a role for Perlecan in maintaining the stability of the ECM surrounding nerve bundles, with loss of neuronal axons and synapses in mutants lacking the protein.

Drosophila larval motoneurons (MNs) and their glutamatergic neuromuscular junctions (NMJs) are a robust system for studying neuronal development and function due to abundant genetic toolkits and their ease of use for live and fixed imaging (Andlauer and Sigrist, 2012; Bellen et al., 2019; Collins and DiAntonio, 2007; Harris and Littleton, 2015; Kanca et al., 2017; Owald and Sigrist, 2009; Sambashivan and Freeman, 2021; Şentürk and Bellen, 2018). Many HSPGs are

highly conserved in *Drosophila* and several function in neuronal development (Dani et al., 2012; Han et al., 2020; Johnson et al., 2006; Kamimura et al., 2019, 2013; Koper et al., 2012; Nguyen et al., 2016). The *Drosophila* Perlecan homolog is encoded by the gene *terribly reduced optic lobes* (*trol*) (Datta and Kankel, 1992; Friedrich et al., 2000; Voigt et al., 2002) and has been suggested to play a signaling role at NMJs by regulating diffusion of synaptically released Wingless (Wg) (Kamimura et al., 2013).

Given Perlecan has important structural functions as an ECM component in other developing tissues (Costell et al., 1999; Skeath et al., 2017), we examined if the protein played a similar role during synapse development or maintenance at *Drosophila* NMJs. Strikingly, $trol^{null}$ MNs developed progressive morphological defects over the course of larval development. Although NMJs developed normally in $trol^{null}$ larvae, they subsequently underwent retraction and displayed characteristic postsynaptic footprints where presynaptic material had been dismantled, similar to other *Drosophila* retraction mutants (Eaton et al., 2002; Massaro et al., 2009; Pielage et al., 2011, 2008, 2005). Although $trol^{null}$ MNs had normal synaptic output prior to retraction, MNs with disrupted NMJ structure lacked synaptic transmission. In addition, $trol^{null}$ MNs displayed an abnormal axonal cytoskeleton and underwent axonal breakage and loss. These phenotypes were independent of Perlecan's role in Wg diffusion and were not prevented by blocking Wallerian degeneration. Cell-type specific knockdown and rescue experiments indicated $trol^{null}$ phenotypes were non-cell autonomous and required Perlecan secretion from multiple cell types. Within the peripheral nervous system (PNS), Perlecan was enriched in the neural lamella, a thick ECM structure that surrounds nerve bundles, the ventral nerve cord (VNC) and brain lobes (Edwards et al., 1993; Stork et al., 2008). Mutations in *trol* disrupted the neural lamella surrounding peripheral nerves, similar to previously identified defects in the CNS neural lamella (Skeath et al., 2017). Consistent with disruption of the neural lamella triggering axonal instability, loss of entire axonal bundles and NMJs temporally coincided within individual larval hemisegments. Together, these data indicate Perlecan plays a key role within the ECM to regulate the integrity and stability of MN axons and synapses.

2.2 Results

2.2.1 Perlecan is a conserved HSPG that localizes to the neural lamella surrounding peripheral nerves in *Drosophila* larvae

Perlecan is an evolutionary conserved HSPG with a similar domain architecture in invertebrates, vertebrates, and the early multicellular eukaryote *Trichoplax adhaerens* (Warren et al., 2015). The *trol* locus on the X chromosome encodes *Drosophila* Perlecan, with 25 predicted splice variants ranging in size from 2853 to 4489 amino acids (**Figure 1A**). To compare the relationship of *Drosophila* Perlecan to other secreted HSPGs, a phylogenetic tree was constructed using homologs of Perlecan, Agrin and *Drosophila* Carrier of Wingless (Cow). One of the longest isoforms of *Drosophila* Perlecan (Trol-RAT) was used for the analysis. *Ciona intestinalis*, *Danio rerio*, *Mus musculus*, *Rattus norvegicus*, *Homo sapiens*, *Caenorhabditis elegans*, and *Trichoplax adhaerens* homologs were identified with NCBI blast searches. FASTA sequences of the longest isoform from each species was used in a Clustal Omega multiple sequence alignment and visualized in Jalview as an average distance phylogenetic tree using the BLOSUM62 algorithm (**Figure 1B**). The *Trichoplax* Perlecan and Agrin homologs were the most distantly related, but still clustered within their specific subfamily. *Drosophila* Perlecan clustered in a leaf with other Perlecan homologs and distinct from the Agrin family. Although Agrin plays a key role in cholinergic NMJ development (Gautam et al., 1996; Nitkin et al., 1987; Sanes and Lichtman, 2001), *Drosophila* contains glutamatergic NMJs and lacks an Agrin homolog. *Drosophila* Cow was more closely aligned with Agrin homologs than the Perlecan family.

As the closest homolog of Agrin, Perlecan might play similar roles in organizing *Drosophila* synaptic proteins. Indeed, a previous study identified Perlecan within NMJ synaptic clefts and observed defects in GluRIIA receptor clustering and Wg diffusion in *trol* mutants (Kamimura et al., 2013). We also identified Perlecan from *Drosophila* adult brain extracts in a proximity-based screen for proteins near the active zone (AZ) scaffold component Bruchpilot (Brp) (**Figure 1C**). Together, these data suggested Perlecan may regulate organization of *Drosophila* synapses, prompting us to further evaluate its function. To examine Perlecan localization within the larval PNS, an endogenous $trol^{GFP}$ insertion allele from the FlyTrap protein-tagging library was characterized (Morin et al., 2001). $Trol^{GFP}$ was enriched along nerve bundles and present at lower levels on the surface of body wall muscles (**Figure 1D**). The enrichment of Perlecan around nerve bundles is consistent with its localization within the neural lamella, a large

ECM compartment that surrounds axons and glia of the CNS and PNS. Indeed, Perlecan has been previously observed within the neural lamella surrounding the VNC and peripheral nerves (Brink et al., 2012; Skeath et al., 2017). In addition, the localization of Viking (Vkg), the *Drosophila* secreted type IV collagen homolog and a known component of the neural lamella (Yasothornsrikul et al., 1997), was disrupted in *trol* mutants (see below). Although immunogold electron microscopy (EM) identified Perlecan in the subsynaptic reticulum (SSR) surrounding NMJs (Kamimura et al., 2013), $Trol^{GFP}$ did not display synaptic enrichment beyond the homogenous expression over the entire muscle surface (**Figure 1D,E**). To confirm the $Trol^{GFP}$ signal was specific to Perlecan, an RNAi construct targeting *trol* (UAS-*trol*-RNAi.1, **Figure 1A**) was recombined with $Trol^{GFP}$ and driven with the ubiquitous *tubulin*-Gal4 driver. $Trol^{GFP}$ was eliminated by co-expression of the RNAi, with no signal observed along nerve bundles or on the muscle surface **(Figure 1E-I)**. The $Trol^{GFP}$ line also displayed normal NMJ growth and maintenance (**Figure 1-figure supplement 1**), in contrast to *trol* mutants (see below), indicating endogenous $Trol^{GFP}$ also produces a functional Perlecan protein.

2.2.2 *trol^{null}* NMJs undergo synaptic retraction

To examine a role for Perlecan in synaptic development and function, a previously generated null mutant that deletes the *trol* locus (**Figure 1A**) was characterized (Voigt et al., 2002). Male *trol^{null}* larvae are smaller than their heterozygous female *trol^{null}*/+ counterparts and display disrupted locomotion and lethality during the 3rd instar stage (Datta and Kankel, 1992; Voigt et al., 2002). To examine synaptic morphology in *trol^{null}* and heterozygous control 3rd instars, immunostaining was performed at muscle 4 NMJs for presynaptic Complexin (Cpx) and postsynaptic Discs-large (Dlg). In *trol^{null}*/+ controls, Cpx and Dlg colocalized at NMJ boutons (**Figure 2A**). Although some *trol^{null}*/y larvae had intact NMJs, many *trol* NMJs displayed Dlg+ boutons that lacked presynaptic Cpx (**Figure 2A**). The presence of postsynaptic "footprints" lacking presynaptic material is a defining feature of mutants that undergo synaptic retraction (Eaton et al., 2002; Graf et al., 2011; Koch et al., 2008; Pielage et al., 2008, 2005). *Trol^{null}* mutants also displayed fewer synaptic boutons (**Figure 2B**), in addition to increased synaptic footprints (**Figure 2C**), compared to control NMJs in abdominal segments A3-A5. Consistent with other retraction mutants (Graf et al., 2011), the *trol^{null}* phenotype was more severe in posterior abdominal segments (**Figure 2B,C**). NMJs showing severe synaptic retraction, defined by retraction

footprints and decreased number of synaptic boutons two standard deviations compared to controls, was only observed in *trol*^{null} larvae with increasing severity in posterior abdominal segments (**Figure 2D**). Together, these data indicate NMJs undergo synaptic retraction in larvae lacking Perlecan (**Figure 2E**).

To determine if synaptic retraction is specific to loss of Perlecan and not the *trol*^{null} genetic background, NMJs were examined in *trol*^{null} larvae in trans to a deficiency (*Df(1)ED411*) that removes the *trol* locus. *Df(1)ED411/+* heterozygous NMJs appeared normal and lacked postsynaptic footprints. In contrast, *Df(1)ED411/trol*^{null} NMJs had significantly reduced bouton number, with 50% of NMJs showing postsynaptic footprints (**Figure 2-figure supplement 1A-C**). In addition, expression of UAS-*trol*-RNAi.2 (**Figure 1A**) with the ubiquitous *tubulin*-Gal4 driver resulted in reduced bouton number, with >65% of NMJs showing postsynaptic footprints compared to RNAi or Gal4 only controls (**Figure 2-figure supplement 1D-F**).

The experiments described above examined synaptic retraction of type Ib glutamatergic MNs. However, larval muscles are also innervated by type Is glutamatergic and type II and III neuromodulatory MNs. The two glutamatergic MNs have distinct morphology and physiology, with tonic-like (Ib) or phasic-like (Is) properties (Aponte-Santiago and Littleton, 2020). To assay if Perlecan is required for stability of other MN subtypes, synaptic retraction was quantified at Is NMJs in *trol*^{null} larvae. Similar to Ib, *trol*^{null} Is NMJs displayed a significant reduction in bouton number, with >30% showing severe retraction phenotypes compared to heterozygous controls (*trol*^{null}/+, **Figure 2-figure supplement 2A-C).** In addition to glutamatergic MNs, type II and III neuromodulatory MNs displayed missing NMJs (data not shown). Together, these data indicate synaptic retraction occurs across all MN subtypes in 3rd instar larvae lacking Perlecan.

2.2.3 Synaptic retraction is independent of Perlecan's role in Wingless signaling

A previous study identified changes in pre- and postsynaptic Wg levels at *trol* mutant NMJs, suggesting Perlecan restricts Wg diffusion within the synaptic cleft. The absence of Perlecan resulted in enhanced presynaptic and reduced postsynaptic Wg signaling (Kamimura et al., 2013). Although synaptic retraction has not been previously associated with the Wg signaling pathway at *Drosophila* NMJs (Franco et al., 2004; Mathew et al., 2005; Mosca and Schwarz, 2010;

Packard et al., 2002; Restrepo et al., 2022), genetic interaction studies were conducted to assay whether increased presynaptic Wg output might contribute to synaptic retraction phenotypes observed in *trol*^{null} mutants. A UAS construct expressing a constitutively active (CA) form of the *Drosophila* GSK3 serine/threonine kinase Shaggy (Sgg, UAS-*sgg*^{S9A}), which dominantly blocks Wg signaling (Cook et al., 1996; Siegfried et al., 1992), was expressed in glutamatergic MNs of *trol*^{null} larvae using *vGlut*-Gal4. NMJ bouton number and synaptic retraction were quantified at muscles 6 and 7 in UAS-*sgg*^{S9A} controls, in *trol*^{null}, *vGlut*-Gal4, and in *trol*^{null} mutants expressing CA-Sgg (*trol*^{null}; *vGlut*-Gal4>*sgg*^{S9A}). Like muscle 4, muscle 6/7 NMJs showed reduced bouton number and postsynaptic footprints in >90% of *trol*^{null} larvae, indicating synaptic retraction is not restricted to MNs innervating muscle 4 (**Figure 3A-C**). Blocking presynaptic Wg signaling with CA-Sgg did not suppress the loss of boutons or prevent synaptic retraction in *trol*^{null} mutants (**Figure 3A-C**). These data indicate Perlecan's function in controlling synaptic stability is independent of its effects on Wg signaling.

2.2.4 *trol*^{null} NMJs develop normally and retract during the 3rd instar larval stage

Although postsynaptic footprints are a hallmark of synaptic retraction, it is possible that Perlecan loss disrupts early MN or synaptic development such that synapses classified as retracted never contained presynaptic material. To dynamically visualize NMJ development, serial intravital imaging of larval muscle 26 NMJs was performed over 4 days in *trol*^{null} and heterozygous controls following brief anesthesia as previously described (Akbergenova et al., 2018). Larvae containing endogenously tagged nSynaptobrevin (nSyb^{GFP}) (Guan et al., 2020) and a construct expressing GluRIIA^{RFP} (Schmid et al., 2008) were used to visualize presynaptic vesicles and postsynaptic receptors, respectively (**Figure 4A**). Although control and *trol*^{null} larvae had similar NMJ area at the 2nd instar stage when imaging began (**Figure 4B**), only control NMJs continued to grow on subsequent days of imaging (**Figure 4C**). In contrast, both pre- and postsynaptic area declined in *trol*^{null} larvae during the 3rd instar imaging window. Control NMJs had greater pre- than postsynaptic area, while *trol*^{null} larva had smaller nSyb^{GFP} than GluRIIA^{RFP} area by the final day of imaging, consistent with loss of presynaptic material and lingering postsynaptic footprints (**Figure 4C**). Several patterns of presynaptic loss were observed in *trol*^{null} NMJs during serial

imaging (**Figure 4A**). In some cases, an entire branch of an axon arbor was lost between imaging days. At other NMJs, presynaptic material was absent from internal boutons in an axon branch, with proximal and distal boutons from the same axon containing $nSyb^{GFP}$. These findings confirm that $trol^{null}$ MNs form NMJs that are subsequently retracted during development.

In vivo imaging indicated $trol^{null}$ NMJs are morphologically intact prior to retraction. However, loss of Perlecan could cause functional disruption of synaptic output earlier in development. To assay synaptic function at intact versus retracting NMJs in $trol^{null}$ 3rd instars, two-electrode voltage-clamp (TEVC) electrophysiology was performed at muscle 6. Following physiology, dissected $trol^{null}$ larvae were bathed with fluorescent anti-Hrp to visualize NMJs and determine if they were intact or retracted at the recording site (**Figure 4D**). At intact $trol^{null}$ NMJs, nerve stimulation resulted in evoked release amplitude similar to controls, indicating normal presynaptic output prior to retraction (**Figure 4E,F**). In contrast, fully retracted $trol^{null}$ NMJs completely lacked evoked or spontaneous release. When the average evoked responses from intact and retracted $trol^{null}$ NMJs were combined and compared to controls, a significant reduction in evoked excitatory junctional current (eEJC) was observed (**Figure 4F**). Together with intravital imaging, these data indicate loss of Perlecan does not have a major effect on early NMJ development and function, but impairs synaptic maintenance as development progresses. The gradual loss of NMJs is consistent with other cell types where Perlecan is dispensable for the initial formation of BMs and only required for their maintenance (Costell et al., 1999; Matsubayashi et al., 2017).

2.2.5 Non-cell autonomous Perlecan secretion is required for synaptic stability

The largest source of Perlecan in *Drosophila* larvae comes from the larval fat body, where it is secreted into the hemolymph and incorporated into the ECM surrounding most cell types (Pastor-Pareja and Xu, 2011). Although abundant in the fat body, *trol* mRNA is also present at lower levels in larval MNs and muscles (Jetti et al., 2023). To determine the cell type(s) responsible for Perlecan secretion that controls synaptic stability, UAS-*trol*-RNAi.2 was driven with a panel of cell-type specific Gal4 drivers. As indicated above, ubiquitous knockdown of *trol* mRNA with *tubulin*-Gal4 abolishes Perlecan expression (**Figure 1D-G**) and causes synaptic retraction (**Figure**

2–figure supplement 1). In contrast, knockdown of Perlecan with UAS-*trol*-RNAi.2 driven by multiple Gal4 lines expressed in specific cell populations, including pan-neuronal (*elav*^{C155}), neuronal and muscle (*elav*^{C155} and *mef2*-Gal4), glial (*repo*-Gal4), fat body (*ppl*-Gal4, *Lsp2*-Gal4), hemocytes (*Hml*-Gal4), and fat body and hemocytes (*c564*-Gal4), failed to trigger synaptic retraction or reduce synaptic bouton number (**Figure 5A,B**). In addition, knockdown of Perlecan in the three cell types that form or surround NMJs (MNs, muscles and glia) failed to reduce Trol^{GFP} signal around larval nerves or on the muscle surface (**Figure 5C-G**). Although it is possible that these individual drivers are weaker than *tubulin*-Gal4, no phenotypes were observed when *trol*-RNAi was driven by *elav*^{C155}, *elav*^{C155} and *mef2*, and *repo* at 29°C to increase Gal4 activity (data not shown). Together, these data suggest Perlecan secretion from multiple cell types is required to stabilize NMJs.

The majority of proteins that control synaptic stability at *Drosophila* NMJs function cell autonomously within the neuron (Eaton et al., 2002; Graf et al., 2011; Koch et al., 2008; Pielage et al., 2008, 2005). To determine whether MN secretion of Perlecan is sufficient to stabilize synapses, UAS-*trol* constructs encoding two different Perlecan isoforms (**Figure 1A**) were overexpressed with *vGlut*-Gal4 in the *trol*^{null} background. Overexpression of Perlecan specifically in MNs did not rescue the reduction in bouton number or synaptic retraction phenotypes in *trol*^{null} larvae (**Figure 5–figure supplement 1A-C**), suggesting neuronally secreted Perlecan is insufficient for maintaining synaptic stability. Together, these data indicate Perlecan acts non-cell autonomously from multiple cell types to stabilize larval NMJs.

2.2.6 NMJ loss in *trol* mutants is not exacerbated by mechanical stress from enhanced muscle contraction

Studies of Perlecan's role within the ECM of other *Drosophila* cell types and in several mammalian tissues indicate the protein helps withstand mechanical stress during tissue development (Arikawa-Hirasawa et al., 2002; Costell et al., 1999; Pastor-Pareja and Xu, 2011; Skeath et al., 2017; Töpfer et al., 2022). Although Perlecan is not enriched at synaptic boutons, *trol*^{null} NMJs could retract due to a failure to withstand mechanical stress from repeated contractions during larval crawling that would normally be buffered by the small amount of Perlecan normally on muscles. To test this model, a mutation in Myosin heavy chain (*Mhc*^{S1}) that

causes a dominant hypercontractive muscle phenotype (Montana and Littleton, 2006, 2004) was brought into the *trol*^{null} background to assay if synaptic retraction phenotypes were enhanced. Despite increased muscle contraction in *trol*^{null}*; Mhc*^{S1}/+ larvae, no enhancement of synaptic retraction or decreases in bouton number were observed (**Figure 6A,B**). Given hypercontraction in *Mhc*^{S1} mutants requires synaptic transmission (Montana and Littleton, 2004) and retracted *trol*^{null} NMJs lack evoked release (**Figure 4C-E**), we cannot exclude the possibility that *Mhc*^{S1} mutants only enhance early stages of synaptic retraction prior to loss of presynaptic output. To examine if muscle hypercontraction increases Perlecan NMJ abundance as a protective mechanism to withstand elevated muscle contraction force, endogenous Trol^{GFP} was brought into the *Mhc*^{S1} mutant background. No enhancement of Perlecan staining was observed around axons, at NMJs, or on muscles in Trol^{GFP}*; Mhc*^{S1}/+ larvae compared to Trol^{GFP} alone (**Figure 6C-E**). Together with the lack of Perlecan enrichment around boutons, the failure of muscle hypercontraction to increase instability of *trol*^{null} NMJs suggest the protein is unlikely to play a mechanical role within the extracellular space around boutons to directly stabilize NMJs.

2.2.7 The absence of Perlecan disrupts the neural lamella and triggers coordinated synaptic loss across abdominal hemisegments

Drosophila MN cell bodies reside within the VNC and their axons exit in segmental nerve bundles that also contain incoming sensory neuron axons. Nerve bundles are wrapped by several layers of glial cells and surrounded by the neural lamella (Edwards et al., 1993; Stork et al., 2008), a specialized ECM structure containing Perlecan. Although *trol*^{null} mutants display synaptic retraction phenotypes at larval NMJs, Perlecan is primarily expressed within the neural lamella surrounding larval nerves and not at NMJs (**Figure 1D-I**). As such, where Perlecan acts to regulate synaptic stability is unclear. If loss of Perlecan compromises the function of the neural lamella as a physical and protective barrier for encapsulated axons over time, NMJ retraction might occur for all axons within a nerve bundle in a temporally coordinated manner across larval hemisegments. To examine if synapses within each segmental nerve bundle showed evidence of coordinated loss, abdominal body wall hemisegments of *trol*^{null} larvae expressing *vGlut*-Gal4; UAS-*10xGFP* were examined. NMJ area on muscle 6/7, 4, and 1 was quantified for each hemisegment and compared to controls. Indeed, NMJs were often completely absent in one hemisegment, while fully intact in

others. *Trol*^{null} NMJs across each hemisegment displayed similar percentages of control NMJ area (**Figure 7A-C**), indicating entire hemisegments undergo coordinated synaptic loss while others remain intact.

To determine if the neural lamella surrounding peripheral nerves was disrupted in the absence of Perlecan, the expression and localization of the neural lamella-localized collagen IV homolog Vkg was assayed. In control segmental nerves, Vkg showed a similar localization to Perlecan and surrounded axon bundles exiting the VNC and at nerve branch points to muscles (**Figure 8A,B,E**). In contrast, Vkg expression in *trol*^{null} nerve bundles was dimmer with gaps in staining around axon segments, along with abnormal aggregation at specific sites along the nerve (**Figure 8A,B,E**). To quantify neural lamella disruption, fluorescence intensity of Vkg and anti-Hrp (to label all axons) was determined for segmental nerve bundles. Unlike controls, Vkg staining in axonal cross sections from *trol*^{null} larvae showed a thinner, or in some cases absent, neural lamella surrounding Hrp+ axon bundles (**Figure 8B**). Anti-Hrp staining was also brighter in *trol*^{null} axon bundles, suggesting there may be greater antibody penetration in the absence of a functional neural lamella (**Figure 8A,B**). The mean fluorescence of Vkg and Hrp signal was calculated in axon bundles traveling over muscle 4. Vkg signal around axons was significantly reduced in *trol*^{null} larvae, with the Vkg/Hrp ratio significantly lower in *trol*^{null} axons than controls (**Figure 8C,D**). This phenotype was independent of whether NMJs had undergone retraction, as nerves for both intact and retracted NMJs displayed a reduced neural lamella.

These data suggest disruption of the neural lamella is an upstream event preceding synaptic retraction in *trol*^{null} mutants. Compared to controls, Vkg staining was also non-evenly distributed along nerves, with multiple sites showing extracellular accumulation of Vkg beyond the traditional boundaries of the neural lamella (**Figure 8E**). In some of these protrusions, Hrp+ axon material also protruded from its normal boundaries to co-localize with Vkg. As such, Perlecan is likely to play a role in capturing or retaining Vkg within the neural lamella surrounding larval nerves.

2.2.8 Mutations in *trol* cause axonal damage independent of the Wallerian degeneration pathway

Prior studies indicated disruptions to the microtubule cytoskeleton often proceeded NMJ loss in other *Drosophila* synaptic retraction mutants (Eaton et al., 2002; Pielage et al., 2005). Given

loss of Perlecan compromises the neural lamella, we examined axonal morphology in *trol*^{null} mutants by visualizing the axonal and synaptic microtubule network by immunostaining for Futsch, the *Drosophila* homolog of microtubule associated protein 1B (MAP1B) (Hummel et al., 2000). Microtubule bundles in MN axons innervating muscle 4 were examined in larvae expressing *vGlut*-Gal4; UAS-*10xGFP* or UAS-*myrRFP*. Microtubules in heterozygous *trol*^{null}/+ control larvae formed filamentous tracks within axons that extended into synaptic boutons (**Figure 9A**). In contrast, *trol*^{null} axons contained fragmented and non-continuous microtubule tracks or lacked Futsch staining altogether at muscle branch points (**Figure 9A**). Quantification of Futsch staining intensity in *trol*^{null} axons revealed a significant reduction (**Figure 9B**). Similar defects were observed within synaptic terminals, where NMJs undergoing retraction lacked Futsch staining or displayed fragmented microtubules (**Figure 9A**). These data indicate disruptions to the microtubule cytoskeleton within *trol*^{null} axons and NMJs accompany synaptic retraction.

To determine if axons showed more severe defects in morphology, axon bundles and microtubules were imaged at different developmental timepoints. In mature 3rd instar control larvae, axon bundles have defined boundaries with smooth tracks of Futsch+ microtubules within them (**Figure 9C**). In contrast, *trol*^{null} axon bundles display progressive defects throughout larval development. 2nd instar *trol*^{null} larvae had relatively well-organized axon bundles, with some swellings, small RFP+ protrusions beyond the normal nerve boundary, and slightly twisted, disorganized Futsch+ microtubule tracts (**Figure 9C**). By early 3rd instar, bundles were disorganized but intact, with numerous protrusions and tangled microtubules (**Figure 9C**). At the mature 3rd instar stage, some axon bundles are entirely severed, with large highly tangled nets of disorganized Futsch at the ends of the severed nerve bundles (**Figure 9C**), similar to previously described retraction balls that form after axonal injury in mammals (Cajal, 1928). The time course of these deficits suggest that axonal damage and breakage occurs upstream of synapse loss, given that 2nd instar *trol*^{null} larvae have normal synaptic area but display altered axonal structure (**Figure 9D,E, Figure 3B**).

Loss of distal axons following damage is a well-known trigger for neurodegeneration in both invertebrates and vertebrates (Gerdts et al., 2016; Perlson et al., 2010). Neurite loss, synaptic retraction and eventual neuronal death following axonal damage often proceeds through a defined molecular cascade known as Wallerian degeneration (Coleman and Höke, 2020; Conforti et al., 2014; Llobet Rosell and Neukomm, 2019; Luo and O'Leary, 2005; Sambashivan and Freeman,

2021; Wang et al., 2012). Inhibiting this protein cascade promotes distal axon survival following injury in multiple systems (DiAntonio, 2019; Fang et al., 2012; Figley et al., 2021; Gerdts et al., 2015; Gilley et al., 2017, 2015; Llobet Rosell et al., 2022; Neukomm et al., 2017; Sasaki et al., 2016). To determine whether NMJ loss in $trol^{null}$ mutants utilizes the Wallerian degeneration signaling cascade, an established RNAi inhibitor of an upstream component of the cascade, dSarm (Gerdts et al., 2015, 2013; Osterloh et al., 2012), was expressed in $trol^{null}$ MNs. Inhibition of this pathway did not rescue distal axon maintenance, as $trol^{null}$ larvae expressing *dSarm* RNAi still had reduced synaptic bouton number, with >80% of NMJs displaying postsynaptic footprints associated with synaptic retraction (**Figure 9F-H**). These data indicate *Drosophila* MNs lacking Perlecan undergo axonal degeneration and synaptic retraction independent of the Wallerian degeneration pathway. Together, these data indicate loss of Perlecan disrupts the neural lamella, leading to axonal insults that cause cytoskeletal disruption and synaptic retraction that are temporally coordinated across individual hemisegment nerve bundles during larval development (**Figure 10**).

2.3 Discussion

In this study, we identified a role for the ECM protein Perlecan in regulating the structure and integrity of the neural lamella surrounding segmental nerve bundles in *Drosophila* larvae. Loss of Perlecan caused defects in neural lamella ECM function, with reduced thickness of the lamella based on staining for the type IV collagen Vkg. In addition, Vkg accumulated at aberrant sites along nerve bundles, with neuronal axons present outside of their normal boundary and within neural lamella protrusions. Although MNs formed functional NMJs in the absence of Perlecan, these synapses destabilized and rapidly retracted during later stages of larval development. Defects in axonal morphology and disruptions to the microtubule cytoskeleton were present before NMJs retracted, suggesting insults to axonal integrity and function were likely early events triggering synaptic retraction in *trol* mutants.

The normal development of *Drosophila* larval MNs and NMJs in *trol* mutants, followed by destabilization and subsequent breakdown, is consistent with a late role for Perlecan in ECM function and stability described in other systems (Hayes et al., 2022). In vertebrates, Perlecan loss causes degeneration of the developing heart only after pumping begins (Costell et al., 1999). The *C. elegans* Perlecan homolog Unc-52 regulates a late stage of muscle-epidermis attachment

(Rogalski et al., 2001, 1995) and can promote ectopic presynaptic growth after synapse formation when other ECM components are missing (Qin et al., 2014). Within developing *Drosophila* egg chambers, Perlecan and type IV Collagen function to establish mechanical properties of the ECM, protecting the egg from osmotic stress (Töpfer et al., 2022). In some contexts, Perlecan and type IV Collagen have opposing roles in regulating ECM rigidity (Pastor-Pareja and Xu, 2011; Skeath et al., 2017). Within the neural lamella surrounding the *Drosophila* VNC and brain, Perlecan acts to reduce ECM stiffness established by Vkg and β-Integrin (Skeath et al., 2017). EM imaging of the VNC neural lamella in *trol* mutants demonstrates a much thinner ECM (Skeath et al., 2017), consistent with reduced Vkg thickness around larval nerve bundles identified in this study. Studies in *Drosophila* embryos indicate Perlecan is a late delivered component of BMs and ECMs, requiring type IV Collagen for its incorporation into the matrix (Matsubayashi et al., 2017; Pastor-Pareja and Xu, 2011). Together, these data support a primary role for Perlecan as a regulator of tissue maturation and maintenance rather than in early development.

Perlecan can be produced in numerous cell types in *Drosophila,* with specific roles requiring secretion from neurons (Cho et al., 2012), muscles (Kamimura et al., 2013), glia (Skeath et al., 2017), hemocytes and fat body (Isabella and Horne-Badovinac, 2015; Pastor-Pareja and Xu, 2011; Ramos-Lewis et al., 2018), intestinal stem cells (You et al., 2014) and wing imaginal discs (Bonche et al., 2021). In contrast to these cases of a single cell type supplying the source of Perlecan, the neural lamella's role in regulating MN axonal and synaptic stability requires Perlecan to act in a non-cell autonomous role and be secreted from multiple cell types. RNAi knockdown of *trol* in neurons, muscles, glia, fat body, or hemocytes was not sufficient to induce synaptic retraction, in contrast to pan-cellular knockdown with *tubulin*-Gal4. In addition, expression of Perlecan specifically in neurons in *trol* mutants was not sufficient to rescue synaptic retraction phenotypes, in contrast to other characterized retraction mutants where the affected gene acts cell-autonomously (Eaton et al., 2002; Eaton and Davis, 2005; Graf et al., 2011; Koch et al., 2008; Massaro et al., 2009; Pielage et al., 2011, 2008, 2005). Our data suggest multiple cell types are required to secrete Perlecan for proper incorporation and function within the neural lamella, consistent with examples where multiple cell types are required to secrete Perlecan for its functional role (Bonche et al., 2022, 2021; You et al., 2014).

Following our initial observations of synaptic retraction in *trol* mutants, we hypothesized that mechanical stress caused by repeated muscle contraction during larval crawling might

destabilize synaptic boutons due to defects in synaptic cleft rigidity. Indeed, Perlecan can act to resist mechanical stress during tissue development in *Drosophila* and other species by providing malleability to the ECM and BM (Costell et al., 1999; Farach-Carson et al., 2014; Khalilgharibi and Mao, 2021; Pastor-Pareja and Xu, 2011; Qin et al., 2014; Ramos-Lewis et al., 2018; Skeath et al., 2017; Töpfer et al., 2022). However, increasing the mechanical stress of muscle contraction with a previously generated hyperactive *Mhc* mutant in the lab (Montana and Littleton, 2004) did not enhance synaptic retraction in *trol* mutants. We also found no role for local regulation of Wg diffusion with the synaptic cleft, as blocking presynaptic Wg output did not prevent retraction. The same genetic approach to block the presynaptic Wg pathway prevented formation of some satellite boutons observed early on in *trol* mutants secondary to Perlecan reducing Wg diffusion following synaptic secretion (Kamimura et al., 2013). As such, the low levels of Perlecan at the NMJ do not appear to be the site of action for how it normally prevents synaptic retraction.

Together with the lack of Perlecan enrichment at synaptic boutons, we focused on the neural lamella surrounding nerve bundles as a potential site of action in regulating synaptic stability. MN axons are under constant tension during larval crawling with fixed points of attachment at somas within the VNC and terminal anchors at the NMJ (Fan et al., 2019, 2017; Siechen et al., 2009; Tofangchi et al., 2016). Consistent with a primary defect downstream of axonal dysfunction, larval axons degenerated over development in *trol* mutants. Synaptic microtubules were absent in retracting NMJs, and fragmented microtubules with breaks at the site where axons enter the synaptic field were often observed, along with breakage of entire axon bundles upstream of the NMJ. Imaging of the Type IV collagen Vkg, an essential component of ECMs and the neural lamella, revealed reduced Vkg thickness and abnormal accumulation of the protein around nerve bundles in *trol* mutants. Axon retraction events were also temporally correlated in individual hemisegments, suggesting catastrophic breakdown of the neural lamella in single segmental nerves is likely the trigger for axon bundle breakage and loss of the entire nerve bundle.

In summary, our study uncovered a critical role for Perlecan in neural lamella integrity that prevents axonal degeneration and synaptic retraction in *Drosophila* MNs. Despite the involvement of axons in Perlecan-dependent synaptic retraction, inhibition of the Wallerian degeneration pathway did not prevent synapse loss in $trol^{null}$ mutants, suggesting loss of Perlecan causes axonal degeneration through a distinct pathway. Although the morphology of glia involved in wrapping

axons and forming the blood brain barrier was not characterized, it would not be surprising if they displayed morphological and functional defects due to disruption of the neural lamella that contributes to axonal injury. Both glia and the neural lamella can signal or interact directly with MNs (Bittern et al., 2021; Edwards et al., 1993; Hunter et al., 2020; Lee and Sun, 2015; Meyer et al., 2014; Stork et al., 2008; Weiss et al., 2022), providing multiple avenues by which loss of Perlecan could disrupt axon integrity. For example, interactions of Perlecan with components regulating the spectrin cytoskeleton could be a key factor. α- and β-Spectrin localize to MN axons and presynaptic RNAi against either protein results in synaptic retraction (Pielage et al., 2005). Integrins are known for their activity as ECM receptors in *Drosophila* (Bittern et al., 2021; Hunter et al., 2020) and could provide a direct link between Perlecan and the axonal spectrin cytoskeleton. Given hypomorphic Perlecan mutations cause Schwartz-Jampel syndrome in humans, a condition characterized by persistent muscle contraction and cartilage and bone abnormalities (Arikawa-Hirasawa et al., 2002; Farach-Carson et al., 2014; Nicole et al., 2000), and null alleles of Perlecan are incompatible with life (Arikawa-Hirasawa et al., 1999; Costell et al., 1999; Farach-Carson et al., 2014; Gubbiotti et al., 2017; Hayes et al., 2022), further characterization of the role of this critical ECM protein in axonal and synaptic maintenance will likely provide insights into its role in tissue integrity.

2.4 Materials and Methods

Drosophila stocks

Flies were maintained at 18-25°C and cultured on standard medium. 3rd instar larvae were used for all experiments unless otherwise noted. Larvae lacking Perlecan were collected at 1st or 2nd instar stage and separated from wild type counterparts and placed on petri dishes containing standard medium to facilitate survival to 3rd instar stage. Male and female larvae were used depending upon genetic background; see figure legends for genotypes. Canton-S (CS) was used as the wild type background in heterozygous controls except in the case of *Df(1)ED411*/+, where the wild type background was w^{1118} (BDSC# 3605). *trol* strains used include *trol^{null}* (Voigt et al., 2002; provided by Brian Stramer and Yutaka Matsubayashi), GFP-tagged *trol* (referred to in text as Trol^{GFP}, KDSC #110-836), *trol* deficiency (*Df(1)ED411*, BDSC #8031, 36516), *trol* overexpression constructs (UAS-*trol*.RD BDSC #65274, UAS-*trol*.RG BDSC #65273), and *trol* RNAis (UAS-*trol*-RNAi.1 VDRC #22642, UAS-*trol*-RNAi.2 VDRC #24549). Gal4 drivers used

were: *tubulin*-Gal4 (BDSC #5138), *vGlut*-Gal4 (provided by Aaron DiAntonio), *elav*^{C155}-Gal4 (BDSC #8765), *mef2*-Gal4 (BDSC #27390), *repo*-Gal4 (Lee and Jones, 2005), *ppl*-Gal4 (BDSC #58768), *Lsp*-Gal4 (BDSC #6357), *Hml*-Gal4 (BDSC #6395), *c564*-Gal4 (BDSC #6982). Overexpression of constitutively active Shaggy was performed using UAS-*sgg*^{S9A} (BDSC #5255). Presynaptic labeling for intravital imaging was performed using CRISPR-generated nSyb^{GFP} (Guan et al., 2020). PSD labeling for intravital imaging was performed using GluRIIA-RFP inserted onto chromosome III under the control of its endogenous promoter (provided by Stephan Sigrist). The hypercontractive *Mhc*^{S1} mutation (Montana and Littleton, 2004) was used to assess mechanical stress. UAS-*dSarm*-RNAi (VDRC #105369, provided by Aaron DiAntonio) was used to inhibit Wallerian degeneration in the *trol*^{null} background. UAS-*10xGFP* (Poukkula et al., 2011) and UAS-*myrRFP* (BDSC #7118) were used to visualize individual motoneuron axon anatomy. Viking^{GFP} (DGRC #110692, G00454 original FlyTrap identifier, provided by David Bilder) was used to visualize the neural lamella surrounding peripheral nerves.

APEX proximity labeling

Apex2 strains used were UAS-Brp^{short}.Apex2.Flag (referred to in text as Brp-tethered Apex, this study) and UAS-NES.Apex2.Flag (referred to in text as cytosolic Apex, this study). Adult brains expressing UAS-Brp^{short}.Apex2.Flag or UAS-NES.Apex2.Flag pan-neuronally were dissected, bathed in H_2O_2 and homogenized. Biotinylated proteins were purified with streptavidin beads and identified with tandem mass spectrometry.

Immunocytochemistry

3rd instar larvae were filleted in Ca^{2+}-free HL3.1 solution (in mM: 70 NaCl, 5 KCl, 4 $MgCl_2$, 10 $NaHCO_3$, 5 trehalose, 115 sucrose, 5 HEPES, pH 7.18) and fixed in 4% paraformaldehyde for 15 minutes, washed in Ca^{2+} -free HL3.1 twice and 0.1-PBT (1x PBS with 0.1% Triton X-100) once, then blocked in 5% normal goat serum (NGS) in 0.5-PBT (1x PBS with 0.5% Triton X-100) for 30 minutes at room temperature or overnight at 4°C. Samples were incubated overnight at 4°C in blocking solution containing primary antibodies, and then washed three times with 0.1-PBT. Samples were incubated for 2 hours at room temperature in blocking solution containing fluorophore-conjugated secondary antibodies. Primary antibodies used in this study were mouse anti-Brp at 1:500 (Nc82 DSHB, Iowa City, IA), rabbit anti-GluRIIC at 1:2000 (Jorquera et al.,

2012), rabbit anti-Cpx at 1:5000 (Huntwork and Littleton, 2007), mouse anti-Dlg at 1:500 (4F3 DSHB, Iowa City, IA), mouse anti-Futsch (22C10 DSHB, Iowa City, IA), and mouse anti-GFP at 1:1000 (#A-11120, Thermo Fisher Scientific, Waltham, MA). Secondary antibodies used in this study were goat anti-mouse Alexa Fluor 488-conjugated IgG at 1:500 (#A-32723, Thermo Fisher Scientific, Waltham, MA), goat anti-rabbit Alexa Fluor 568-conjugated IgG at 1:500 (#A-11011, Thermo Fisher Scientific, Waltham, MA), goat anti-mouse 555-conjugated IgG at 1:500 (#A-32727, Thermo Fisher Scientific, Waltham, MA) and goat anti-mouse 647-conjugated IgG at 1:500 (#A-32728, Thermo Fisher Scientific, Waltham, MA). For Hrp staining, samples were incubated in DyLight 649 or 488 conjugated Hrp at 1:500 (#123-605-021, #123-485-021; Jackson ImmunoResearch Laboratories, West Grove, PA, USA). For Phalloidin staining, samples were incubated in Texas Red-X Phalloidin at 1:500 (#T7471, Thermo Fisher Scientific, Waltham, MA). Samples were mounted in Vectashield Vibrance hard setting antifade mounting medium (#H-1700, Vector Laboratories, Burlingame, CA).

Confocal imaging and imaging data analysis

Images of fixed NMJs were acquired on a Zeiss Pascal confocal microscope (Carl Zeiss Microscopy, Zena, Germany) using a 63X Zeiss pan-APOCHROMAT oil-immersion objective with a 1.3 NA. 3D image stacks were merged into a maximum intensity projection using Zen (Zeiss) software. Abdominal segments and muscle numbers imaged are listed in figure legends or in results text. Boutons were counted manually using the parameters specified in each experiment (e.g. Dlg+ or Hrp/GluRIIC+). Severe retraction was calculated by taking the mean bouton number of control genotype(s) in an individual experiment and calculating the standard deviation. A bouton number of < mean – 2*SD and presence of postsynaptic footprints indicated severe retraction. Line profiles of fluorescence intensity across axons or boutons were generated in Volocity 3D Image Analysis software (PerkinElmer) using the "measure line profile" algorithm in Volocity 3.2 or 5 software. Lines were drawn between 4.17-4.22 μm for axon line profiles and 2.4-2.6 μm boutons were chosen and lines extended 2 μm in either direction for bouton line profiles. Mean Vkg and Hrp intensity were calculated from maximum intensity projections using Volocity 3D Image Analysis software with the "Find Objects" algorithm and a Vkg threshold that identified neural lamella area in both genotypes. Images of live NMJs and live and fixed axons were acquired on a Zeiss Axio Imager 2 with a spinning-disk confocal head (CSU-X1; Yokagawa)

and ImagEM X2 EM-CCD camera (Hamamatsu) using an Olympus LUMFL N 60X water-immersion objective with a 1.10 NA. Low magnification images of fixed larvae were acquired on a Zeiss LSM 800 confocal microscope using a 10x objective. A 3D image stack was acquired for each axon, NMJ, or larvae imaged. Futsch nets were counted manually. Mean fluorescence intensity of Futsch signal was calculated from the maximum intensity projection using Volocity 3D Image Analysis software. A 5μm^2 ROI at the point of individual axon exit from the nerve bundle (muscle branch point) was generated and Volocity calculated the mean intensity within this ROI.

Live intravital imaging and data analysis

Larvae were anesthetized with SUPRANE (desflurane, USP) from Amerinet Choice. Larvae were covered with a thin layer of halocarbon oil and incubated with a small paper towel containing Suprane for 1-2 minutes in a fume hood. Anesthetized larvae were arranged ventral side up on a glass slide between spacers made by tape. Larvae were covered with a fresh thin film of halocarbon oil and then with a cover glass. After each imaging session, larvae were placed in numbered chambers with food at room temperature. The same data acquisition settings were used to visualize NMJs at each session. Larvae were imaged every 24 hours. Area of pre- and postsynaptic material was calculated from maximum intensity projections using Volocity 3D Image Analysis software with the "Find Objects" algorithm and a pre- or postsynaptic threshold that identified presynaptic boutons or postsynaptic receptor fields in both genotypes. The same threshold was used to analyze images from each day of analysis.

Two-electrode voltage clamp electrophysiology and post-hoc imaging

Postsynaptic currents were recorded with a -80 mV holding potential. Experiments were performed in room temperature HL3.1 saline solution as previously described with final [Ca^{2+}] adjusted to 0.3 mM (Jorquera et al., 2012). Recordings were performed at muscle 6 of segments A3 and A4 in 3rd instar larvae. Motor axon bundles were cut and individual bundles were suctioned into a glass electrode for stimulation. Action potentials were stimulated at 0.33 Hz using a programmable stimulator (Master8, AMPI; Jerusalem, Israel). Data acquisition and analysis was performed using Axoscope 9.0 and Clampfit 9.0 software (Molecular Devices, Sunnyvale, CA, USA). Inward currents are labeled on a reverse axis. For post-hoc Hrp staining, samples were incubated for 5

minutes in DyLight 488 conjugated Hrp (2 µL of stock solution applied directly to filleted larvae and washed twice with HL3.1 before imaging) (#123-485-021; Jackson ImmunoResearch Laboratories, West Grove, PA, USA). Live imaging was performed as described above.

Bioinformatics

NCBI BLAST and NCBI Gene search were used to identify Perlecan homologs and to select the longest isoforms of Perlecan, Agrin, and Carrier of Wingless (Cow) in the genomes of *D. melanogaster*, *C. elegans*, *C. intestinalis*, *D. rerio*, *M. musculus*, *H. sapiens*, and *T. adhaerens*. Clustal Omega multiple sequence alignment (with default parameters) was used to align all of the sourced sequences (Madeira et al., 2022). Jalview was used to generate a phylogenetic tree using a BLOSUM62 matrix and average distance clustering. Sequences used for alignment and phylogenetic tree included:

Protein	**Species**	**Accession number (NCBI)**
Carrier of Wingless	*D. melanogaster*	NP_001262857.1
Agrin	*H. sapiens*	XP_005244806.1
	M. musculus	XP_006538554.1
	C. intestinalis	XP_026691460.1
	D. rerio	XP_021325505.1
	C. elegans	NP_001022152.3
	T. adhaerens	XP_002113830.1
Perlecan	*H. sapiens*	XP_011539620.1
	M. musculus	XP_030109089.1
	C. intestinalis	XP_018666843.1
	D. rerio	XP_021325650.1
	D. melanogaster	NP_001027034.2
	C. elegans	NP_001364664.1
	T. adhaerens	AKE31564.1

Statistical analysis

Graphing and statistical analysis were performed using GraphPad Prism (San Diego, CA, USA).

For comparisons between two groups, statistical significance was determined using a Student's t-test. For comparisons between three or more groups, statistical significance was determined using a one-way ANOVA followed by multiple comparisons with p-values corrected for multiple hypothesis testing using either Tukey, Šidák, or Dunnett's multiple comparisons tests (individual test chosen based on Prism recommendation). Figures depict the mean of each distribution and individual data points. *N* indicates the number of individual NMJs analyzed unless otherwise noted. Number of larvae per group, mean ± SEM, *n*, and the p values are indicated in figure legends. Asterisks in the figures denote p-values of: *, $p \leq 0.05$; **, $p \leq 0.01$; ***, $p \leq 0.001$; and ****, $p \leq 0.0001$.

Figures

Figure 1

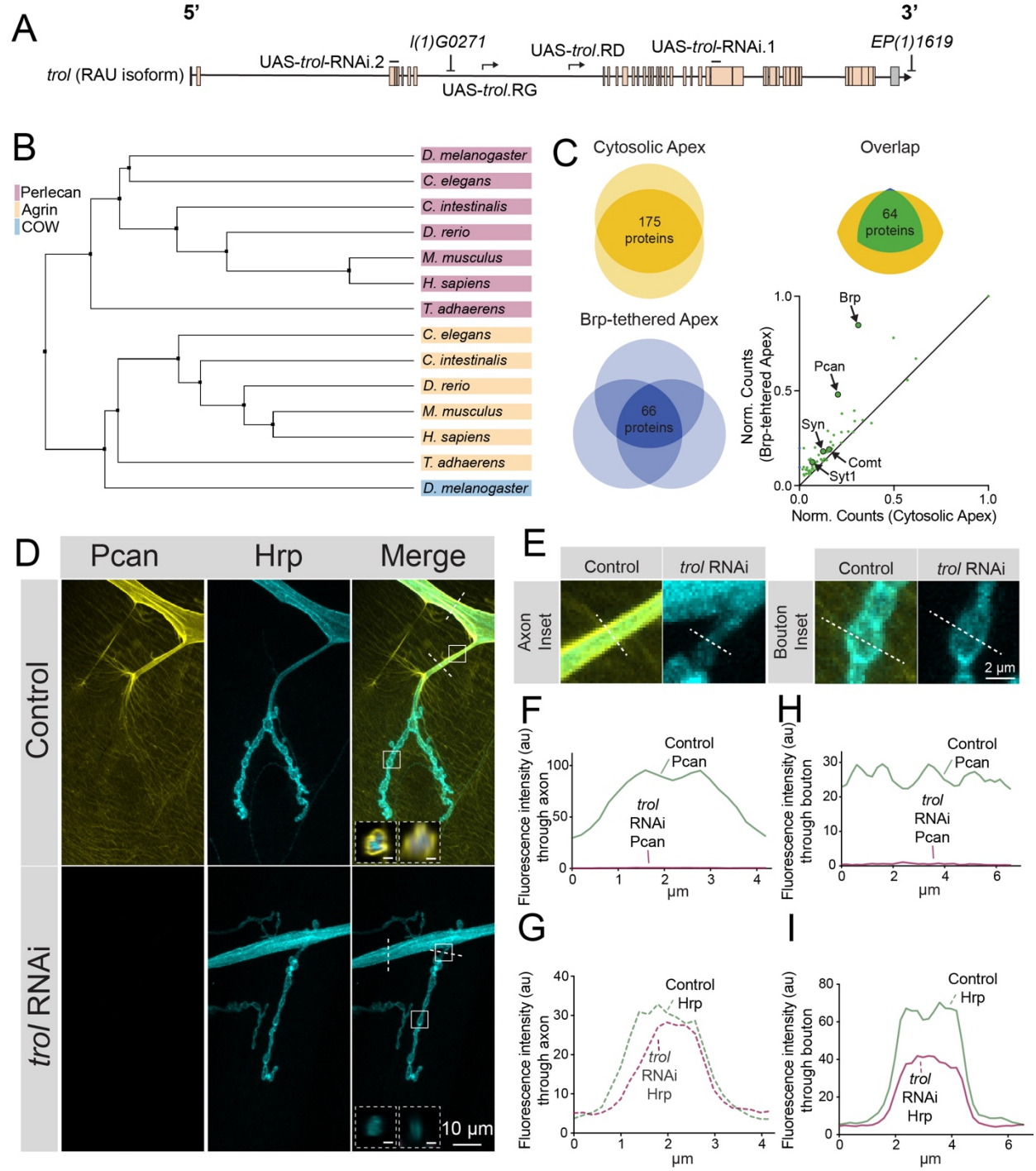
A
5'
3'
trol (RAU isoform)
UAS-trol-RNAi.2
l(1)G0271
UAS-trol.RG
UAS-trol.RD
UAS-trol-RNAi.1
EP(1)1619
B
Perlecan
Agrin
COW
D. melanogaster
C. elegans
C. intestinalis
D. rerio
M. musculus
H. sapiens
T. adhaerens
C
Cytosolic Apex
175 proteins
Overlap
64 proteins
Brp-tethered Apex
66 proteins
Brp
Pcan
Syn
Comt
Syt1
Norm. Counts (Brp-tehtered Apex)
Norm. Counts (Cytosolic Apex)
D
Pcan
Hrp
Merge
Control
trol RNAi
10 µm
E
Control
trol RNAi
Axon Inset
Bouton Inset
2 µm
F
Fluorescence intensity (au) through axon
Control
Pcan
trol RNAi Pcan
µm
H
Fluorescence intensity (au) through bouton
Control
Pcan
trol RNAi Pcan
µm
G
Fluorescence intensity (au) through axon
Control
Hrp
trol RNAi Hrp
µm
I
Fluorescence intensity (au) through bouton
Control
Hrp
trol RNAi Hrp
µm

Figure 1. Perlecan conservation and localization within the *Drosophila* PNS.

(**A**) Diagram of the *trol*-RAU isoform with exons (boxes) and introns (lines) indicated. Sequence locations targeted by two UAS-*trol* RNAi lines and start sites for two overexpression constructs (UAS-*trol*.RD and UAS-*trol*.RG) used in this study are noted. The location of P-elements *l(1)G0271* and *EP(1)1619* previously mobilized to generate the $trol^{null}$ deletion allele (Voigt et al., 2002) is also shown. (**B**) Phylogenetic tree of Perlecan, Agrin and Carrier of Wingless (Cow) from the indicated species generated using BLOSUM62 average distance. (**C**) Graphs of overlap in protein targets identified from two cytosolic Apex (tagged with a nuclear export signal (NES)) labeling experimental replicates (top left) and three synaptic Brp-Apex labeling experiments (bottom left), with overlapping targets identified by both shown on the right. To assess enrichment for targets labeled by Brp-Apex, normalized counts for proteins identified by both baits were plotted (bottom right). The bait protein Brp was the most enriched protein in Brp-Apex labeling experiments. Other enriched proteins included Perlecan (Pcan), Synapsin (Syn), NSF (Comt) and Synaptotagmin 1 (Syt1). (**D**) Representative images of muscle 4 NMJs stained for Perlecan (Pcan) and Hrp in control ($trol^{GFP}$, *UAS-trol-RNAi.1/+;+;+*) or Perlecan knockdown ($trol^{GFP}$, *UAS-trol-RNAi.1/+;+;tub-Gal4/+*) larvae. White boxes denote location of insets depicted in E. Dashed white lines denote location of insets depicted in lower left corner. Left inset displays orthogonal section through axon bundles, showing Perlecan signal in the neural lamella (scale bar 2 μm). Right inset displays orthogonal section through individual axon, showing Perlecan signal in the neural lamella (scale bar 1 μm). (**E**) Magnified view of control and *trol* RNAi axons and boutons, highlighting loss of Perlecan following RNAi knockdown. Dashed lines show representative sites for line scanning quantification for panels F-I. (**F-I**) Line scan profiles of Perlecan (**F,H**) or Hrp (**G,I**) mean fluorescent intensity through axons (**F,G**) or synaptic boutons (**H,I**) at muscle 4 in segment A2 (control: 14 axons from 8 larvae; *trol* RNAi: 19 axons from 11 larvae; control: 14 NMJs from 8 larvae; *trol* RNAi: 22 NMJs from 11 larvae). Control measurements are denoted in green and *trol* RNAi in magenta.

Figure 1 - figure supplement 1

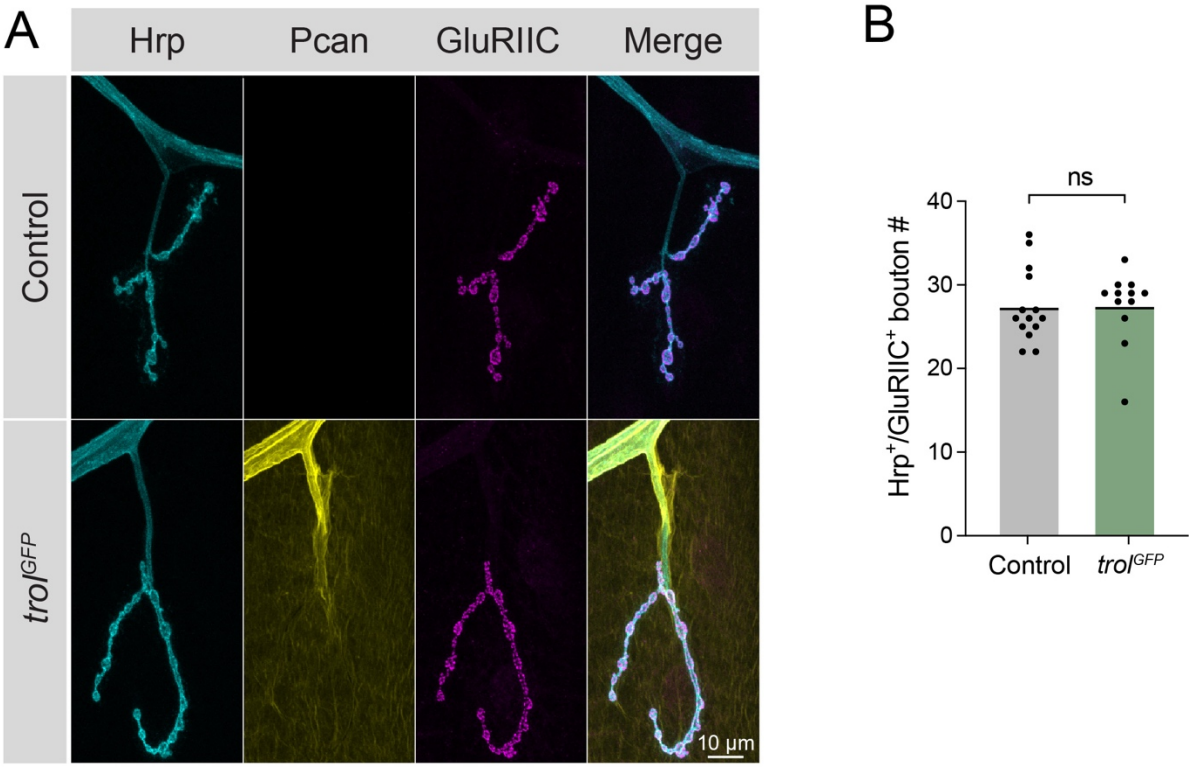

Figure 1–figure supplement 1. Endogenous Trol^{GFP} strain produces a functional Perlecan protein.

(**A**) Representative images of muscle 4 NMJs from segment A4 in control (CS) and Trol^{GFP} (*trol^{GFP}/y;+;+*) larvae stained for Hrp, Perlecan (Pcan) and the glutamate receptor subunit GluRIIC. Merged images are shown on the right. (**B**) Quantification of Hrp^{+}/GluRIIC^{+} Ib synaptic bouton number in control (27.4 ± 1.2, 14 NMJs from 7 larvae) and Trol^{GFP} (27.5 ± 1.3, 12 NMJs from 6 larvae, p=0.9654) larvae. Each point represents the number of boutons at one muscle 4 NMJ in segment A4. The mean is depicted by the solid black line.

Figure 2

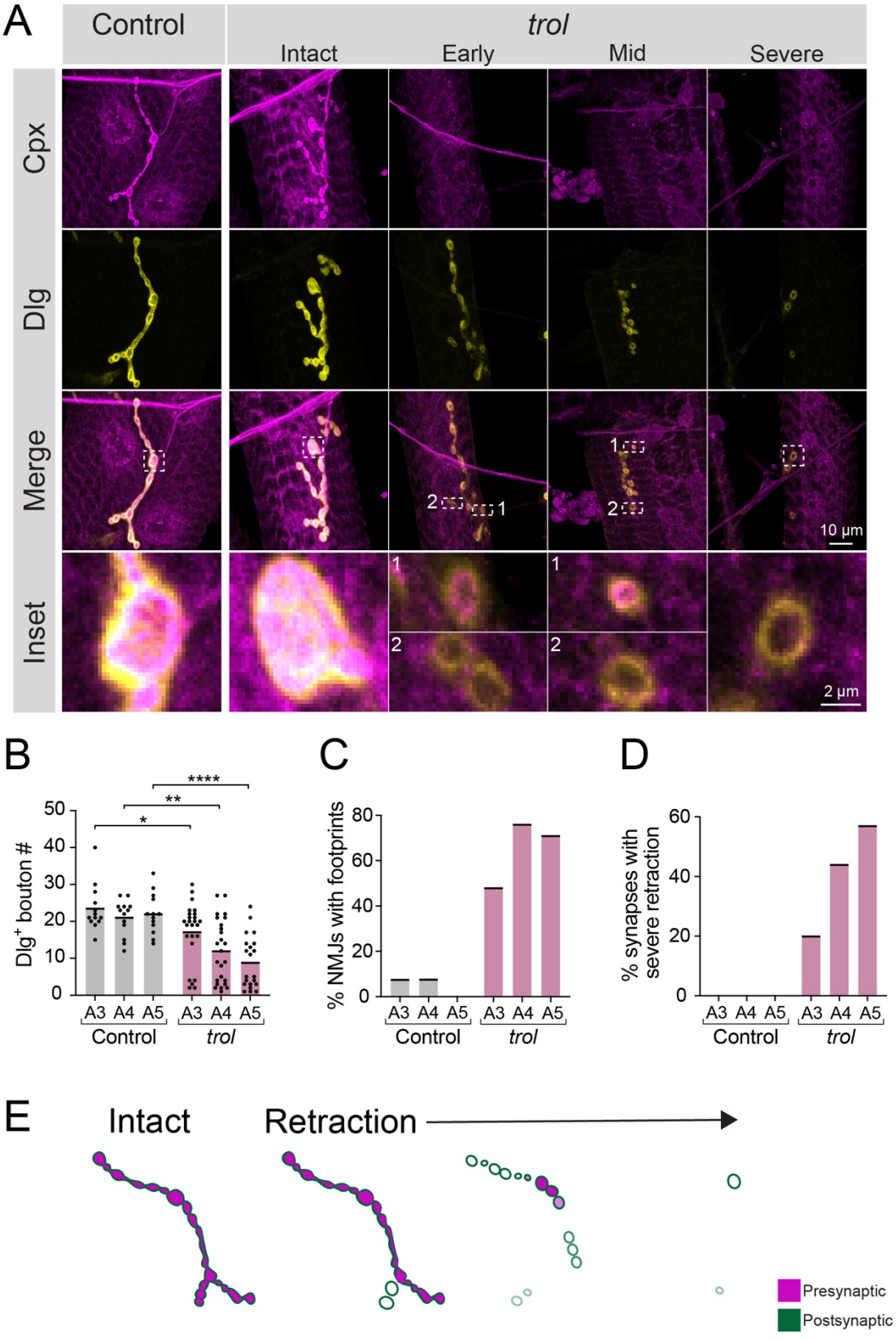
A
Control
trol
Intact
Early
Mid
Severe
Cpx
Dlg
Merge
Inset
10 µm
2 µm
B
Dlg+ bouton #
A3 A4 A5 A3 A4 A5
Control
trol
C
% NMJs with footprints
D
% synapses with severe retraction
E
Intact
Retraction
Presynaptic
Postsynaptic

Figure 2. Synaptic retraction in *trol*^{null} motoneurons.

(**A**) Representative images of muscle 4 NMJs in control (*trol*^{null}/+;+;+, left panel) and *trol*^{null} (*trol*^{null}/y;+;+) larvae stained for Cpx (magenta) and Dlg (yellow). Example *trol* NMJs of increasing retraction severity are shown in the right panels. Highlighted areas in the merged image are shown as insets at the bottom. For mild and moderately retracted NMJs, inset 1 displays a bouton with pre- and postsynaptic material still co-localized while inset 2 highlights a synaptic footprint with only postsynaptic material remaining. (**B**) Quantification of Dlg+ Ib bouton number from control and *trol* muscle 4 NMJs for abdominal segments A3-A5. Each point represents the number of boutons at one NMJ, with mean bouton number indicated with the solid black line. Quantification of bouton number: control A3: 23.5 ± 1.8, 13 NMJs from 7 larvae; *trol* A3: 17.2 ± 1.6, 25 NMJs from 13 larvae, $p<0.05$; control A4: 21.1 ± 1.3, 13 NMJs from 7 larvae; *trol* A4: 12.0 ± 1.7, 25 NMJs from 13 larvae, $p<0.01$; control A5: 22.1 ± 1.5, 13 NMJs from 7 larvae; *trol* A5: 8.9 ± 1.6, 21 NMJs from 13 larvae, $p<0.0001$. (**C**) Percentage of control or *trol* NMJs with one or more postsynaptic footprints (Dlg bouton lacking Cpx) for segments A3-A5 from the dataset in B. (**D**) Percentage of control or *trol* NMJs with severe retraction for segments A3-A5 from the dataset in B. (**E**) Representation of synaptic retraction phenotypes observed at *trol* NMJs. The appearance of initial synaptic footprints (2nd NMJ) still leaves connected boutons remaining within the synaptic area. As retraction proceeds (3rd NMJ), many boutons lack presynaptic material completely or have only residual presynaptic staining. Severely retracted synapses (4th NMJ) have only a few or no boutons.

Figure 2 - figure supplement 1

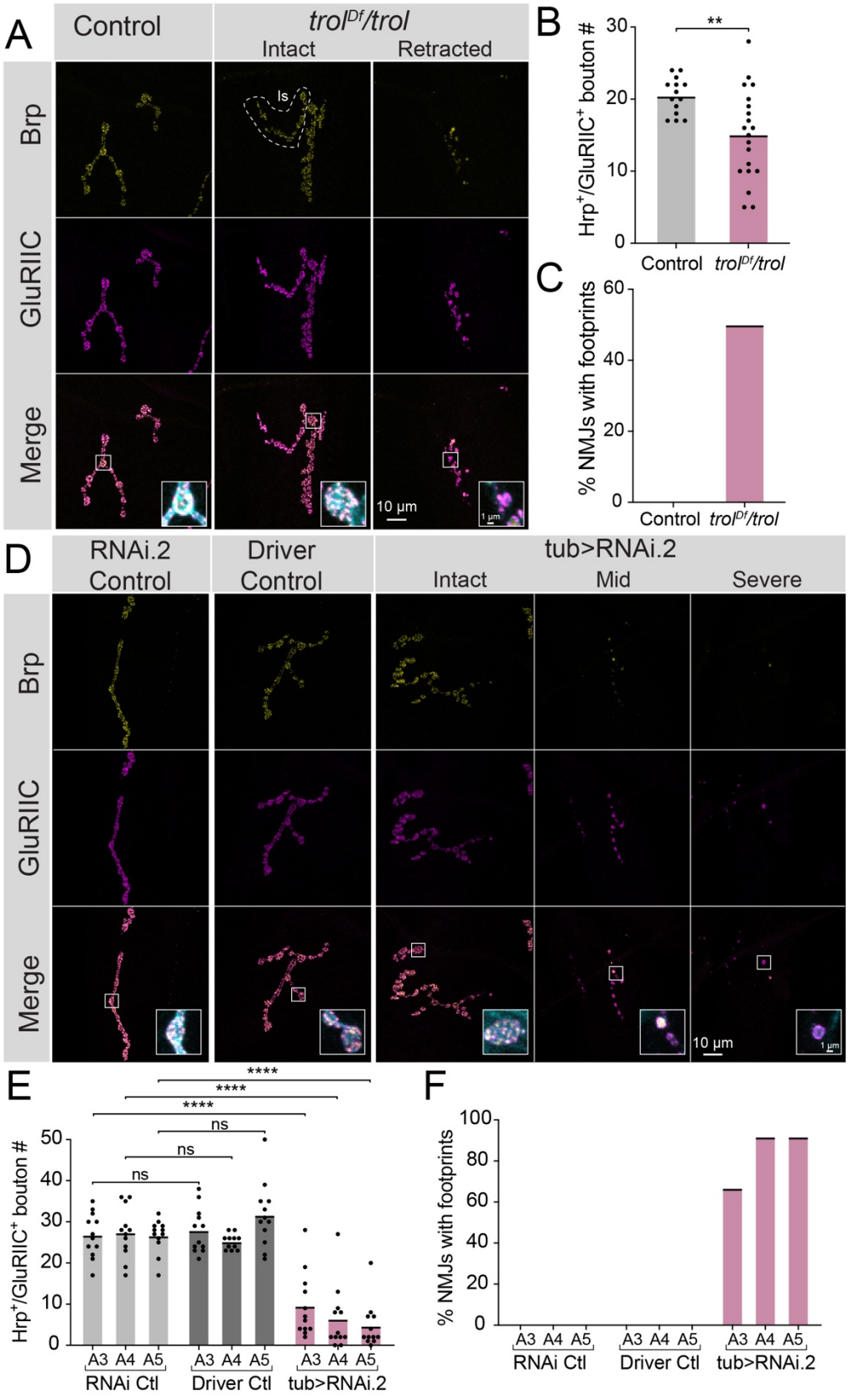

Figure 2–figure supplement 1. Synapse retraction occurs in *trol*^{null} mutants over deficiency and in *trol* RNAi knockdown larvae.

(**A**) Representative images of muscle 4 NMJs in *Df(1)ED411/+* controls and *Df(1)ED411/trol*^{null} larvae stained for the presynaptic AZ protein Brp (yellow), glutamate receptor GluRIIC (magenta) and anti-Hrp (cyan, only shown in inset). The merged image is shown below with location of insets boxed. Insets show a control bouton and an intact and retracting bouton from *trol*^{Df}*/trol*^{null} NMJs. (**B**) Quantification of Hrp+/GluRIIC+ Ib bouton number from control and *trol*^{Df}*/trol*^{null} muscle 4 NMJs in segments A3 and A4. Each point represents the number of boutons at one NMJ, with mean bouton number indicated with the solid black line. Quantification of bouton number: control: 20.4 ± 0.7, 14 NMJs from 4 larvae; *trol*^{Df}*/trol*^{null}: 15.1 ± 1.4, 20 NMJs from 5 larvae, $p<0.005$. (**C**) Percentage of control or *trol*^{Df}*/trol*^{null} NMJs with one or more postsynaptic footprints from the dataset in B. (**D**) Representative images of muscle NMJs in RNAi (*+;UAS-trol-RNAi.2/+;+*) and Gal4 driver (*+;+;tubulin-Gal4/+*) controls and *trol* knockdown (*+;UAS-trol-RNAi.2/+;tubulin-Gal4/+*) larvae stained stained for Brp (yellow), GluRIIC (magenta) and anti-Hrp (cyan, only shown in inset). The merged image is shown below with location of the insets boxed. Insets show control or intact, moderate or severe retraction boutons in *trol* RNAi knockdown larvae. (**E**) Quantification of Hrp+/GluRIIC+ Ib bouton number from controls and *trol* RNAi knockdown muscle 4 NMJs in segments A3-A5. Each point represents the number of boutons at one NMJ, with mean bouton number indicated with the solid black line. Quantification of bouton number: RNAi control A3: 26.8 ± 1.6, 12 NMJs from 6 larvae; Gal4 driver control A3: 27.9 ± 1.6, 12 NMJs from 6 larvae; *tub*>RNAi A3: 9.5 ± 2.3, 12 NMJs from 6 larvae, RNAi versus driver controls $p=0.99$, RNAi control and *tub*>RNAi $p<0.0001$; RNAi control A4: 27.3 ± 1.8, 12 NMJs from 6 larvae; Gal4 control A4: 25.2 ± 0.6, 11 NMJs from 6 larvae; *tub*>RNAi A4: 6.3 ± 2.2, 12 NMJs from 6 larvae, RNAi versus driver controls $p=0.95$, RNAi control and *tub*>RNAi $p<0.0001$; RNAi control A5: 26.6 ± 1.2, 12 NMJs from 6 larvae; Gal4 control A5: 31.6 ± 2.3, 12 NMJs from 6 larvae; *tub*>RNAi A5: 4.7 ± 1.6, 12 NMJs from 6 larvae, RNAi versus driver controls $p=0.25$, RNAi control and *tub*>RNAi $p<0.0001$. (**F**) Percentage of control or *trol* RNAi knockdown NMJs with one or more postsynaptic footprints for segments A3-A5 from the dataset in E.

Figure 2 - figure supplement 2

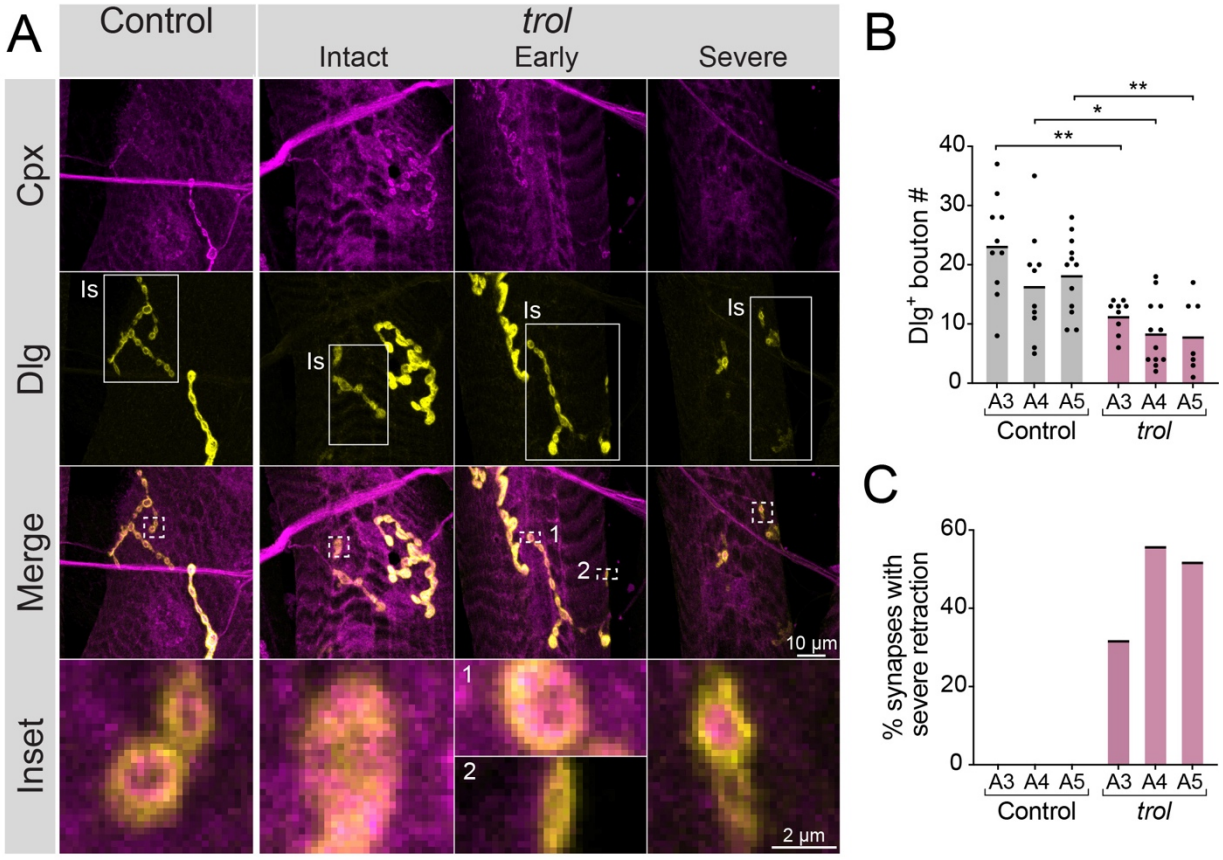

Figure 2–figure supplement 2. *trol*^{null} Is synapses retract.

(**A**) Representative images of Is muscle 4 NMJs in control (*trol*^{null}*/+;+;+*) and *trol*^{null} (*trol*^{null}*/y;+;+*) larvae stained for Cpx (magenta) and Dlg (yellow). Example *trol* NMJs that are intact or in the early or severe stages of retraction are shown in the right panels. White boxes in the 2nd row of images highlight Is innervation, with the remaining Dlg staining coming from the co-innervating Ib MN. Highlighted areas in the merged image are shown as insets in the bottom panel. For the NMJ in early stages of retraction, inset 1 displays a bouton containing both pre- and postsynaptic material, while inset 2 highlights a synaptic footprint with only postsynaptic material remaining. For the severely retracted NMJ, inset displays a bouton with pre- and postsynaptic material remaining (top) and one with only postsynaptic material (bottom). (**B**) Quantification of Dlg+ Is bouton number from control and *trol*^{null} muscle 4 NMJs for segments A3-A5. Each point represents the number of boutons at one NMJ, with mean bouton number indicated with the solid black line. Quantification of bouton number: control A3: 23.3 ± 2.7, 10 NMJs from 7 larvae; *trol* A3: 11.4 ± 1.0, 6 NMJs from 13 larvae, $p<0.001$; control A4: 16.5 ± 2.9, 10 NMJs from 7 larvae; *trol* A4: 8.5 ± 1.6, 12 NMJs from 13 larvae, $p<0.03$; control A5: 18.3 ± 1.9, 12 NMJs from 7 larvae; *trol* A5: 8.0 ± 2.3, 7 NMJs from 13 larvae, $p<0.01$. (**C**) Percentage of control or *trol*^{null} Is NMJs with severe retraction for segments A3-A5 from the dataset in B.

Figure 3

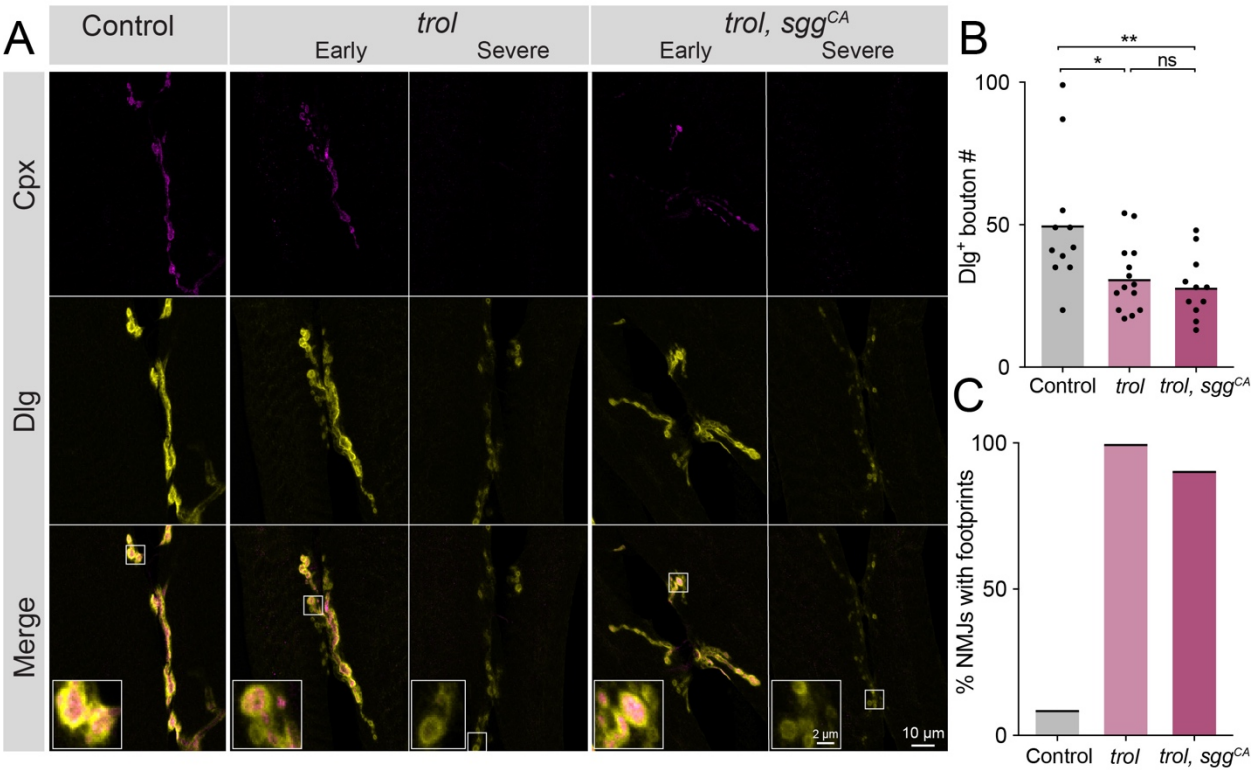
A
Control
trol
Early
Severe
trol, sggCA
Early
Severe
Cpx
Dlg
Merge
2 µm
10 µm
B
**
*
ns
100
50
0
Dlg+ bouton #
Control
trol
trol, sggCA
C
100
50
0
% NMJs with footprints
Control
trol
trol, sggCA

Figure 3. Synaptic retraction in *trol* mutants is not prevented by blocking presynaptic Wg signaling.

(**A**) Representative images of muscle 6/7 NMJs at segment A4 in control (*+;UAS-sgg^{S9A}/+;+,* left panel), *trol^{null}* (*trol^{null},vGlut-Gal4/y;+;+*, middle panels) and *trol^{null}, sgg^{CA}* (*trol^{null},vGlut-Gal4/y;UAS-sgg^{S9A}/+;+*, right panels) larvae stained for Cpx (magenta) and Dlg (yellow). Example NMJs that are in early or severe stages of retraction are shown for both *trol* genotypes. Highlighted areas in the merge are shown as insets in the bottom panel with either intact (early) or retracting (severe) boutons. (**B**) Quantification of Dlg+ Ib and Is bouton number from control, *trol^{null}* and *trol^{null}, sgg^{CA}* muscle 6/7 NMJs for abdominal segment A4. Each point represents the number of boutons at one NMJ, with mean bouton number indicated with the solid black line. Quantification of bouton number: control: 50.1 ± 7.0, 11 NMJs from 6 larvae; *trol*: 31.3 ± 3.2, 14 NMJs from 7 larvae, $p<0.05$ compared to control; *trol, sgg^{CA}*: 28.2 ± 3.4, 11 NMJs from 6 larvae; $p<0.01$ compared to control, $p=0.8814$ compared to *trol*. (**C**) Percentage of control, *trol,* or *trol, sgg^{CA}* NMJs with one or more postsynaptic footprints for the dataset in B.

Figure 4

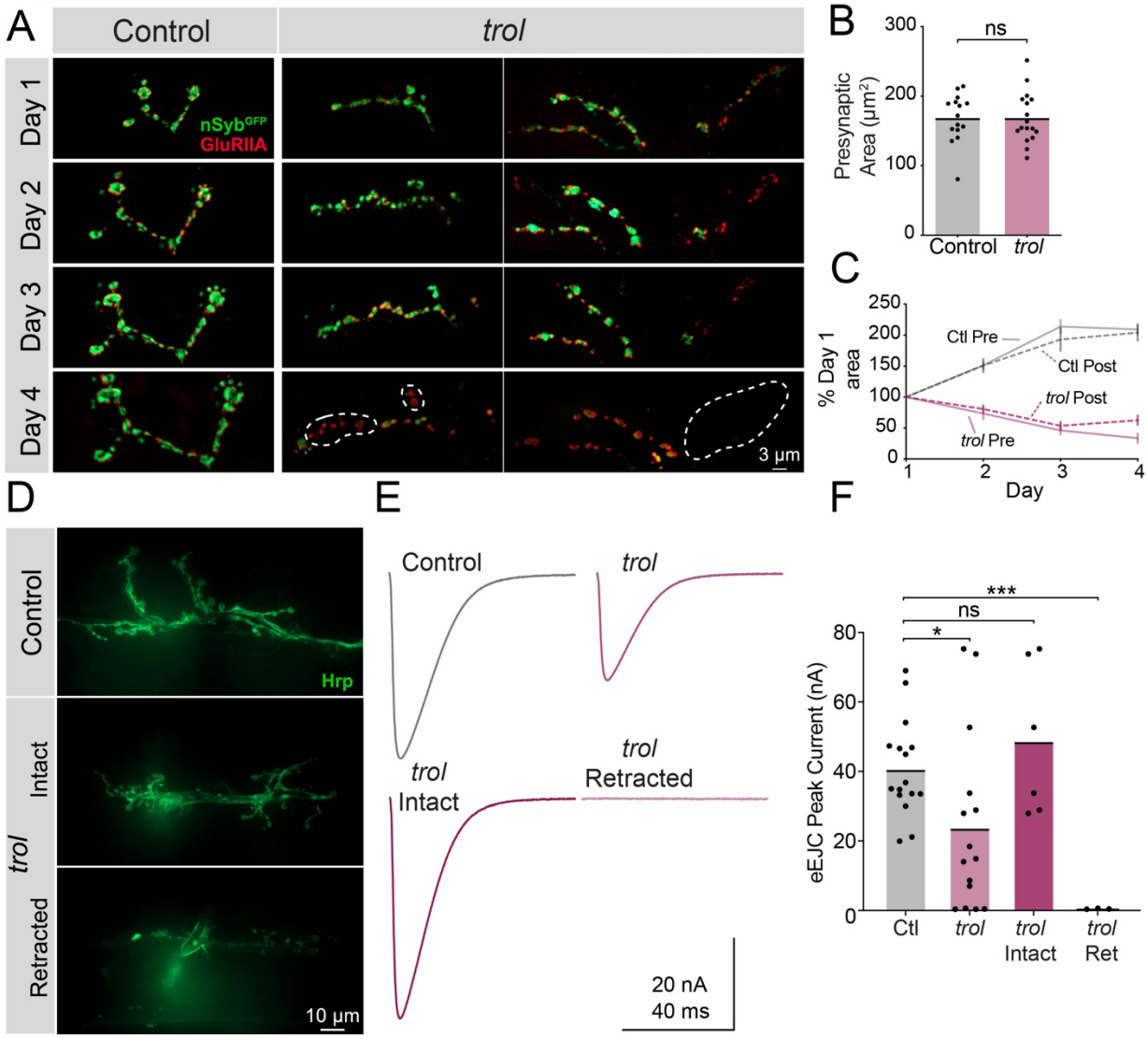
A
Control
trol
Day 1
Day 2
Day 3
Day 4
nSyb^GFP
GluRIIA
3 µm
B
ns
Presynaptic Area (µm²)
300
200
100
0
Control
trol
C
% Day 1 area
250
200
150
100
50
0
Ctl Pre
Ctl Post
trol Post
trol Pre
1
2
3
4
Day
D
Control
trol
Intact
Retracted
Hrp
10 µm
E
Control
trol
trol Intact
trol Retracted
20 nA
40 ms
F
***
ns
*
eEJC Peak Current (nA)
80
60
40
20
0
Ctl
trol
trol Intact
trol Ret

Figure 4. *Trol* mutant NMJs form normally but are not maintained over development.

(**A**) Representative NMJ images during serial intravital imaging of muscle 26 in control (*trol*^{null}*/+;+;nSyb*^{GFP}*/GluRIIA*^{RFP}, left) and *trol*^{null} (*trol*^{null}*/y;+;nSyb*^{GFP}*/GluRIIA*^{RFP}, right) larvae over 4 days starting at the 2nd instar stage. nSyb^{GFP} is shown in green and GluRIIA^{RFP} in red. Dashed lines highlight areas where presynaptic nSyb is missing while postsynaptic GluRIIA remains (retraction footprints). Severe NMJ retraction is seen in both example *trol*^{null} NMJs by day 4, while control NMJs continue to grow. (**B**) Quantification of muscle 26 presynaptic NMJ area in control and *trol*^{null} 2nd instar larvae at the beginning of serial intravital imaging sessions. No differences in NMJ area are present during this stage of early development. Quantification of NMJ area: control: 168.5 ± 8.974, 15 NMJs from 4 larvae; *trol*: 168.5 ± 8.855, 17 NMJs from 4 larvae, p=0.9991. NMJs from multiple abdominal segments were imaged. (**C**) Percent change in NMJ area during each day of imaging for control and *trol*^{null} larvae. Both presynaptic and postsynaptic area continue to increase in controls, while synaptic area is lost in *trol*^{null} larvae. (**D**) Representative images of muscle 6/7 NMJs stained with anti-Hrp following TEVC physiology in control (*trol*^{null}*/+;+;+*) and *trol*^{null} (*trol*^{null}*/y;+;+*) 3rd instar larvae. Examples of intact (middle) and retracted (bottom) NMJs are shown. (**E**) Average eEJC traces in 0.3 mM Ca^{2+} saline in control and all *trol*^{null} NMJs combined (top), together with average traces from NMJs of only intact or retracted *trol*^{null} NMJs (bottom). (**F**) Quantification of average eEJC peak amplitude (nA) per NMJ in segments A3 and A4 for the indicated genotypes. Intact and retracted *trol* NMJs were determined post-hoc blinded following anti-Hrp staining and paired with their corresponding eEJC data. Quantification of EJC amplitude: control: 40.8 ± 3.5 nA, 16 NMJs from 7 larvae; *trol* combined: 23.8 ± 6.6, 15 NMJs from 6 larvae, p<0.05 compared to control; *trol* intact: 48.8 ± 8.9 nA, 6 NMJs from 4 larvae, p=0.3189 compared to control; *trol* retracted: 0.5 ± 0.1, 3 NMJs from 2 larvae, p<0.0001 compared to control.

Figure 5

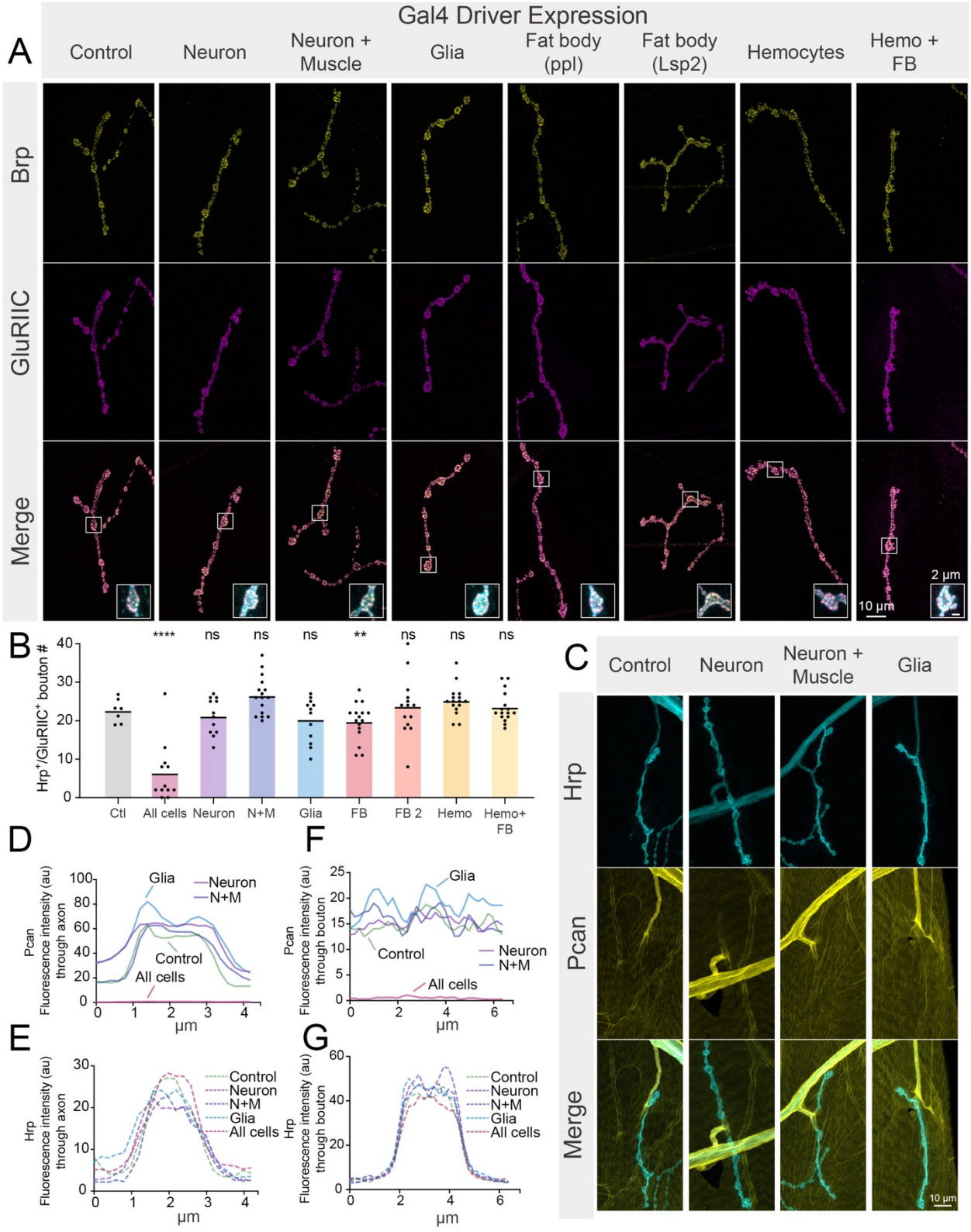
A
Gal4 Driver Expression
Control
Neuron
Neuron + Muscle
Glia
Fat body (ppl)
Fat body (Lsp2)
Hemocytes
Hemo + FB
Brp
GluRIIC
Merge
2 µm
10 µm
B
Hrp+/GluRIIC+ bouton #
****
ns
ns
ns
**
ns
ns
ns
Ctl
All cells
Neuron
N+M
Glia
FB
FB 2
Hemo
Hemo+ FB
C
Control
Neuron
Neuron + Muscle
Glia
Hrp
Pcan
Merge
10 µm
D
Pcan Fluorescence intensity (au) through axon
Glia
Neuron
N+M
Control
All cells
µm
E
Hrp Fluorescence intensity (au) through axon
Control
Neuron
N+M
Glia
All cells
µm
F
Pcan Fluorescence intensity (au) through bouton
Glia
Control
Neuron
N+M
All cells
µm
G
Hrp Fluorescence intensity (au) through bouton
Control
Neuron
N+M
Glia
All cells
µm

Figure 5. Perlecan acts in non-cell autonomous fashion to control synaptic maintenance.
(**A**) Representative images of larval muscle 4 NMJs at segment A4 stained for Brp (yellow), GluRIIC (magenta) and anti-Hrp (cyan, only shown in inset) in control (*+;UAS-trol-RNAi.2/+;+*) and *trol* RNAi knockdown in the indicated cell types (UAS-*trol*-RNAi.2 (one copy) driven by $elav^{C155}$, $elav^{C155}$ and *mef2*-Gal4, *repo*-Gal4, *ppl*-Gal4, *Lsp2*-Gal4, *Hml*-Gal4, and *c564*-Gal4 (one copy)). The merged image is shown below with location of the insets highlighting single boutons. (**B**) Quantification of Hrp+/GluRIIC+ positive Ib bouton number at muscle 4 NMJs in segment A4 in controls and following cell-type specific *trol* RNAi knockdown. Each knockdown was analyzed in separate experiments with both UAS only and Gal4 only controls. Significance was calculated for each experimental comparison, but a single control that represents the average bouton number of every experiment is plotted for ease of visualization. Quantification of *trol* knockdown with *tubulin*-Gal4 at A4 (from **Figure 2–figure supplement 1**) is included for comparison. Unlike pan-cellular RNAi, cell-type specific RNAi does not induce synaptic retraction. Quantification of bouton number: neuron UAS only control: 23.25 ± 1.399, 12 NMJs from 6 larvae; neuron Gal4 only control: 23.75 ± 1.226, 12 NMJs from 6 larvae; $elav^{C155}$>UAS-*trol*-RNAi.2: 21.17 ± 1.359, 12 NMJs from 6 larvae; p=0.4424 compared to UAS control; p=0.2994 compared to Gal4 control; neuron and muscle UAS only control: 21.21 ± 1.130, 14 NMJs from 7 larvae; neuron and muscle Gal4 only control: 23.43 ± 1.189, 14 NMJs from 7 larvae; $elav^{C155}$, *mef2*>UAS-*trol*-RNAi.2: 26.44 ± 1.248, 16 NMJs from 8 larvae; p=0.0066 (<0.01) compared to UAS control; p=0.1437 compared to Gal4 control; glia UAS only control: 26.83 ± 1.375, 12 NMJs from 6 larvae; glia Gal4 only control: 23.79 ± 1.407, 14 NMJs from 7 larvae; *repo*>UAS-*trol*-RNAi.2: 20.25 ± 1.643, 12 NMJs from 6 larvae; p=0.0078 (<0.01) compared to UAS control; p=0.1666 compared to Gal4 control; fat body (*ppl*) UAS only control: 25.57 ± 1.312, 14 NMJs from 7 larvae; fat body (*ppl*) Gal4 only control: 26.21 ± 0.7644, 14 NMJs from 7 larvae; *ppl*>UAS-*trol*-RNAi.2: 19.75 ± 1.216, 16 NMJs from 8 larvae; p<0.01 compared to UAS and Gal4 controls (0.0014 compared to UAS; 0.0004 compared to Gal4); fat body 2 (*Lsp2*) UAS only control: 19.08 ± 1.412, 13 NMJs from 7 larvae; fat body 2 (*Lsp2*) Gal4 only control: 25.07 ± 0.7593, 14 NMJs from 7 larvae; *Lsp2*>UAS-*trol*-RNAi.2: 23.64 ± 2.053, 14 NMJs from 7 larvae; p=0.0731 compared to UAS control; p=0.7249 compared to Gal4 control; hemocyte UAS only control: 18.93 ± 0.8285, 14 NMJs from 7 larvae; hemocyte Gal4 only control: 26 ± 1.441, 14 NMJs from 7 larvae; *Hml*>UAS-*trol*-RNAi.2: 25.19 ± 0.9841, 16 NMJs from 8 larvae; p=0.0005 (<0.001) compared to UAS control; p=0.8242

compared to Gal4 control; hemocyte and fat body UAS only control: 23.14 ± 1.181, 14 NMJs from 7 larvae; hemocyte and fat body Gal4 only control: 24.25 ± 0.8972, 12 NMJs from 6 larvae; *c564*>UAS-*trol*-RNAi.2: 23.44 ± 0.9999, 16 NMJs from 8 larvae; p=0.9705 compared to UAS control; p=0.8149 compared to Gal4 control. (**C**) Representative images of muscle 4 NMJs stained for Perlecan and Hrp in control (Trol^{GFP},UAS-*trol*-RNAi.1) or *trol* RNAi knockdown by *elav*^{C155}, *elav*^{C155} and *mef2*-Gal4, or *repo*-Gal4 (one copy of UAS and Gal4 constructs). (**D-G**) Line scanning profiles of Perlecan (**D,F**) or Hrp (**E,G**) mean fluorescent intensity through axons (**D,E**) or synaptic boutons (**F,G**) at muscle 4 in segment A4. Measurements are color-coded as indicated: control (green), *trol* RNAi in neurons (magenta), neurons and muscles (blue), or glia (light blue). No reduction in Perlecan around nerves or on the muscle surface surrounding boutons was observed compared with *tubulin*-Gal4 knockdown (**Figure 1F-I**, replicated here ("All cells") for comparison).

Figure 5 - figure supplement 1

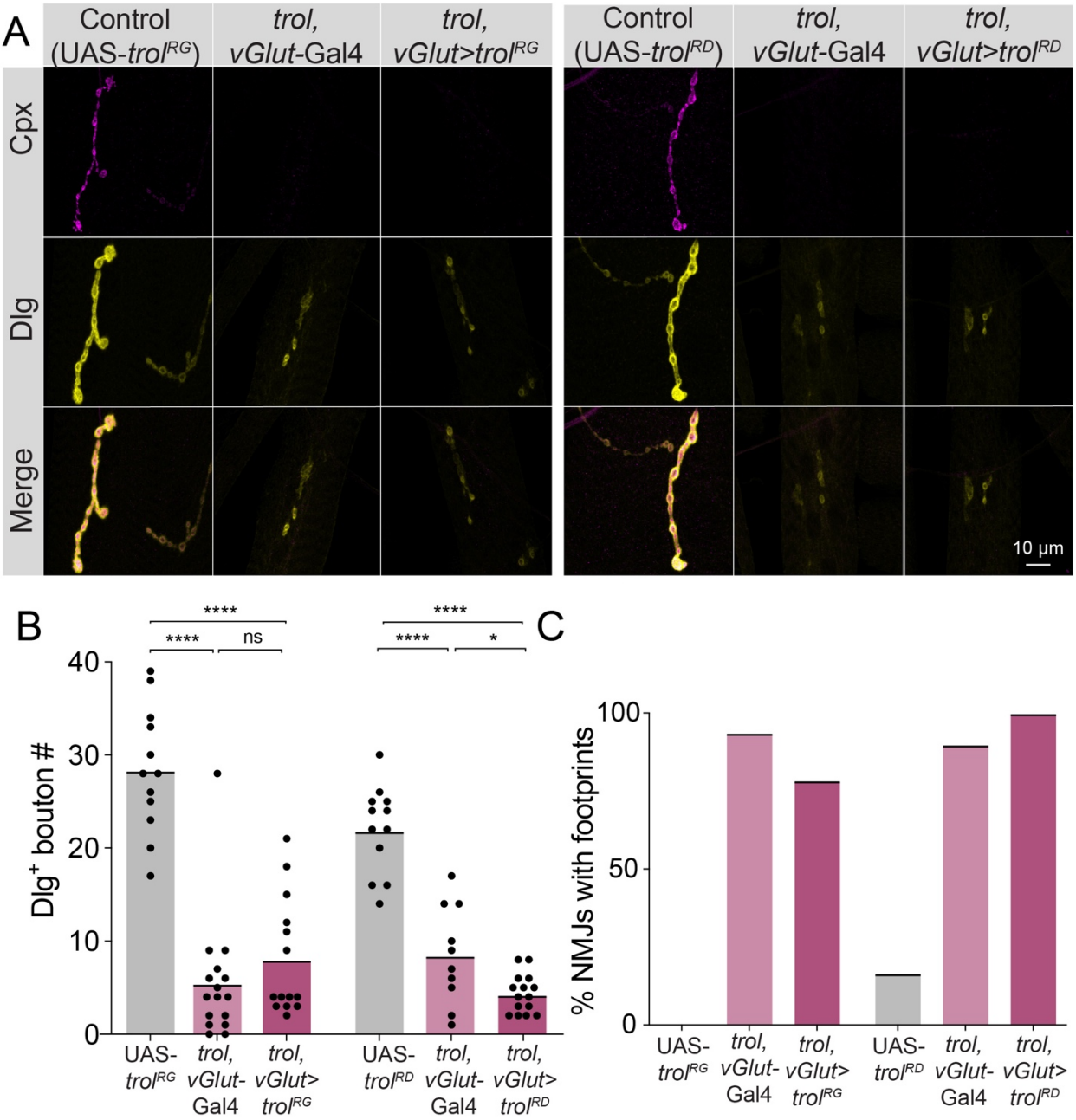

Figure 5 – figure supplement 1. Overexpression of Perlecan in *trol^{null}* motoneurons does not rescue synaptic retraction phenotypes.

(**A**) Representative images of muscle 4 NMJs in larval segments A4 for controls (*+;+;UAS-trol.RG/+*, 1st panel; *+;+;UAS-trol.RD/+*, 4th panel), *trol^{null}* larvae expressing Gal4 only (*trol^{null}, vGlut-Gal4/y;+;+*, 2nd and 5th panels) and *trol^{null}* larvae expressing UAS-*trol.*RG or UAS-*trol.*RD with *vGlut*-Gal4 (*trol^{null}, vGlut-Gal4/y;+;UAS-trol.RG/+,* 3rd panel; *trol^{null}, vGlut-Gal4/y;+;UAS-trol.RD/+,* 6th panel). Larvae were stained for Cpx (magenta) and Dlg (yellow), with the merged image below. In this set of panels, retracting NMJs had brightness enhanced to facilitate visualization of dim synaptic material. (**B**) Quantification of Dlg+ Ib bouton number from control, *trol* (*trol^{null}, vGlut*-Gal4), or *trol* rescues (*trol^{null}, vGlut*-Gal4 driving UAS-*trol^{RG}* or *trolRD*) at muscle 4 NMJs from segment A4. Each point represents the number of boutons at one NMJ, with mean bouton number indicated with the solid black line. Quantification of bouton number: RG experiments - UAS-*trol^{RG}*: 28.4 ± 2.0, 12 NMJs from 6 larvae; *trol^{null}, vGlut*-Gal4: 5.5 ± 1.7, 16 NMJs from 8 larvae, $p<0.0001$ compared to control; *trol*, *vGlut*>UAS-*trol^{RG}* rescues: 8.1 ± 1.7, 14 NMJs from 7 larvae; $p<0.0001$ compared to control, $p=0.54$ compared to *trol^{null}, vGlut*-Gal4; RD experiments - UAS-*trolRD*: 22.0 ± 1.4, 12 NMJs from 6 larvae; *trol^{null}, vGlut*-Gal4: 8.5 ± 1.7, 10 NMJs from 5 larvae, $p<0.0001$ compared to control; *trol*, *vGlut*>UAS-*trolRD* rescues: 4.3 ± 0.5, 15 NMJs from 8 larvae; $p<0.0001$ compared to control, $p=0.043$ (<0.05) compared to *trol^{null}, vGlut*-Gal4. (**C**) Percentage of NMJs with one or more postsynaptic footprints for segments A4 from the genotypes in panel B.

Figure 6

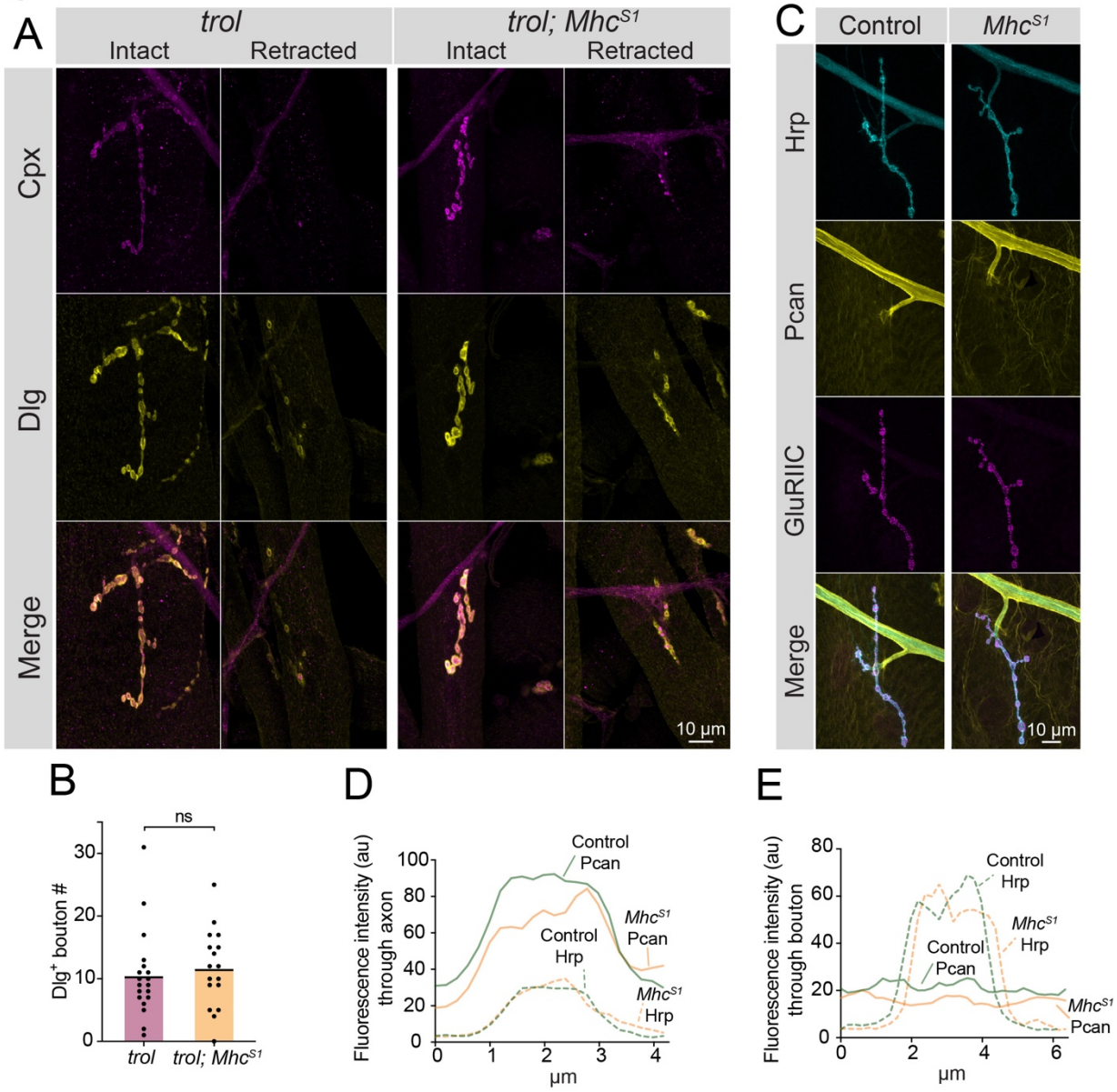
A
trol
Intact
Retracted
trol; Mhc^S1
Intact
Retracted
Cpx
Dlg
Merge
10 µm
C
Control
Mhc^S1
Hrp
Pcan
GluRIIC
Merge
10 µm
B
ns
Dlg+ bouton #
0
10
20
30
trol
trol; Mhc^S1
D
Fluorescence intensity (au) through axon
0
20
40
60
80
100
0
1
2
3
4
µm
Control Pcan
Mhc^S1 Pcan
Control Hrp
Mhc^S1 Hrp
E
Fluorescence intensity (au) through bouton
0
20
40
60
80
0
2
4
6
µm
Control Hrp
Mhc^S1 Hrp
Control Pcan
Mhc^S1 Pcan

Figure 6. Enhanced muscle contraction does not exacerbate synaptic retraction in *trol* mutants.

(**A**) Representative images of muscle 4 NMJs at segment A3 in *trol* (*trol*^{null}*/y;+;+*) and *trol; Mhc*^{S1} (*trol*^{null}*/y;Mhc*^{S1}*/+;+*) larvae stained for Cpx (magenta) and Dlg (yellow). Examples of intact and retracted NMJs are shown for both genotypes. Brightness for images of retracted NMJs was enhanced to show residual synaptic material. (**B**) Quantification of Dlg+ Ib bouton number from *trol* and *trol; Mhc*^{S1} muscle 4 NMJs at segment A3. Each point represents the number of boutons at one NMJ, with mean bouton number indicated with the solid black line. Quantification of bouton number: *trol*: 10.5 ± 1.6, 19 NMJs from 10 larvae; *trol; Mhc*^{S1}: 11.7 ± 1.5, 19 NMJs from 10 larvae, p = 0.597. (**C**) Representative images of muscle 4 NMJs stained for Perlecan, Hrp and GluRIIC in control (*trol*^{GFP}*/y*;+;+) or *Mhc*^{S1} (*trol*^{GFP}*/y;Mhc*^{S1}*/+;+*.) larvae. (**D,E**) Line scanning profiles of Perlecan and Hrp fluorescent intensity through axons (**D**) or synaptic boutons (**E**) at muscle 4 in segment A4. For both axons and boutons, line profiles from 12 control NMJs from 6 larvae and 10 *Mhc*^{S1} NMJs from 5 larvae were averaged. Control measurements are denoted in green and *Mhc*^{S1} in orange.

Figure 7

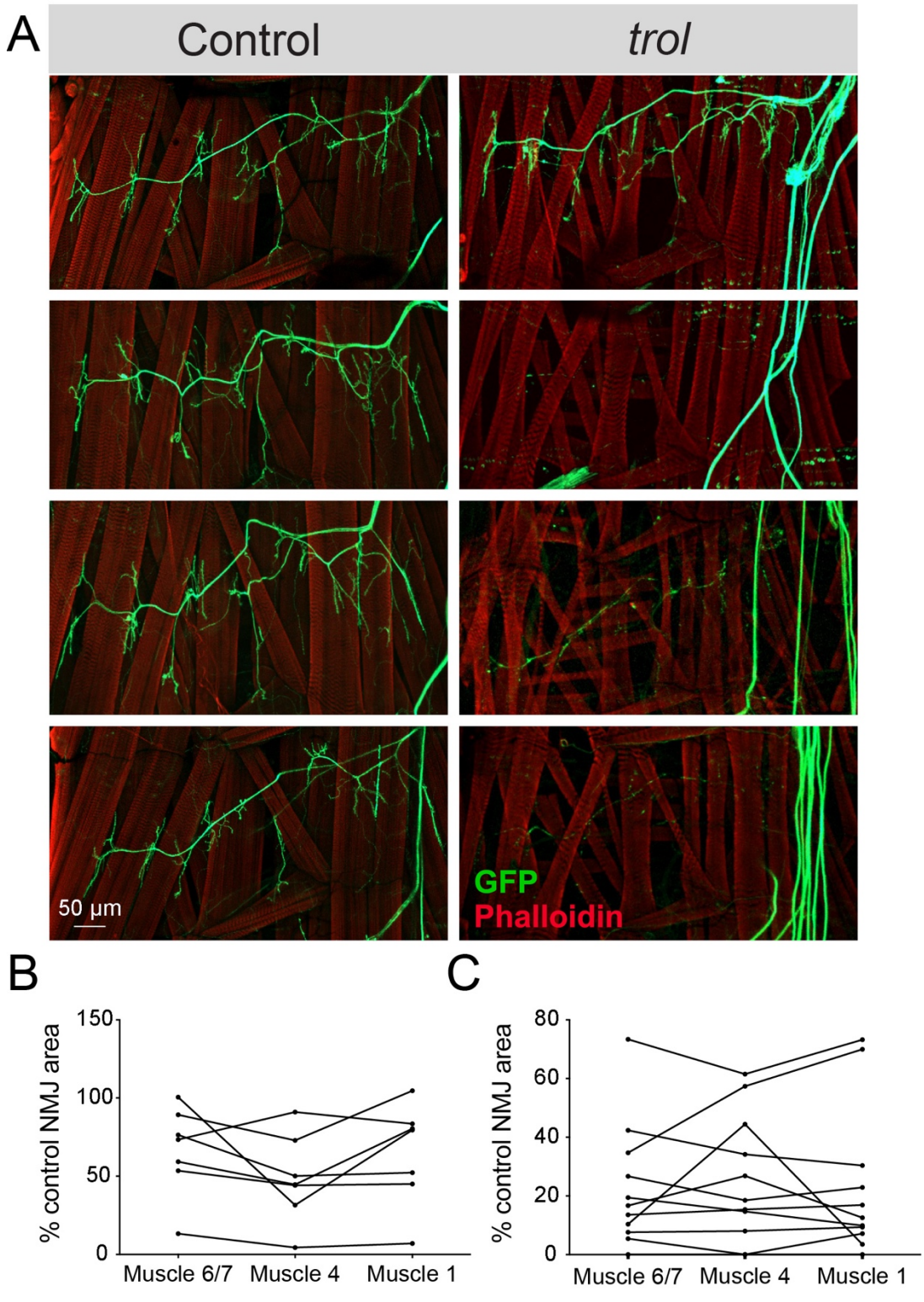
A
Control
trol
50 µm
GFP
Phalloidin
B
% control NMJ area
150
100
50
0
Muscle 6/7
Muscle 4
Muscle 1
C
% control NMJ area
80
60
40
20
0
Muscle 6/7
Muscle 4
Muscle 1

Figure 7. NMJ loss occurs in a temporally coordinated manner across abdominal hemisegments in *trol* mutants.

(**A**) Representative images of larval hemisegments in four control (*trol^{null},vGlut-Gal4/+;+;UAS-10xGFP/+*, left panels) or *trol^{null}* (*trol^{null},vGlut-Gal4/y;+;UAS-10xGFP/+,* right panels) larvae expressing 10X-GFP in motoneurons (green) and stained for Phalloidin to label muscle Actin (red). (**B**) Area of listed NMJs (muscle 6/7, muscle 4, muscle 1) in *trol* segment A2 as a percentage of mean control NMJ area. Percent area is largely consistent across synapses along the hemisegment, indicating synapses retract or are maintained together with their hemisegment. (**C**) Area of listed NMJs (muscle 6/7, muscle 4, muscle 1) in *trol* segment A3 as a percentage of mean control NMJ area.

Figure 8

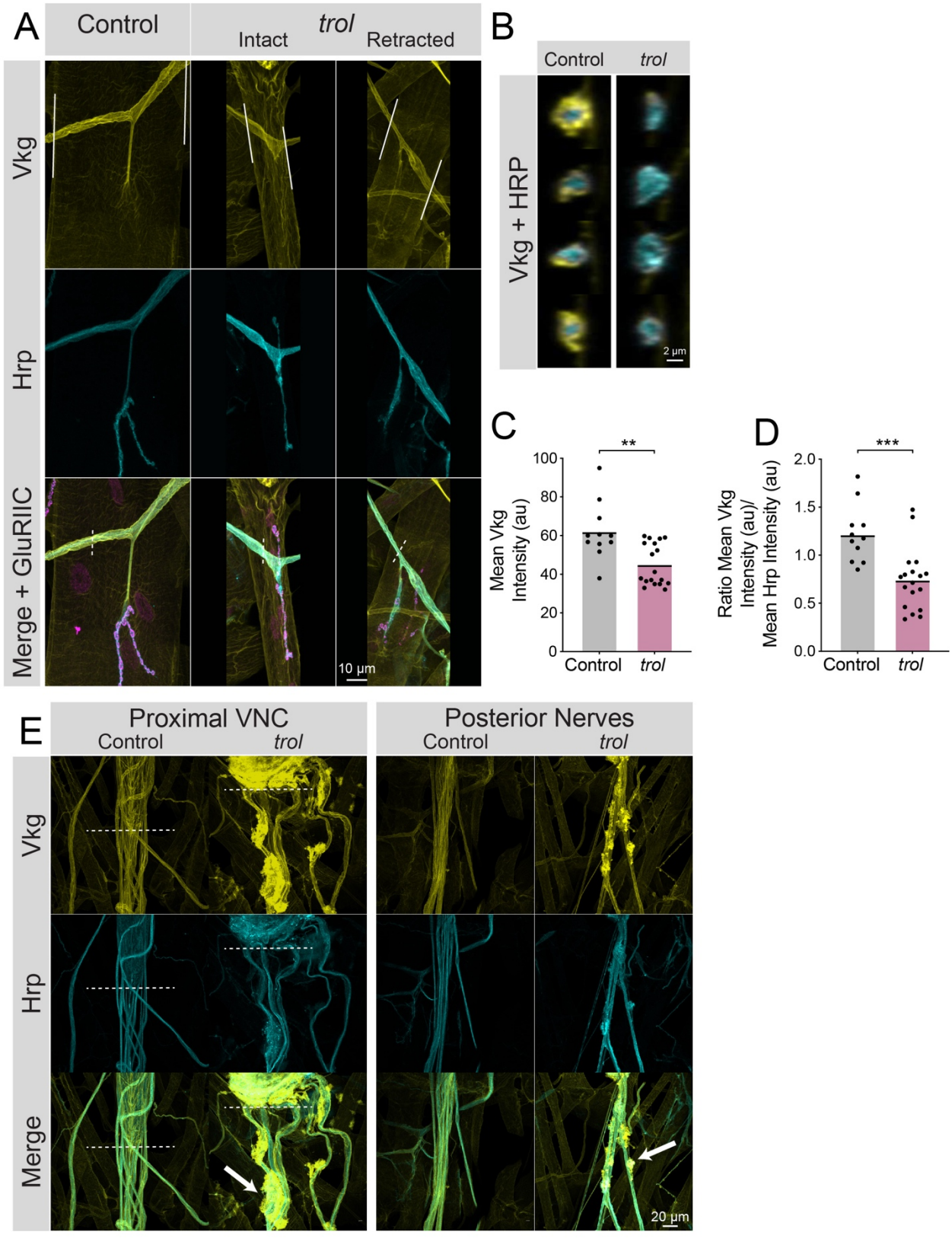
A
Control
trol
Intact
Retracted
Vkg
Hrp
Merge + GluRIIC
10 µm
B
Control
trol
Vkg + HRP
2 µm
C
**
Mean Vkg Intensity (au)
100
80
60
40
20
0
Control
trol
D
***
Ratio Mean Vkg Intensity (au)/ Mean Hrp Intensity (au)
2.0
1.5
1.0
0.5
0.0
Control
trol
E
Proximal VNC
Control
trol
Posterior Nerves
Control
trol
Vkg
Hrp
Merge
20 µm

Figure 8. Loss of Perlecan disrupts the neural lamella.

(**A**) Representative images of muscle 4 NMJs in control (*trol*^{null}*/+;vkg*^{GFP}*/+;+*) and *trol*^{null} (*trol*^{null}*/y;vkg*^{GFP}*/+;+*) larvae stained for Vkg (yellow), Hrp (cyan) and GluRIIC (magenta). Images of intact and retracted *trol* NMJs are shown. White lines in Vkg panels indicate borders for quantification of axon bundle fluorescence in panels C and D. (**B**) Representative cross-sections of control (left) and *trol* (right) axon bundles with Vkg in yellow and Hrp in cyan. (**C**) Quantification of mean Vkg fluorescence in the axon bundle crossing over muscle 4. Each point represents one axonal segment measurement. (Control: 7 larvae; $n = 11$; 62.00 ± 4.476; *trol*: 9 larvae; $n = 18$; 45.04 ± 2.549; $p = 0.0014$). (**D**) Quantification of the ratio of mean Vkg fluorescence divided by mean Hrp fluorescence in the axon bundle crossing over muscle 4. Each point represents the ratio for one axonal segment measurement. (Control: 7 larvae; $n = 11$; 1.219 ± 0.08998; *trol*: 9 larvae; $n = 18$; 0.7402 ± 0.07467, $p < 0.001$). (**E**) Representative images of axon bundles stained for Vkg (yellow) and Hrp (cyan) exiting the proximal VNC or those located more posteriorly. Control nerve bundles are on the left, with *trol* nerve bundles on the right. White dashed lines indicate the posterior tip of the VNC. White arrows note areas of Vkg accumulation and protrusions from the neural lamella.

Figure 9

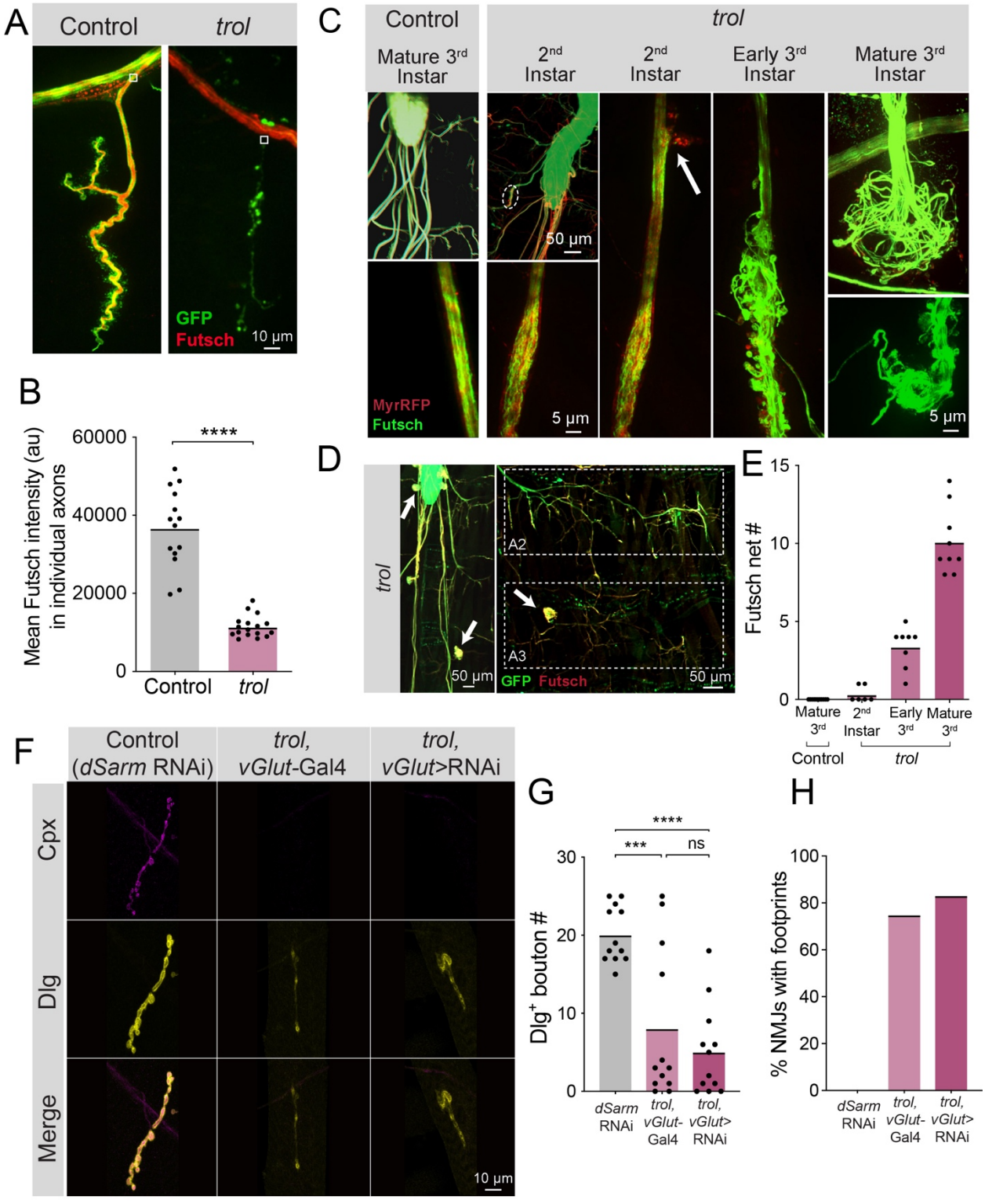
A
Control
trol
GFP
Futsch
10 µm
B
Mean Futsch intensity (au) in individual axons
60000
40000
20000
0
****
Control
trol
C
Control
trol
Mature 3rd Instar
2nd Instar
2nd Instar
Early 3rd Instar
Mature 3rd Instar
50 µm
MyrRFP
Futsch
5 µm
5 µm
D
trol
A2
A3
50 µm
GFP Futsch
50 µm
E
Futsch net #
15
10
5
0
Mature 3rd
2nd Instar
Early 3rd
Mature 3rd
Control
trol
F
Control (dSarm RNAi)
trol, vGlut-Gal4
trol, vGlut>RNAi
Cpx
Dlg
Merge
10 µm
G
Dlg+ bouton #
30
20
10
0
****
***
ns
dSarm RNAi
trol, vGlut-Gal4
trol, vGlut> RNAi
H
% NMJs with footprints
100
80
60
40
20
0
dSarm RNAi
trol, vGlut-Gal4
trol, vGlut> RNAi

Figure 9. The microtubule cytoskeleton and axons are fragmented in *trol* mutants and NMJ retraction occurs independent of the Wallerian degeneration pathway.

(**A**) Representative images of Ib neurons innervating muscle 4 in control (*trol^{null},vGlut-Gal4/+;+; UAS-10xGFP/+*, left panel) or *trol* (*trol^{null},vGlut-Gal4/y;+;UAS-10xGFP/+,* right panel) larvae expressing 10X-GFP in motoneurons (green) and stained for Futsch to label microtubules (red). White boxes indicate area of axon with Futsch fluorescence quantified in B. (**B**) Quantification of mean Futsch fluorescence in individual axons. Each point represents the average fluorescence in one axon. Quantification of mean fluorescence: control: 36725 ± 2679, 14 NMJs from 6 larvae; trol: 11476 ± 675.7, 17 NMJs from 7 larvae, $p<0.0001$. Multiple abdominal segments were imaged. (**C**) Representative images of VNCs and axon bundles stained for Futsch (green) and expressing MyrRFP (red) in control (*trol^{null},vGlut-Gal4/+;UAS-myrRFP/+;+*) and *trol* (*trol^{null},vGlut-Gal4/y; UAS-myrRFP/+;+*) larvae at the listed larval stage. Mature 3rd instar control axon bundles have continuous tracks of microtubules within unbroken membranes of fairly uniform size. Disruption of *trol* axons is mild at the 2nd instar stage, with swelling of axon material in some areas and mildly twisted microtubules (white dashed oval depicts location of swollen axon and twisted microtubule shown in inset). The 2nd instar axon bundle image is replicated in the next panel to also indicate an area of membrane material leaving the axon boundary (white arrow). In early 3rd instar *trol* larvae, microtubules are severely tangled and leave the boundary of the axon along with membrane material. By late 3rd instar, *trol* axons are severed and nets of tangled microtubules form balls at either end of the axon bundle breakage. (**D**) Representative image of 3rd instar *trol* VNC (*trol^{null}, vGlut-Gal4/y;+;UAS-10xGFP/+*, left panel) expressing 10X-GFP in motoneurons (green) and stained for Futsch to label microtubules (red). White arrows indicate microtubule nets at either end of axon bundle breakage. Right panels: representative images of *trol* hemisegments (intact top; retracted bottom) indicating that retracted synapses are present following axon breakage and formation of Futsch nets (white arrow). **(E)** Quantification of the number of Futsch nets in mature 3rd instar control larvae and *trol* larvae at multiple developmental stages. Control larvae have no Futsch nets. *Trol* larvae accumulate Futsch nets over the course of development. Each point indicates the number of Futsch nets in one larvae. (**F**) Representative images of larval muscle 4 NMJs stained for Cpx (magenta) and Dlg (yellow) in control (*+;UAS-dSarm-RNAi/+;+*), *trol*, *vGlut*-Gal4 (*trol^{null},vGlut-Gal4/y;+;+*) and *trol^{null}* expressing *dSarm* RNAi (*trol^{null},vGlut-Gal4/y;UAS-dSarm-RNAi/+,+*). Brightness for images of retracted NMJs was enhanced to show

residual synaptic material. (**G**) Quantification of Dlg+ Ib bouton number at muscle 4 NMJs in segment 4 in control, *trol*, *vGlut*-Gal4, and $trol^{null}$ expressing *dSarm*-RNAi. Each point represents bouton number from one NMJ with the mean indicated by the solid black line. Quantification of bouton number: control: 20.08 ± 1.048, 12 NMJs from 6 larvae; *trol*, *vGlut*-Gal4: 8.083 ± 2.811, 12 NMJs from 7 larvae, $p<0.001$ compared to control; $trol^{null}$ expressing *dSarm*-RNAi: 5.083 ± 1.667, 12 NMJs from 6 larvae, $p<0.0001$ compared to control, $p=0.5387$ compared to $trol^{null}$. (**H**) Percentage of control, *trol*, *vGlut*-Gal4 or $trol^{null}$ expressing *dSarm*-RNAi NMJs with footprints from the dataset in F.

Figure 10

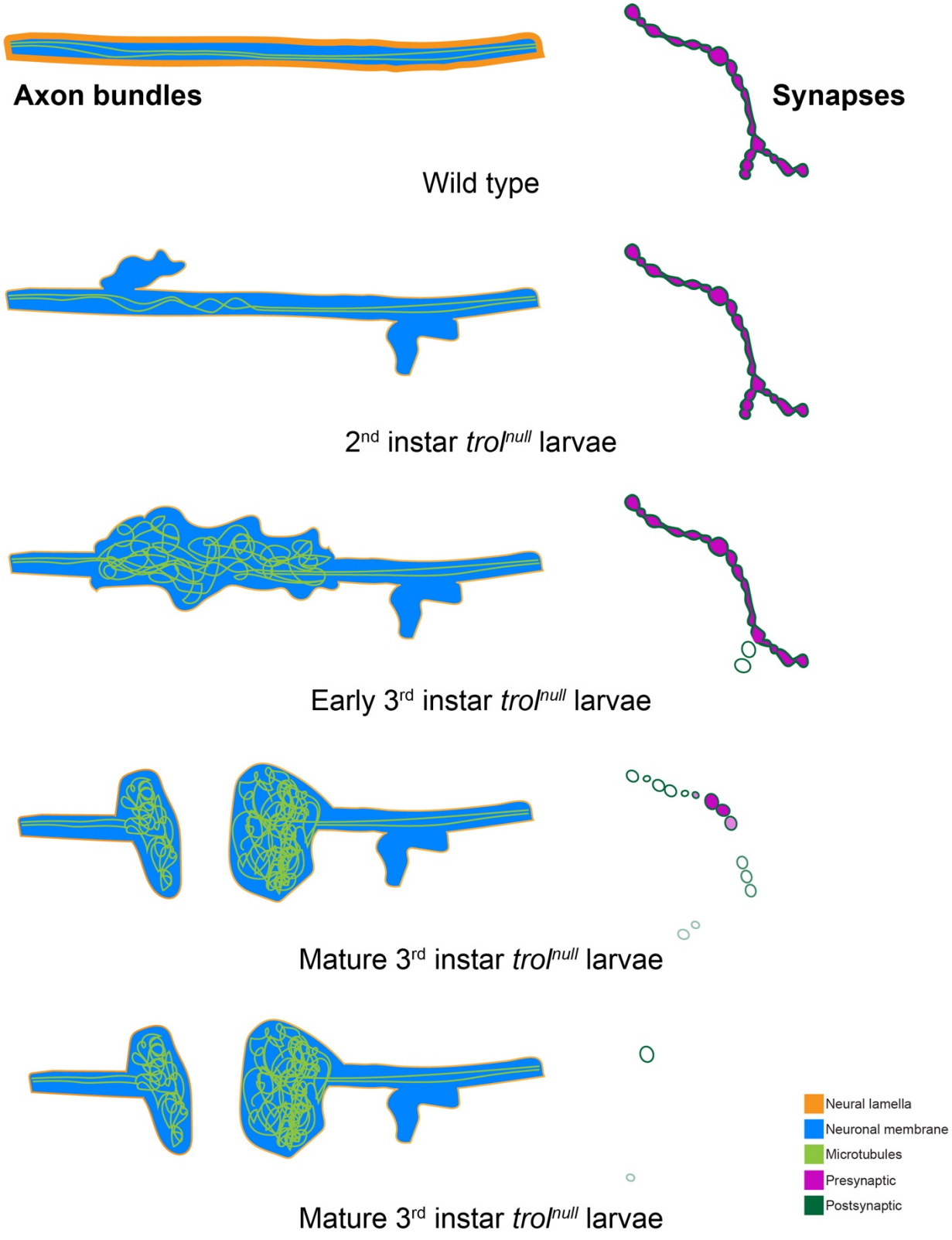
Axon bundles
Synapses
Wild type
2nd instar trolnull larvae
Early 3rd instar trolnull larvae
Mature 3rd instar trolnull larvae
Mature 3rd instar trolnull larvae
Neural lamella
Neuronal membrane
Microtubules
Presynaptic
Postsynaptic

Figure 10. Model of progressive axonal and synaptic defects in the absence of Perlecan.
In wild type animals, axon bundles (neuronal membrane in cyan) have a thick neural lamella (orange) and continuous, straight tracks of microtubules (light green). Synapses have good co-localization of pre- (magenta) and postsynaptic (dark green) material. In 2nd instar *trol*^{null} larvae, microtubules have begun to appear twisted and some small protrusions of neuronal membrane occur. The neural lamella is thin and protrudes prior to neuronal material and remains surrounding membrane protrusions. Synapses are still intact. In early 3rd instar larvae lacking Perlecan, microtubules are severely disorganized and lamella and membrane protrusions in axon bundles are larger. Some presynaptic material is lost from synapses in the first stages of retraction. By the mature 3rd instar larval stage, axons have broken entirely and tangled nets of microtubules bulge on either side of the breakage. Synapses are retracting and continue to retract until very few or no boutons remain. Synapse portion of model is replicated from **Figure 2**.

References

Akbergenova, Y., Cunningham, K.L., Zhang, Y.V., Weiss, S., Littleton, J.T., 2018. Characterization of developmental and molecular factors underlying release heterogeneity at Drosophila synapses. Elife 7. doi:10.7554/eLife.38268

Andlauer, T.F.M., Sigrist, S.J., 2012. In vivo imaging of Drosophila larval neuromuscular junctions to study synapse assembly. Cold Spring Harb. Protoc. 2012, 407–413. doi:10.1101/pdb.top068577

Aponte-Santiago, N.A., Littleton, J.T., 2020. Synaptic properties and plasticity mechanisms of invertebrate tonic and phasic neurons. Front. Physiol. 11, 611982. doi:10.3389/fphys.2020.611982

Arikawa-Hirasawa, E., Le, A.H., Nishino, I., Nonaka, I., Ho, N.C., Francomano, C.A., Govindraj, P., Hassell, J.R., Devaney, J.M., Spranger, J., Stevenson, R.E., Iannaccone, S., Dalakas, M.C., Yamada, Y., 2002. Structural and functional mutations of the perlecan gene cause Schwartz-Jampel syndrome, with myotonic myopathy and chondrodysplasia. Am. J. Hum. Genet. 70, 1368–1375. doi:10.1086/340390

Arikawa-Hirasawa, E., Watanabe, H., Takami, H., Hassell, J.R., Yamada, Y., 1999. Perlecan is essential for cartilage and cephalic development. Nat. Genet. 23, 354–358. doi:10.1038/15537

Aviezer, D., Hecht, D., Safran, M., Eisinger, M., David, G., Yayon, A., 1994. Perlecan, basal lamina proteoglycan, promotes basic fibroblast growth factor-receptor binding, mitogenesis, and angiogenesis. Cell 79, 1005–1013. doi:10.1016/0092-8674(94)90031-0

Bellen, H.J., Wangler, M.F., Yamamoto, S., 2019. The fruit fly at the interface of diagnosis and pathogenic mechanisms of rare and common human diseases. Hum. Mol. Genet. 28, R207–R214. doi:10.1093/hmg/ddz135

Bernfield, M., Götte, M., Park, P.W., Reizes, O., Fitzgerald, M.L., Lincecum, J., Zako, M., 1999. Functions of cell surface heparan sulfate proteoglycans. Annu. Rev. Biochem. 68, 729–777. doi:10.1146/annurev.biochem.68.1.729

Bishop, J.R., Schuksz, M., Esko, J.D., 2007. Heparan sulphate proteoglycans fine-tune mammalian physiology. Nature 446, 1030–1037. doi:10.1038/nature05817

Bittern, J., Pogodalla, N., Ohm, H., Brüser, L., Kottmeier, R., Schirmeier, S., Klämbt, C., 2021. Neuron-glia interaction in the Drosophila nervous system. Dev. Neurobiol. 81, 438–452. doi:10.1002/dneu.22737

Bonche, R., Chessel, A., Boisivon, S., Smolen, P., Thérond, P., Pizette, S., 2021. Two different sources of Perlecan cooperate for its function in the basement membrane of the Drosophila wing imaginal disc. Dev. Dyn. 250, 542–561. doi:10.1002/dvdy.274

Bonche, R., Smolen, P., Chessel, A., Boisivon, S., Pisano, S., Voigt, A., Schaub, S., Thérond, P., Pizette, S., 2022. Regulation of the collagen IV network by the basement membrane protein perlecan is crucial for squamous epithelial cell morphogenesis and organ architecture. Matrix Biol 114, 35–66. doi:10.1016/j.matbio.2022.10.004

Brink, D.L., Gilbert, M., Xie, X., Petley-Ragan, L., Auld, V.J., 2012. Glial processes at the Drosophila larval neuromuscular junction match synaptic growth. PLoS One 7, e37876. doi:10.1371/journal.pone.0037876

Cajal, R., 1928. Degeneration and regeneration of the nervous system. . Clarendon Press.

Carson, D.D., Tang, J.P., Julian, J., 1993. Heparan sulfate proteoglycan (perlecan) expression by

mouse embryos during acquisition of attachment competence. Dev. Biol. 155, 97–106. doi:10.1006/dbio.1993.1010
Cheng, X.-T., Huang, N., Sheng, Z.-H., 2022. Programming axonal mitochondrial maintenance and bioenergetics in neurodegeneration and regeneration. Neuron 110, 1899–1923. doi:10.1016/j.neuron.2022.03.015
Cho, J.Y., Chak, K., Andreone, B.J., Wooley, J.R., Kolodkin, A.L., 2012. The extracellular matrix proteoglycan perlecan facilitates transmembrane semaphorin-mediated repulsive guidance. Genes Dev. 26, 2222–2235. doi:10.1101/gad.193136.112
Coleman, M.P., Höke, A., 2020. Programmed axon degeneration: from mouse to mechanism to medicine. Nat. Rev. Neurosci. 21, 183–196. doi:10.1038/s41583-020-0269-3
Collins, C.A., DiAntonio, A., 2007. Synaptic development: insights from Drosophila. Curr. Opin. Neurobiol. 17, 35–42. doi:10.1016/j.conb.2007.01.001
Conforti, L., Gilley, J., Coleman, M.P., 2014. Wallerian degeneration: an emerging axon death pathway linking injury and disease. Nat. Rev. Neurosci. 15, 394–409. doi:10.1038/nrn3680
Cook, D., Fry, M.J., Hughes, K., Sumathipala, R., Woodgett, J.R., Dale, T.C., 1996. Wingless inactivates glycogen synthase kinase-3 via an intracellular signalling pathway which involves a protein kinase C. EMBO J. 15, 4526–4536.
Costell, M., Gustafsson, E., Aszódi, A., Mörgelin, M., Bloch, W., Hunziker, E., Addicks, K., Timpl, R., Fässler, R., 1999. Perlecan maintains the integrity of cartilage and some basement membranes. J. Cell Biol. 147, 1109–1122. doi:10.1083/jcb.147.5.1109
Dani, N., Nahm, M., Lee, S., Broadie, K., 2012. A targeted glycan-related gene screen reveals heparan sulfate proteoglycan sulfation regulates WNT and BMP trans-synaptic signaling. PLoS Genet. 8, e1003031. doi:10.1371/journal.pgen.1003031
Datta, S., Kankel, D.R., 1992. l(1)trol and l(1)devl, loci affecting the development of the adult central nervous system in Drosophila melanogaster. Genetics 130, 523–537.
De Vos, K.J., Grierson, A.J., Ackerley, S., Miller, C.C.J., 2008. Role of axonal transport in neurodegenerative diseases. Annu. Rev. Neurosci. 31, 151–173. doi:10.1146/annurev.neuro.31.061307.090711
DiAntonio, A., 2019. Axon degeneration: mechanistic insights lead to therapeutic opportunities for the prevention and treatment of peripheral neuropathy. Pain 160 Suppl 1, S17–S22. doi:10.1097/j.pain.0000000000001528
Eaton, B.A., Davis, G.W., 2005. LIM Kinase1 controls synaptic stability downstream of the type II BMP receptor. Neuron 47, 695–708. doi:10.1016/j.neuron.2005.08.010
Eaton, B.A., Fetter, R.D., Davis, G.W., 2002. Dynactin is necessary for synapse stabilization. Neuron 34, 729–741. doi:10.1016/s0896-6273(02)00721-3
Edwards, J.S., Swales, L.S., Bate, M., 1993. The differentiation between neuroglia and connective tissue sheath in insect ganglia revisited: the neural lamella and perineurial sheath cells are absent in a mesodermless mutant of Drosophila. J. Comp. Neurol. 333, 301–308. doi:10.1002/cne.903330214
Erickson, A.C., Couchman, J.R., 2000. Still more complexity in mammalian basement membranes. J. Histochem. Cytochem. 48, 1291–1306. doi:10.1177/002215540004801001
Fan, A., Joy, M.S.H., Saif, T., 2019. A connected cytoskeleton network generates axonal tension in embryonic Drosophila. Lab Chip 19, 3133–3139. doi:10.1039/c9lc00243j
Fan, A., Tofangchi, A., Kandel, M., Popescu, G., Saif, T., 2017. Coupled circumferential and

axial tension driven by actin and myosin influences in vivo axon diameter. Sci. Rep. 7, 14188. doi:10.1038/s41598-017-13830-1

Fang, Y., Soares, L., Teng, X., Geary, M., Bonini, N.M., 2012. A novel Drosophila model of nerve injury reveals an essential role of Nmnat in maintaining axonal integrity. Curr. Biol. 22, 590–595. doi:10.1016/j.cub.2012.01.065

Farach-Carson, M.C., Warren, C.R., Harrington, D.A., Carson, D.D., 2014. Border patrol: insights into the unique role of perlecan/heparan sulfate proteoglycan 2 at cell and tissue borders. Matrix Biol 34, 64–79. doi:10.1016/j.matbio.2013.08.004

Fernandopulle, M.S., Lippincott-Schwartz, J., Ward, M.E., 2021. RNA transport and local translation in neurodevelopmental and neurodegenerative disease. Nat. Neurosci. 24, 622–632. doi:10.1038/s41593-020-00785-2

Figley, M.D., Gu, W., Nanson, J.D., Shi, Y., Sasaki, Y., Cunnea, K., Malde, A.K., Jia, X., Luo, Z., Saikot, F.K., Mosaiab, T., Masic, V., Holt, S., Hartley-Tassell, L., McGuinness, H.Y., Manik, M.K., Bosanac, T., Landsberg, M.J., Kerry, P.S., Mobli, M., Hughes, R.O., Milbrandt, J., Kobe, B., DiAntonio, A., Ve, T., 2021. SARM1 is a metabolic sensor activated by an increased NMN/NAD+ ratio to trigger axon degeneration. Neuron 109, 1118–1136.e11. doi:10.1016/j.neuron.2021.02.009

Fox, A.N., Zinn, K., 2005. The heparan sulfate proteoglycan syndecan is an in vivo ligand for the Drosophila LAR receptor tyrosine phosphatase. Curr. Biol. 15, 1701–1711. doi:10.1016/j.cub.2005.08.035

Franco, B., Bogdanik, L., Bobinnec, Y., Debec, A., Bockaert, J., Parmentier, M.-L., Grau, Y., 2004. Shaggy, the homolog of glycogen synthase kinase 3, controls neuromuscular junction growth in Drosophila. J. Neurosci. 24, 6573--6577.

Friedrich, M.V., Schneider, M., Timpl, R., Baumgartner, S., 2000. Perlecan domain V of Drosophila melanogaster. Sequence, recombinant analysis and tissue expression. Eur. J. Biochem. 267, 3149–3159. doi:10.1046/j.1432-1327.2000.01337.x

Gautam, M., Noakes, P.G., Moscoso, L., Rupp, F., Scheller, R.H., Merlie, J.P., Sanes, J.R., 1996. Defective neuromuscular synaptogenesis in agrin-deficient mutant mice. Cell 85, 525–535. doi:10.1016/s0092-8674(00)81253-2

Gerdts, J., Brace, E.J., Sasaki, Y., DiAntonio, A., Milbrandt, J., 2015. SARM1 activation triggers axon degeneration locally via NAD^+ destruction. Science 348, 453–457. doi:10.1126/science.1258366

Gerdts, J., Summers, D.W., Milbrandt, J., DiAntonio, A., 2016. Axon Self-Destruction: New Links among SARM1, MAPKs, and NAD+ Metabolism. Neuron 89, 449–460. doi:10.1016/j.neuron.2015.12.023

Gerdts, J., Summers, D.W., Sasaki, Y., DiAntonio, A., Milbrandt, J., 2013. Sarm1-mediated axon degeneration requires both SAM and TIR interactions. J. Neurosci. 33, 13569–13580. doi:10.1523/JNEUROSCI.1197-13.2013

Gilley, J., Orsomando, G., Nascimento-Ferreira, I., Coleman, M.P., 2015. Absence of SARM1 rescues development and survival of NMNAT2-deficient axons. Cell Rep. 10, 1974–1981. doi:10.1016/j.celrep.2015.02.060

Gilley, J., Ribchester, R.R., Coleman, M.P., 2017. Sarm1 deletion, but not wlds, confers lifelong rescue in a mouse model of severe axonopathy. Cell Rep. 21, 10–16. doi:10.1016/j.celrep.2017.09.027

Graf, E.R., Heerssen, H.M., Wright, C.M., Davis, G.W., DiAntonio, A., 2011. Stathmin is required for stability of the Drosophila neuromuscular junction. J. Neurosci. 31, 15026–

15034. doi:10.1523/JNEUROSCI.2024-11.2011
Guan, Z., Quiñones-Frías, M.C., Akbergenova, Y., Littleton, J.T., 2020. Drosophila Synaptotagmin 7 negatively regulates synaptic vesicle release and replenishment in a dosage-dependent manner. Elife 9. doi:10.7554/eLife.55443
Gubbiotti, M.A., Neill, T., Iozzo, R.V., 2017. A current view of perlecan in physiology and pathology: A mosaic of functions. Matrix Biol 57–58, 285–298. doi:10.1016/j.matbio.2016.09.003
Häcker, U., Nybakken, K., Perrimon, N., 2005. Heparan sulphate proteoglycans: the sweet side of development. Nat. Rev. Mol. Cell Biol. 6, 530–541. doi:10.1038/nrm1681
Han, K.A., Kim, Y.-J., Yoon, T.H., Kim, H., Bae, S., Um, J.W., Choi, S.-Y., Ko, J., 2020. LAR-RPTPs Directly Interact with Neurexins to Coordinate Bidirectional Assembly of Molecular Machineries. J. Neurosci. 40, 8438–8462. doi:10.1523/JNEUROSCI.1091-20.2020
Harris, K.P., Littleton, J.T., 2015. Transmission, development, and plasticity of synapses. Genetics 201, 345–375. doi:10.1534/genetics.115.176529
Hassell, J.R., Robey, P.G., Barrach, H.J., Wilczek, J., Rennard, S.I., Martin, G.R., 1980. Isolation of a heparan sulfate-containing proteoglycan from basement membrane. Proc. Natl. Acad. Sci. USA 77, 4494–4498. doi:10.1073/pnas.77.8.4494
Hayes, A.J., Farrugia, B.L., Biose, I.J., Bix, G.J., Melrose, J., 2022. Perlecan, A Multi-Functional, Cell-Instructive, Matrix-Stabilizing Proteoglycan With Roles in Tissue Development Has Relevance to Connective Tissue Repair and Regeneration. Front. Cell Dev. Biol. 10, 856261. doi:10.3389/fcell.2022.856261
Hummel, T., Krukkert, K., Roos, J., Davis, G., Klämbt, C., 2000. Drosophila Futsch/22C10 is a MAP1B-like protein required for dendritic and axonal development. Neuron 26, 357–370. doi:10.1016/s0896-6273(00)81169-1
Hunter, A.C., Petley-Ragan, L.M., Das, M., Auld, V.J., 2020. Basigin Associates with Integrin in Order to Regulate Perineurial Glia and Drosophila Nervous System Morphology. J. Neurosci. 40, 3360–3373. doi:10.1523/JNEUROSCI.1397-19.2020
Huntwork, S., Littleton, J.T., 2007. A complexin fusion clamp regulates spontaneous neurotransmitter release and synaptic growth. Nat. Neurosci. 10, 1235–1237. doi:10.1038/nn1980
Isabella, A.J., Horne-Badovinac, S., 2015. Dynamic regulation of basement membrane protein levels promotes egg chamber elongation in Drosophila. Dev. Biol. 406, 212–221. doi:10.1016/j.ydbio.2015.08.018
Jetti, S.J., Crane, A.B., Akbergenova, Y., Aponte-Santiago, N.A., Cunningham, K.L., Whittaker, C.W., Littleton, J.T., 2023. Molecular logic of synaptic diversity between drosophila tonic and phasic motoneurons. BioRxiv. doi:10.1101/2023.01.17.524447
Johnson, K.G., Tenney, A.P., Ghose, A., Duckworth, A.M., Higashi, M.E., Parfitt, K., Marcu, O., Heslip, T.R., Marsh, J.L., Schwarz, T.L., Flanagan, J.G., Van Vactor, D., 2006. The HSPGs Syndecan and Dallylike bind the receptor phosphatase LAR and exert distinct effects on synaptic development. Neuron 49, 517–531. doi:10.1016/j.neuron.2006.01.026
Jorquera, R.A., Huntwork-Rodriguez, S., Akbergenova, Y., Cho, R.W., Littleton, J.T., 2012. Complexin controls spontaneous and evoked neurotransmitter release by regulating the timing and properties of synaptotagmin activity. J. Neurosci. 32, 18234–18245. doi:10.1523/JNEUROSCI.3212-12.2012
Kamimura, K., Maeda, N., 2021. Glypicans and heparan sulfate in synaptic development, neural

plasticity, and neurological disorders. Front. Neural Circuits 15, 595596. doi:10.3389/fncir.2021.595596
Kamimura, K., Odajima, A., Ikegawa, Y., Maru, C., Maeda, N., 2019. The HSPG Glypican Regulates Experience-Dependent Synaptic and Behavioral Plasticity by Modulating the Non-Canonical BMP Pathway. Cell Rep. 28, 3144–3156.e4. doi:10.1016/j.celrep.2019.08.032
Kamimura, K., Ueno, K., Nakagawa, J., Hamada, R., Saitoe, M., Maeda, N., 2013. Perlecan regulates bidirectional Wnt signaling at the Drosophila neuromuscular junction. J. Cell Biol. 200, 219–233. doi:10.1083/jcb.201207036
Kanca, O., Bellen, H.J., Schnorrer, F., 2017. Gene tagging strategies to assess protein expression, localization, and function in drosophila. Genetics 207, 389–412. doi:10.1534/genetics.117.199968
Khalilgharibi, N., Mao, Y., 2021. To form and function: on the role of basement membrane mechanics in tissue development, homeostasis and disease. Open Biol 11, 200360. doi:10.1098/rsob.200360
Kinnunen, T.K., 2014. Combinatorial roles of heparan sulfate proteoglycans and heparan sulfates in Caenorhabditis elegans neural development. PLoS One 9, e102919. doi:10.1371/journal.pone.0102919
Koch, I., Schwarz, H., Beuchle, D., Goellner, B., Langegger, M., Aberle, H., 2008. Drosophila ankyrin 2 is required for synaptic stability. Neuron 58, 210–222. doi:10.1016/j.neuron.2008.03.019
Koper, A., Schenck, A., Prokop, A., 2012. Analysis of adhesion molecules and basement membrane contributions to synaptic adhesion at the Drosophila embryonic NMJ. PLoS One 7, e36339. doi:10.1371/journal.pone.0036339
Krench, M., Littleton, J.T., 2013. Modeling Huntington disease in Drosophila: Insights into axonal transport defects and modifiers of toxicity. Fly (Austin) 7, 229–236. doi:10.4161/fly.26279
Lee, B.P., Jones, B.W., 2005. Transcriptional regulation of the Drosophila glial gene repo. Mech. Dev. 122, 849–862. doi:10.1016/j.mod.2005.01.002
Lee, Y.-M., Sun, Y.H., 2015. Drosophila as a model to study the role of glia in neurodegeneration. J Neurogenet 29, 69–79. doi:10.3109/01677063.2015.1076816
Lin, X., 2004. Functions of heparan sulfate proteoglycans in cell signaling during development. Development 131, 6009–6021. doi:10.1242/dev.01522
Lindner, J.R., Hillman, P.R., Barrett, A.L., Jackson, M.C., Perry, T.L., Park, Y., Datta, S., 2007. The Drosophila Perlecan gene trol regulates multiple signaling pathways in different developmental contexts. BMC Dev. Biol. 7, 121. doi:10.1186/1471-213X-7-121
Llobet Rosell, A., Neukomm, L.J., 2019. Axon death signalling in Wallerian degeneration among species and in disease. Open Biol 9, 190118. doi:10.1098/rsob.190118
Llobet Rosell, A., Paglione, M., Gilley, J., Kocia, M., Perillo, G., Gasparrini, M., Cialabrini, L., Raffaelli, N., Angeletti, C., Orsomando, G., Wu, P.-H., Coleman, M.P., Loreto, A., Neukomm, L.J., 2022. The NAD+ precursor NMN activates dSarm to trigger axon degeneration in Drosophila. Elife 11. doi:10.7554/eLife.80245
Luo, L., O'Leary, D.D.M., 2005. Axon retraction and degeneration in development and disease. Annu. Rev. Neurosci. 28, 127–156. doi:10.1146/annurev.neuro.28.061604.135632
Madeira, F., Pearce, M., Tivey, A.R.N., Basutkar, P., Lee, J., Edbali, O., Madhusoodanan, N., Kolesnikov, A., Lopez, R., 2022. Search and sequence analysis tools services from

EMBL-EBI in 2022. Nucleic Acids Res. 50, W276-9. doi:10.1093/nar/gkac240
Mariano, V., Domínguez-Iturza, N., Neukomm, L.J., Bagni, C., 2018. Maintenance mechanisms of circuit-integrated axons. Curr. Opin. Neurobiol. 53, 162–173. doi:10.1016/j.conb.2018.08.007
Martin, G.R., Timpl, R., 1987. Laminin and other basement membrane components. Annu. Rev. Cell Biol. 3, 57–85. doi:10.1146/annurev.cb.03.110187.000421
Martin, G.R., Timpl, R., Kühn, K., 1988. Basement membrane proteins: molecular structure and function. Adv. Protein Chem. 39, 1–50. doi:10.1016/s0065-3233(08)60374-5
Massaro, C.M., Pielage, J., Davis, G.W., 2009. Molecular mechanisms that enhance synapse stability despite persistent disruption of the spectrin/ankyrin/microtubule cytoskeleton. J. Cell Biol. 187, 101–117. doi:10.1083/jcb.200903166
Mathew, D., Ataman, B., Chen, J., Zhang, Y., Cumberledge, S., Budnik, V., 2005. Wingless signaling at synapses is through cleavage and nuclear import of receptor DFrizzled2. Science (New York, NY) 310, 1344--1347.
Matsubayashi, Y., Louani, A., Dragu, A., Sánchez-Sánchez, B.J., Serna-Morales, E., Yolland, L., Gyoergy, A., Vizcay, G., Fleck, R.A., Heddleston, J.M., Chew, T.-L., Siekhaus, D.E., Stramer, B.M., 2017. A moving source of matrix components is essential for de novo basement membrane formation. Curr. Biol. 27, 3526–3534.e4. doi:10.1016/j.cub.2017.10.001
Meyer, S., Schmidt, I., Klämbt, C., 2014. Glia ECM interactions are required to shape the Drosophila nervous system. Mech. Dev. 133, 105–116. doi:10.1016/j.mod.2014.05.003
Montana, E.S., Littleton, J.T., 2004. Characterization of a hypercontraction-induced myopathy in Drosophila caused by mutations in Mhc. J. Cell Biol. 164, 1045–1054. doi:10.1083/jcb.200308158
Montana, E.S., Littleton, J.T., 2006. Expression profiling of a hypercontraction-induced myopathy in Drosophila suggests a compensatory cytoskeletal remodeling response. J. Biol. Chem. 281, 8100–8109. doi:10.1074/jbc.M512468200
Morin, X., Daneman, R., Zavortink, M., Chia, W., 2001. A protein trap strategy to detect GFP-tagged proteins expressed from their endogenous loci in Drosophila. Proc. Natl. Acad. Sci. USA 98, 15050–15055. doi:10.1073/pnas.261408198
Mosca, T.J., Schwarz, T.L., 2010. The nuclear import of Frizzled2-C by Importins-beta11 and alpha2 promotes postsynaptic development. Nat. Neurosci. 13, 935–943. doi:10.1038/nn.2593
Mouw, J.K., Ou, G., Weaver, V.M., 2014. Extracellular matrix assembly: a multiscale deconstruction. Nat. Rev. Mol. Cell Biol. 15, 771–785. doi:10.1038/nrm3902
Neukomm, L.J., Burdett, T.C., Seeds, A.M., Hampel, S., Coutinho-Budd, J.C., Farley, J.E., Wong, J., Karadeniz, Y.B., Osterloh, J.M., Sheehan, A.E., Freeman, M.R., 2017. Axon death pathways converge on axundead to promote functional and structural axon disassembly. Neuron 95, 78–91.e5. doi:10.1016/j.neuron.2017.06.031
Neukomm, L.J., Freeman, M.R., 2014. Diverse cellular and molecular modes of axon degeneration. Trends Cell Biol. 24, 515–523. doi:10.1016/j.tcb.2014.04.003
Nguyen, M.U., Kwong, J., Chang, J., Gillet, V.G., Lee, R.M., Johnson, K.G., 2016. The extracellular and cytoplasmic domains of syndecan cooperate postsynaptically to promote synapse growth at the drosophila neuromuscular junction. PLoS One 11, e0151621. doi:10.1371/journal.pone.0151621
Nicole, S., Davoine, C.S., Topaloglu, H., Cattolico, L., Barral, D., Beighton, P., Hamida, C.B.,

Hammouda, H., Cruaud, C., White, P.S., Samson, D., Urtizberea, J.A., Lehmann-Horn, F., Weissenbach, J., Hentati, F., Fontaine, B., 2000. Perlecan, the major proteoglycan of basement membranes, is altered in patients with Schwartz-Jampel syndrome (chondrodystrophic myotonia). Nat. Genet. 26, 480–483. doi:10.1038/82638

Nitkin, R.M., Smith, M.A., Magill, C., Fallon, J.R., Yao, Y.M., Wallace, B.G., McMahan, U.J., 1987. Identification of agrin, a synaptic organizing protein from Torpedo electric organ. J. Cell Biol. 105, 2471–2478. doi:10.1083/jcb.105.6.2471

Noonan, D.M., Fulle, A., Valente, P., Cai, S., Horigan, E., Sasaki, M., Yamada, Y., Hassell, J.R., 1991. The complete sequence of perlecan, a basement membrane heparan sulfate proteoglycan, reveals extensive similarity with laminin A chain, low density lipoprotein-receptor, and the neural cell adhesion molecule. J. Biol. Chem. 266, 22939–22947. doi:10.1016/S0021-9258(18)54445-8

Osterloh, J.M., Yang, J., Rooney, T.M., Fox, A.N., Adalbert, R., Powell, E.H., Sheehan, A.E., Avery, M.A., Hackett, R., Logan, M.A., MacDonald, J.M., Ziegenfuss, J.S., Milde, S., Hou, Y.-J., Nathan, C., Ding, A., Brown, R.H., Conforti, L., Coleman, M., Tessier-Lavigne, M., Züchner, S., Freeman, M.R., 2012. dSarm/Sarm1 is required for activation of an injury-induced axon death pathway. Science 337, 481–484. doi:10.1126/science.1223899

Owald, D., Sigrist, S.J., 2009. Assembling the presynaptic active zone. Curr. Opin. Neurobiol. 19, 311–318. doi:10.1016/j.conb.2009.03.003

Packard, M., Koo, E.S., Gorczyca, M., Sharpe, J., Cumberledge, S., Budnik, V., 2002. The Drosophila Wnt, wingless, provides an essential signal for pre- and postsynaptic differentiation. Cell 111, 319–330. doi:10.1016/s0092-8674(02)01047-4

Park, Y., Rangel, C., Reynolds, M.M., Caldwell, M.C., Johns, M., Nayak, M., Welsh, C.J.R., McDermott, S., Datta, S., 2003. Drosophila perlecan modulates FGF and hedgehog signals to activate neural stem cell division. Dev. Biol. 253, 247–257. doi:10.1016/s0012-1606(02)00019-2

Pastor-Pareja, J.C., Xu, T., 2011. Shaping cells and organs in Drosophila by opposing roles of fat body-secreted Collagen IV and perlecan. Dev. Cell 21, 245–256. doi:10.1016/j.devcel.2011.06.026

Perlson, E., Maday, S., Fu, M.-M., Moughamian, A.J., Holzbaur, E.L.F., 2010. Retrograde axonal transport: pathways to cell death? Trends Neurosci. 33, 335–344. doi:10.1016/j.tins.2010.03.006

Pielage, J., Bulat, V., Zuchero, J.B., Fetter, R.D., Davis, G.W., 2011. Hts/Adducin controls synaptic elaboration and elimination. Neuron 69, 1114–1131. doi:10.1016/j.neuron.2011.02.007

Pielage, J., Cheng, L., Fetter, R.D., Carlton, P.M., Sedat, J.W., Davis, G.W., 2008. A presynaptic giant ankyrin stabilizes the NMJ through regulation of presynaptic microtubules and transsynaptic cell adhesion. Neuron 58, 195–209. doi:10.1016/j.neuron.2008.02.017

Pielage, J., Fetter, R.D., Davis, G.W., 2005. Presynaptic spectrin is essential for synapse stabilization. Curr. Biol. 15, 918–928. doi:10.1016/j.cub.2005.04.030

Qin, J., Liang, J., Ding, M., 2014. Perlecan antagonizes collagen IV and ADAMTS9/GON-1 in restricting the growth of presynaptic boutons. J. Neurosci. 34, 10311–10324. doi:10.1523/JNEUROSCI.5128-13.2014

Ramos-Lewis, W., LaFever, K.S., Page-McCaw, A., 2018. A scar-like lesion is apparent in basement membrane after wound repair in vivo. Matrix Biol 74, 101–120.

doi:10.1016/j.matbio.2018.07.004
Restrepo, L.J., DePew, A.T., Moese, E.R., Tymanskyj, S.R., Parisi, M.J., Aimino, M.A., Duhart, J.C., Fei, H., Mosca, T.J., 2022. γ-secretase promotes Drosophila postsynaptic development through the cleavage of a Wnt receptor. Dev. Cell 57, 1643–1660.e7. doi:10.1016/j.devcel.2022.05.006
Rogalski, T.M., Gilchrist, E.J., Mullen, G.P., Moerman, D.G., 1995. Mutations in the unc-52 gene responsible for body wall muscle defects in adult Caenorhabditis elegans are located in alternatively spliced exons. Genetics 139, 159–169. doi:10.1093/genetics/139.1.159
Rogalski, T.M., Mullen, G.P., Bush, J.A., Gilchrist, E.J., Moerman, D.G., 2001. UNC-52/perlecan isoform diversity and function in Caenorhabditis elegans. Biochem. Soc. Trans. 29, 171–176. doi:10.1042/bst0290171
Sambashivan, S., Freeman, M.R., 2021. SARM1 signaling mechanisms in the injured nervous system. Curr. Opin. Neurobiol. 69, 247–255. doi:10.1016/j.conb.2021.05.004
Sanes, J.R., Lichtman, J.W., 2001. Induction, assembly, maturation and maintenance of a postsynaptic apparatus. Nat. Rev. Neurosci. 2, 791–805. doi:10.1038/35097557
Sanes, J.R., Marshall, L.M., McMahan, U.J., 1978. Reinnervation of muscle fiber basal lamina after removal of myofibers. Differentiation of regenerating axons at original synaptic sites. J. Cell Biol. 78, 176–198. doi:10.1083/jcb.78.1.176
Sarrazin, S., Lamanna, W.C., Esko, J.D., 2011. Heparan sulfate proteoglycans. Cold Spring Harb. Perspect. Biol. 3. doi:10.1101/cshperspect.a004952
Sasaki, Y., Nakagawa, T., Mao, X., DiAntonio, A., Milbrandt, J., 2016. NMNAT1 inhibits axon degeneration via blockade of SARM1-mediated NAD+ depletion. Elife 5. doi:10.7554/eLife.19749
Schaefer, L., Schaefer, R.M., 2010. Proteoglycans: from structural compounds to signaling molecules. Cell Tissue Res. 339, 237–246. doi:10.1007/s00441-009-0821-y
Schmid, A., Hallermann, S., Kittel, R.J., Khorramshahi, O., Frölich, A.M.J., Quentin, C., Rasse, T.M., Mertel, S., Heckmann, M., Sigrist, S.J., 2008. Activity-dependent site-specific changes of glutamate receptor composition in vivo. Nat. Neurosci. 11, 659–666. doi:10.1038/nn.2122
Şentürk, M., Bellen, H.J., 2018. Genetic strategies to tackle neurological diseases in fruit flies. Curr. Opin. Neurobiol. 50, 24–32. doi:10.1016/j.conb.2017.10.017
Siechen, S., Yang, S., Chiba, A., Saif, T., 2009. Mechanical tension contributes to clustering of neurotransmitter vesicles at presynaptic terminals. Proc. Natl. Acad. Sci. USA 106, 12611–12616. doi:10.1073/pnas.0901867106
Siegfried, E., Chou, T.B., Perrimon, N., 1992. wingless signaling acts through zeste-white 3, the Drosophila homolog of glycogen synthase kinase-3, to regulate engrailed and establish cell fate. Cell 71, 1167–1179. doi:10.1016/s0092-8674(05)80065-0
Skeath, J.B., Wilson, B.A., Romero, S.E., Snee, M.J., Zhu, Y., Lacin, H., 2017. The extracellular metalloprotease AdamTS-A anchors neural lineages in place within and preserves the architecture of the central nervous system. Development 144, 3102–3113. doi:10.1242/dev.145854
Stork, T., Engelen, D., Krudewig, A., Silies, M., Bainton, R.J., Klämbt, C., 2008. Organization and function of the blood-brain barrier in Drosophila. J. Neurosci. 28, 587--597.
Tofangchi, A., Fan, A., Saif, M.T.A., 2016. Mechanism of axonal contractility in embryonic drosophila motor neurons in vivo. Biophys. J. 111, 1519–1527. doi:10.1016/j.bpj.2016.08.024

Töpfer, U., Guerra Santillán, K.Y., Fischer-Friedrich, E., Dahmann, C., 2022. Distinct contributions of ECM proteins to basement membrane mechanical properties in Drosophila. Development 149. doi:10.1242/dev.200456

Voigt, A., Pflanz, R., Schäfer, U., Jäckle, H., 2002. Perlecan participates in proliferation activation of quiescent Drosophila neuroblasts. Dev. Dyn. 224, 403–412. doi:10.1002/dvdy.10120

Wang, J.T., Medress, Z.A., Barres, B.A., 2012. Axon degeneration: molecular mechanisms of a self-destruction pathway. J. Cell Biol. 196, 7–18. doi:10.1083/jcb.201108111

Warren, C.R., Kassir, E., Spurlin, J., Martinez, J., Putnam, N.H., Farach-Carson, M.C., 2015. Evolution of the perlecan/HSPG2 gene and its activation in regenerating Nematostella vectensis. PLoS One 10, e0124578. doi:10.1371/journal.pone.0124578

Weiss, S., Clamon, L.C., Manoim, J.E., Ormerod, K.G., Parnas, M., Littleton, J.T., 2022. Glial ER and GAP junction mediated Ca2+ waves are crucial to maintain normal brain excitability. Glia 70, 123–144. doi:10.1002/glia.24092

Yasothornsrikul, S., Davis, W.J., Cramer, G., Kimbrell, D.A., Dearolf, C.R., 1997. viking: identification and characterization of a second type IV collagen in Drosophila. Gene 198, 17–25. doi:10.1016/s0378-1119(97)00274-6

You, J., Zhang, Y., Li, Z., Lou, Z., Jin, L., Lin, X., 2014. Drosophila perlecan regulates intestinal stem cell activity via cell-matrix attachment. Stem Cell Rep. 2, 761–769. doi:10.1016/j.stemcr.2014.04.007

Ellen Guss performed all the work described in this chapter.

Chapter 3

Conclusions and Future Directions

3.1 Conclusions

In this thesis, I have characterized a structural role for the HSPG Perlecan in maintaining the normal ECM environment of the NL that surrounds *Drosophila* larval nerve bundles. Loss of Perlecan disrupts the NL and causes axonal breakage, cytoskeletal disruption and synaptic retraction of motoneurons within the nerve bundle. HSPGs are key components of ECMs and BMs and many of them regulate signaling molecule diffusion and physically provide cues to guide NS development and maturation across phyla (see **Chapter 1**; (Bishop et al., 2007; Condomitti and de Wit, 2018; Dreyfuss et al., 2009; Farach-Carson et al., 2014; Sarrazin et al., 2011). At the *Drosophila* larval NMJ, Perlecan has a previously characterized role regulating cell-cell signaling. Postsynaptically secreted and localized Perlecan ensures the proper balance of the Wg ligand pre- and postsynaptically to prevent ectopic growth of satellite and ghost boutons caused by abnormal Wg diffusion within the synaptic cleft (Kamimura et al., 2013). Perlecan also participates in the development of other aspects of the *Drosophila* NS, from regulating midline crossing of axons to controlling neuroblast proliferation and maintaining the structure of the VNC (Cho et al., 2012; Datta, 1995; Datta and Kankel, 1992; Friedrich et al., 2000; Lindner et al., 2007; Park et al., 2003b, 2003a, 1998; Skeath et al., 2017; Voigt et al., 2002). Despite Perlecan's structural role in other *Drosophila* NS tissues (Skeath et al., 2017), no structural role had previously been described for the protein in the PNS.

Here I establish that Perlecan is required for the maintenance of NMJ synapses through an upstream mechanism where the protein acts within the NL to control axonal stability. In the absence of Perlecan, NMJs contain boutons with postsynaptic material, while presynaptic synaptic vesicle and active zone components are lost. These postsynaptic "footprints" are hallmarks of *Drosophila* NMJ retraction events that have been observed in the absence of other proteins required for synaptic maintenance (Eaton et al., 2002; Eaton and Davis, 2005; Graf et al., 2011; Koch et al., 2008; Massaro et al., 2009; Pielage et al., 2011, 2008, 2005). To eliminate the possibility that synapses were experiencing a failure to develop initially, we assessed morphological and functional growth and activity. $Trol^{null}$ and control synapses had indistinguishable presynaptic area at the 2nd instar larval stage, but $trol^{null}$ synapses failed to grow over the course of 4 days when performing live imaging through the transparent larval cuticle in contrast to control synapses. Intact $trol^{null}$ synapses were also functionally indistinguishable from controls in electrophysiology experiments, but retracted synapses had no detectable physiological

response to stimulation. Together, these data confirmed that NMJ synapses are initially morphologically and functionally normal prior to synaptic retraction. During the deposition of ECM and BM material, Perlecan is delivered later than components such as Laminin (Matsubayashi et al., 2017; Pöschl et al., 2004). In other cellular contexts, Perlecan is often necessary for the maintenance of tissues and cells, rather than their initial development (Costell et al., 1999; Qin et al., 2014; Rogalski et al., 2001, 1995). Thus, this novel role of Perlecan in maintaining NMJ synapses is consistent with both its delivery to the ECM and its known functions in other contexts and species. Although I initially thought Perlecan was likely to act physically at the NMJ itself, my imaging of GFP-tagged Perlecan indicated the protein was primarily present around larval nerves at the NL ECM, and not enriched at the synapse. Subsequent work showed that the NL was disrupted, and that axonal breakage was an early event that preceded synaptic retraction.

Although maintenance of synapses appears to represent a secondary effect due to a structural role for Perlecan within the NL ECM surrounding nerve bundles, it is possible the very small amount of Perlecan on the muscle surface might play a role in how synapses are stabilized through a local action. Prior studies suggest Wg diffusion and signaling is regulated by Perlecan locally at the NMJ and in the developing VNC (Kamimura et al., 2013; Lindner et al., 2007). During presynaptic growth of the larval NMJ, excess presynaptic Wg signaling results in bouton overgrowth in the form of small, clumped satellite boutons (Kamimura et al., 2013). This phenotype was reported in *trol* mutants, suggesting a potential role in the Wg pathway. During my studies of synaptic development of *trol* mutants, I did not observe an abundance of satellite boutons at NMJs as previously described. It is unclear if this represents issues with genetic background between the two studies, or a small number of satellite boutons that perhaps form earlier in development that were missed due to the synaptic retraction I found. However, the Kamimura study did perform EM at the NMJ of *trol* mutants, revealing detachment of the pre- and postsynaptic membranes of the neuronal bouton and muscle membrane, consistent with an early process in the retraction biology I describe (Kamimura et al., 2013). To assay if excess presynaptic Wg signaling could also result in synaptic retraction, I overexpressed a constitutively active form of *Drosophila* Shaggy, the GSK3β homolog, in motoneurons to block presynaptic Wg output. This manipulation of Wg signaling, which Kamimura et al. found could prevent the formation of satellite boutons they observed, was unable to rescue synaptic retraction, confirming that the role

of Perlecan in the context of synapse stabilization is independent of any role it might have in localizing Wg at the synapse (Kamimura et al., 2013). Although we cannot fully rule out a role for Perlecan having a physical role in stabilizing synapses directly at the NMJ, the lack of any enrichment for the protein at the synapse, together with the observation of axonal breaks in larval nerves and the temporally correlated nerve fragmentation and synapse loss in individual hemisegments, argues in favor of an axonal mechanism for synaptic retraction that is triggered when an entire nerve bundle breaks following a catastrophic failure of the NL ECM within that individual nerve bundle.

Perlecan is a secreted component of the ECM which surrounds all cells and can be secreted by numerous cell types in *Drosophila*, including neurons (Bonche et al., 2021; Cho et al., 2012; Isabella and Horne-Badovinac, 2015; Kamimura et al., 2013; Pastor-Pareja and Xu, 2011; Ramos-Lewis and Page-McCaw, 2019; Skeath et al., 2017; You et al., 2014). As such, I sought to identify which cell types secrete Perlecan to regulate synaptic stability at the *Drosophila* NMJ. Despite the use of strong cell type-specific Gal4 drivers and multiple RNAi constructs which eliminate Perlecan expression and function when driven pan-cellularly, elimination of Perlecan secretion from any single cell type (neurons, muscles, glia, fat body, hemocytes) was unable to recapitulate synaptic retraction or to eliminate Perlecan signal in muscles and NMJ-proximal axons. There are some known instances in *Drosophila* where Perlecan secretion from a single cell type is sufficient for its function (Cho et al., 2012; Díaz-Torres et al., 2021; Kamimura et al., 2013; Skeath et al., 2017). In other situations, however, Perlecan is derived from multiple cell types to function in tissue morphogenesis, cell attachment, or other roles (Bonche et al., 2021; You et al., 2014). It appears that the role of Perlecan in stabilizing *Drosophila* synapses and axons falls under the latter category, where multiple sources of Perlecan form the ECM that stabilizes larval nerves and thus, redundant deposition of Perlecan can compensate for its loss in one individual cell type. During other synaptic retraction paradigms at the *Drosophila* NMJ, loss of cell-autonomous cytoskeletal interactors or components result in synapse destabilization (Eaton et al., 2002; Eaton and Davis, 2005; Graf et al., 2011; Koch et al., 2008; Massaro et al., 2009; Pielage et al., 2011, 2008, 2005). Consistent with the idea that multiple sources of Perlecan stabilize motoneuron axonal morphology, overexpression of Perlecan in motoneurons is not sufficient to rescue retraction.

At the *Drosophila* NMJ, Perlecan localizes to the NL which surrounds both axon bundles and individual axons (Edwards et al., 1993; Skeath et al., 2017; Stork et al., 2008). Perlecan also

covers larval body wall muscles at a lower level of protein expression. As a component of ECMs and NL, Perlecan is responsible for providing malleability to these structures, often in contrast to Collagen IV (Costell et al., 1999; Farach-Carson et al., 2014; Pastor-Pareja and Xu, 2011; Qin et al., 2014; Ramos-Lewis and Page-McCaw, 2019; Skeath et al., 2017; Töpfer et al., 2022). In this role, Perlecan often allows tissues to resist mechanical stress and in its absence, tissues may break apart or disorganize due to loss of malleability (Costell et al., 1999). To further test whether a source of muscle-localized Perlecan would allow synapses to withstand the mechanical stress of larval crawling and repeated muscle contraction, I used a hypercontractive allele previously characterized in the lab (Montana and Littleton, 2006, 2004). This allele did not enhance Perlecan-dependent synaptic retraction, nor did it enhance deposition of Perlecan onto the muscle in wild type animals expressing a fluorescently tagged Perlecan protein. Given that muscle-localized Perlecan does not appear to regulate synaptic stability, we assessed the contribution of NL-localized Perlecan. I analyzed the localization and expression of Viking (Vkg), the *Drosophila* Collagen IV homolog. As the other marker of mature ECM, Vkg is delivered late in development like Perlecan and localizes to the NL surrounding axon bundles (Edwards et al., 1993; Matsubayashi et al., 2017; Stork et al., 2008). In the absence of Perlecan, Vkg signal is dramatically disrupted near NMJs and VNC. Vkg signal in $trol^{null}$ NMJ-proximal axon bundles is significantly dimmer than in controls, and orthogonal slices of axon bundles confirm that the NL is very thin in the absence of Perlecan. Near the VNC, the NL protrudes well beyond its usual borders and axonal material also appears disorganized within this new NL boundary. Although Vkg is required for initial Perlecan deposition in ECM (Matsubayashi et al., 2017; Pastor-Pareja and Xu, 2011), it appears that Perlecan is critical for the maintenance of Vkg localization within the NL and for the stability of the NL as a whole. In conjunction with loss of NL stability, synapses in $trol^{null}$ animals retract together with their entire hemisegment, and all MN subtypes are vulnerable to Perlecan-dependent destabilization. These NL phenotypes occur upstream of synapse retraction, as intact and retracted synapses displayed abnormal Vkg signal and NL morphology.

Axons are also under tension throughout development and indeed, maintenance of that tension is important for axonal and synaptic function (Fan et al., 2019, 2017; Siechen et al., 2009; Tofangchi et al., 2016). To assess whether loss of Perlecan and disorganized NL results in disrupted axonal form or function, we assessed axonal morphology and trafficking. Futsch staining revealed that microtubules, normally in long, unbroken tracks through NMJ axons, are broken in

axons and absent from synapses. Further upstream of the synaptic region, entire axon bundles are broken and form disorganized nets of Futsch+ microtubules at either end of the breakage. This disruption occurs well before retraction in the course of larval development, confirming that axons are compromised upstream of synapse instability.

Loss of functional microtubules is the first step in axonal degeneration which proceeds by the well-characterized Wallerian degeneration pathway (Coleman and Höke, 2020; Conforti et al., 2014; Lincoln et al., 2015; Lincoln and Keller, 2016; Llobet Rosell and Neukomm, 2019; Waller, 1850; Wang et al., 2012) and indeed, other proteins which regulate stability of the *Drosophila* NMJ synapse interact with this pathway (Massaro et al., 2009). I drove an RNAi against an upstream component of the pathway, *dSarm*, in *Drosophila* MNs, but this disruption of the Wallerian degeneration pathway was unable to suppress synapse retraction. Although Wallerian degeneration and synapse loss in $trol^{null}$ animals both begin with microtubule degeneration, the pathways are independent of one another downstream.

The data presented in this thesis establish and characterize a novel structural role for the conserved HSPG Perlecan in stabilizing *Drosophila* axons and synapses through its action in the NL ECM, a role that is consistent with functions of Perlecan in other contexts. Future experiments can continue to dissect the molecular mechanisms which underlie Perlecan's ability to stabilize Drosophila MNs and provide additional insights which may be relevant to neurodegeneration or to Perlecan-derived human disease (see below) (Arikawa-Hirasawa et al., 2002, 2001a, 2001b; Bangratz et al., 2012; Farach-Carson et al., 2014; Gubbiotti et al., 2017; Nicole et al., 2000).

3.2 Future Directions

3.2.1 Cell type requirements for Perlecan-dependent axon and synapse stability

In multiple contexts, including development of *Drosophila* wing imaginal discs and attachment of intestinal stem cells to ECM (Bonche et al., 2021; You et al., 2014), Perlecan is secreted by multiple cell types in order to establish BM or ECM. The data described in this thesis suggest that Perlecan is derived from multiple redundant cellular sources in order to establish a functional NL.

During *Drosophila* development, synthesis of BM components occurs in fat body, hemocytes, and cell-autonomously within the cells establishing the BM (Isabella and Horne-Badovinac, 2015). Although we used a *trol* RNAi that eliminates Perlecan signal and function when driven pan-cellularly in conjunction with strong Gal4 drivers to knock down Perlecan secretion from neurons, glia, muscles, fat body, and hemocytes, we were unable to recapitulate the synaptic retraction phenotype that occurs as a result of compromised NL in $trol^{null}$ larvae. Future work should aim to combine multiple drivers in order to assess what combinatorial cell type code is required to deposit Perlecan within the NL. Given that the past work in wing imaginal discs and intestinal stem cells describe a requirement for cell-autonomous and non-cell-autonomous sources of Perlecan (Bonche et al., 2021; You et al., 2014), first efforts should involve combining pan-neuronal or MN-specific Gal4 drivers with hemocyte or fat body Gal4 drivers. Given that glia- and muscle-derived Perlecan also play known roles in *Drosophila* NS development (Kamimura et al., 2013; Skeath et al., 2017), the next round of driver combinations should be glia or muscle Gal4 drivers with hemocyte or fat body Gal4 drivers.

It is possible that none of these combinations of drivers will yield synaptic retraction as witnessed in *trol* mutants and in pan-cellular *trol* knockdown. In that case, it is possible that maternally deposited Perlecan is responsible for establishing NL stability early in embryonic development and that zygotic NL Perlecan is then provided with numerous redundancies that can only be overcome by pan-cellular elimination of translation. *Trol* transcripts are maternally deposited in *Drosophila* embryos and maternal *trol* can compensate for loss of zygotic *trol* in other contexts (Perrimon et al., 1989; Trisnadi and Stathopoulos, 2014). This model could also explain the initial successful development of NMJ synapses in the absence of Perlecan if maternally-supplied transcripts are sufficient during embryonic and early larval development. Indeed, this model may even explain the successful early development of tissues in mammals in the absence of Perlecan, followed quickly by their degradation over the course of maturation (Costell et al., 1999). It is also equally likely, however, that the initial successful formation of synapses is due to late deposition of Perlecan into the NL (Matsubayashi et al., 2017; Pöschl et al., 2004). To parse these two models, maternal Gal4 drivers could be used with the characterized *trol* RNAis to assess if maternally-supplied *trol* is important for its function in MN axons and synapses.

It is also unclear if any one cell type supplies Perlecan that could be sufficient to stabilize axons and/or synapses in *trol* mutants. Due to strong genetic pressure to recombine when *trol* on

X is in a genetic background with balancers on other chromosomes, it was impossible to establish a stable stock with *trol* mutants and muscle, glia, hemocyte, and fat body drivers on II and III. Future work should identify alternative drivers on X to facilitate recombination with the $trol^{null}$ allele and perform rescue experiments. Another alternative is utilizing a multiple-cross scheme in order to combine the $trol^{null}$ allele, driver, and rescue construct in one larva, rather than attempting to create a stock. Together, these future experiments will provide valuable insights into which cells are necessary and sufficient for Perlecan to establish a stable NL throughout larval development.

3.2.2 Interaction of Perlecan with known synaptic stability regulators at the *Drosophila* NMJ

Numerous components of the larval MN cytoskeleton are required for NMJ synapse stability (Eaton et al., 2002; Eaton and Davis, 2005; Graf et al., 2011; Massaro et al., 2009; Pielage et al., 2011, 2008, 2005). Although Perlecan is not required cell-autonomously to stabilize synapses itself, it seems likely that loss of Perlecan and compromise of the NL may destabilize some of these known regulators of synaptic stability, particularly given the massive disruptions in the microtubule cytoskeleton and axons in $trol^{null}$ larvae. Future experiments should attempt to determine which, if any, known NMJ stability regulators are involved in Perlecan-dependent synaptic retraction.

I have undertaken some preliminary work to address these open questions. First, loss of Perlecan results in a significant reduction of β-Spectrin signal surrounding intact $trol^{null}$ synaptic boutons (**Figure 1A,B**). This reduction is consistent with the decrease in bouton-localized spectrin cytoskeleton noted in mutants for *Drosophila* homologs of human neurodegeneration genes like Presenilin (Restrepo et al., 2022). Interestingly, however, α-Spectrin signal is not reduced in $trol^{null}$ larvae (**Figure 1C,D**). Preliminary rescue experiments indicate that MN-driven overexpression of components of the spectrin cytoskeleton and the microtubule interactor dLIMK1 are not sufficient to suppress synaptic retraction (**Figure 1E-I**), suggesting either that increased supply of cytoskeletal components and binding partners is not sufficient to protect axons from the massive defects that precede synaptic instability or that loss of β-Spectrin around boutons is merely a harbinger of retraction, rather than an indicator of mechanistic interaction. Future work should

analyze *trans*-heterozygous animals with one copy of *trol*^{null} and one copy of mutants known to regulate synaptic stability to fully rule out any genetic interactions.

3.2.3 The role of glia in Perlecan-dependent axon and synapse stability

The *Drosophila* NL surrounds the VNC and peripheral nerves and performs a protective role in preventing inappropriate signaling and cell-cell contacts, immune insults, and other dangers (Edwards et al., 1993; Skeath et al., 2017; Stork et al., 2008). The NL is aided in this role by three layers of glia in between the NL and the neurons that act as the *Drosophila* equivalent of the BBB (Edwards et al., 1993; Hunter et al., 2020; Matzat et al., 2015; Meyer et al., 2014; Skeath et al., 2017; Stork et al., 2008). Given the severe disruptions of neuronal material and NL in the axon bundles of *trol*^{null} larvae, it would be shocking if the glial layers in between axons and the NL were left unscathed. In fact, these layers of glia could be playing an active role in stabilizing or destabilizing axons and synapses by interacting with the NL.

During the development of the VNC, the organ undergoes condensation, where it pulls back from covering the entire ventral embryonic surface to occupying a small number of segments in the larvae, a process which is dependent upon the glial layers in between the NL and the neuropil (Meyer et al., 2014; Olofsson and Page, 2005; Page and Olofsson, 2008). Perlecan itself plays a role in proper VNC condensation (Pastor-Pareja and Xu, 2011; Skeath et al., 2017), suggesting that a Perlecan-glia interaction is necessary for normal development of *Drosophila* NS material. Previous work has established that one class of ECM receptors, the Integrins, are critical in glia in order to drive this VNC condensation (Bittern et al., 2021; Brown, 1994; Hunter et al., 2020; Meyer et al., 2014; Xie and Auld, 2011). Together, this previous work implies that Perlecan interactions with glial Integrins may be important for maintaining MN axons and synapses during larval development. Indeed, Perlecan is already known to bind Integrin subunits in other contexts (Cho et al., 2012; You et al., 2014; Yurchenco, 2011). Future work should absolutely aim to further understand this potential connection.

First, a systematic review of glial morphology in *trol*^{null} larvae should be performed. By driving fluorescent markers with pan-glial Gal4 constructs or available glial subtype-specific constructs, glial deficits along the axon bundle can be examined. Next, the potential role for

Integrin proteins in this biology should be assessed. Preliminarily, I did quantify a significant reduction in Myospheroid, a *Drosophila* β-Integrin at intact synapses in $trol^{null}$ larvae (**Figure 2A,B**). Future work should focus on expression of that protein and other Integrin subunits around axon bundles, where NL and neurons are compromised and glia are localized. Although glia can send processes into the synaptic region of the NMJ (Brink et al., 2012), it is not likely that these transient processes into individual synapses would be responsible for synapse-wide Integrin signal or broken axon bundles seen in $trol^{null}$ larvae. Should it appear that glial-derived Integrins are critical for synaptic stability downstream of Perlecan, specific manipulations of Integrin levels in glia should be performed (e.g. glia-specific Integrin RNAi to recapitulate retraction, glia-specific Integrin overexpression to rescue of $trol^{null}$ retraction) to confirm both the direct involvement of glia in axon and synapse stabilization and the interaction between Perlecan and Integrin subtypes.

It is also possible that glia in the absence of Perlecan play an actively destructive role in axons after NL breakdown. Glia in *Drosophila* express the phagocytic/engulfment receptor Draper, which can serve to clear damaged neuronal material after axon breakage or other injuries (Lu et al., 2017; MacDonald et al., 2006; Purice et al., 2017, 2016). Overactive Draper signaling can also result in neurodegeneration independent of initial injury (Hakim-Mishnaevski et al., 2019). Future work should assess whether $trol^{null}$ glia have upregulated Draper expression or overactive expression of other phagocytic proteins, causing glia to destroy MN axons following NL disruption.

3.2.4 Potential roles for canonical cell-cell signaling pathways in Perlecan-dependent axon and synapse stability

The data in this thesis are consistent with a structural role for Perlecan in maintaining the normal architecture of the NL and consequently maintaining axon and synapse stability. Perlecan and other HPSGs can, however, bind to a wealth of cell-cell signaling molecules (Bishop et al., 2007; Dreyfuss et al., 2009; Sarrazin et al., 2011), suggesting that Perlecan-specific localization of a ligand or receptor that functions to stabilize MNs should not be completely excluded without experimentation. Perhaps most promising are members of the FGF family, since HS chains bind FGF proteins with high affinity (Sarrazin et al., 2011; Schlessinger et al., 2000). There are established roles for Perlecan-dependent FGF localization and signaling in *Drosophila* and

vertebrate NS development (Girós et al., 2007; Kerever et al., 2014; Lindner et al., 2007; Mashayekhi et al., 2011; Park et al., 2003b). FGF signaling through its receptor Heartless in *Drosophila* controls glial maturation and axon wrapping (Muha and Müller, 2013). To assess whether FGF signaling is also important for maintaining axonal and synaptic integrity of larval MNs, I would first want to assess protein levels of FGF ligands and receptors in $trol^{null}$ axons, synapses, and NL. If disruption of the localization or expression of these components occurs in the absence of Perlecan, I would proceed with genetic interaction assessments and cell-specific knockdown or rescue with FGF ligands and receptors.

3.3 Materials and Methods

Drosophila stocks

Flies were maintained at 18-25°C and cultured on standard medium. 3rd instar larvae were used for all experiments in this chapter. Larvae lacking Perlecan were collected at 1st or 2nd instar stage (separate from wild type counterparts) and placed on petri dishes containing standard medium to facilitate survival to 3rd instar stage. Male and female larvae were used depending upon genetic background; see figure legends for genotypes. Canton-S was used as the wild type background. Other fly strains used: $trol^{null}$ (Voigt et al., 2002; provided by Brian Stramer and Yutaka Matsubayashi), *vGlut*-Gal4 (provided by Aaron DiAntonio), UAS-*β-Spectrin* (provided by Tom Hays), and UPS-*α-Spectrin* (BDSC #32005).

Immunocytochemistry

3rd instar larvae were filleted in Ca^{2+}-free HL3.1 solution (in mM: 70 NaCl, 5 KCl, 4 $MgCl_2$, 10 $NaHCO_3$, 5 trehalose, 115 sucrose, 5 HEPES, pH 7.18) and fixed in 4% paraformaldehyde for 15 minutes, washed in Ca^{2+} -free HL3.1 twice and 0.1-PBT (1x PBS with 0.1% Triton X-100) once, then blocked in 5% normal goat serum (NGS) in 0.5-PBT (1x PBS with 0.5% Triton X-100) for 30 minutes at room temperature or overnight at 4°C. Samples were incubated overnight at 4°C in blocking solution containing primary antibodies, and then washed three times with 0.1-PBT. Samples were incubated for 2 hours at room temperature in blocking solution containing fluorophore-conjugated secondary antibodies. Primary antibodies used in this chapter were mouse anti-α-Spectrin at 1:50 (3A9 DSHB, Iowa City, IA), rabbit anti-β-Spectrin at 1:500 (Byers et al., 1989), rabbit anti-Cpx at 1:5000 (Huntwork and Littleton, 2007), mouse anti-Dlg at 1:500 (4F3

DSHB, Iowa City, IA), and mouse anti-Mys at 1:500 (CF.6G11 DSHB, Iowa City, IA). Secondary antibodies used in this study were goat anti-mouse Alexa Fluor 488-conjugated IgG at 1:500 (#A-32723, Thermo Fisher Scientific, Waltham, MA) and goat anti-rabbit Alexa Fluor 568-conjugated IgG at 1:500 (#A-11011, Thermo Fisher Scientific, Waltham, MA). For Hrp staining, samples were incubated in DyLight 649 conjugated Hrp at 1:500 (#123-605-021, Jackson ImmunoResearch Laboratories, West Grove, PA, USA). Samples were mounted in Vectashield Vibrance hard setting antifade mounting medium (#H-1700, Vector Laboratories, Burlingame, CA).

Confocal imaging and imaging data analysis

Images of NMJs were acquired on a Zeiss Pascal confocal microscope (Carl Zeiss Microscopy, Zena, Germany) using a 63X Zeiss pan-APOCHROMAT oil-immersion objective with a 1.3 NA. 3D image stacks were merged into a maximum intensity projection using Zen (Zeiss) software. Abdominal segments and muscle numbers imaged are listed in figure legends. Boutons were counted manually using the Dlg antibody signal. Mean fluorescence intensity was calculated using Volocity 3D Image Analysis software (PerkinElmer) from the maximum intensity projection using the "Find Objects" algorithm in Volocity 3.2 or 5 software with an Hrp threshold that identified synaptic area in all genotypes.

Statistical analysis

Graphing and statistical analysis were performed using GraphPad Prism (San Diego, CA, USA). For comparisons between two groups, statistical significance was determined using a Student's t-test. For comparisons between three groups, statistical significance was determined using a one-way ANOVA followed by multiple comparisons with p-values corrected for multiple hypothesis testing using either Tukey or Šidák multiple comparisons tests (individual test chosen based on Prism recommendation). Figures depict the mean of each distribution and individual data points. *N* indicates the number of individual NMJs analyzed unless otherwise noted. Number of larvae per group, mean ± SEM, *n*, and the p values are indicated in figure legends. Asterisks in the figures denote p-values of: *, $p \leq 0.05$; **, $p \leq 0.01$; ***, $p \leq 0.001$; and ****, $p \leq 0.0001$.

Figures

Figure 1

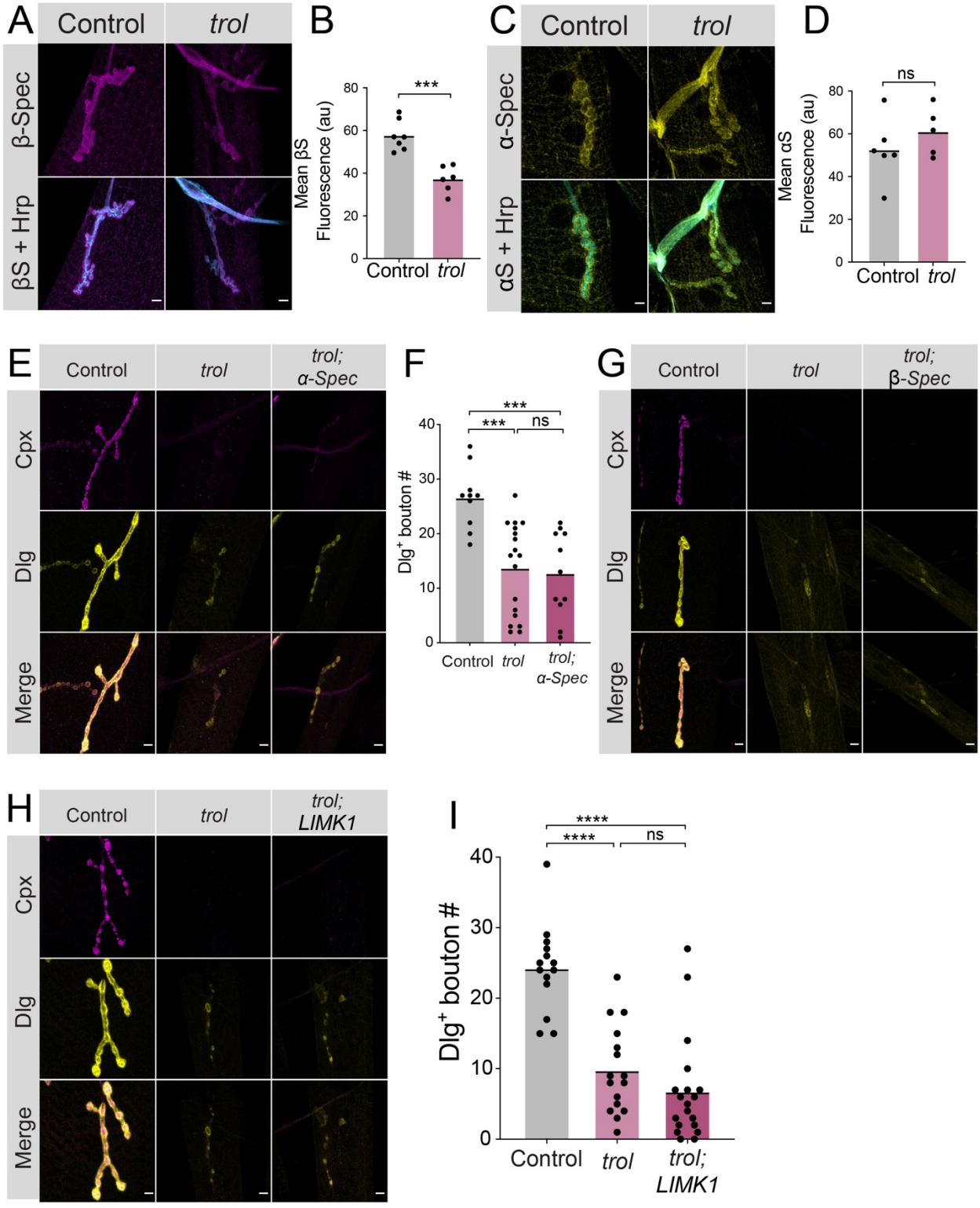
A
Control
trol
β-Spec
βS + Hrp
B
Mean βS Fluorescence (au)
***
Control
trol
C
Control
trol
α-Spec
αS + Hrp
D
Mean αS Fluorescence (au)
ns
Control
trol
E
Control
trol
trol; α-Spec
Cpx
Dlg
Merge
F
Dlg+ bouton #
***
***
ns
Control
trol
trol; α-Spec
G
Control
trol
trol; β-Spec
Cpx
Dlg
Merge
H
Control
trol
trol; LIMK1
Cpx
Dlg
Merge
I
Dlg+ bouton #
****
****
ns
Control
trol
trol; LIMK1

Figure 1. Perlecan may interact with known cytoskeletal regulators of synaptic stability.
(**A**) Representative images of muscle 4 NMJs in control (CS, left panel) and *trol*^{null} (*trol*^{null}*/y;+;+*) larvae stained for β-Spectrin (magenta) and Hrp (cyan). (**B**) Quantification of mean fluorescence intensity of β-Spectrin signal from control and intact *trol* muscle 4 NMJs at abdominal segment A3 or A4. Each point represents the mean intensity at one NMJ, with mean intensity indicated with the solid black line. Quantification of fluorescence intensity: control: 57.68 ± 2.713, 7 NMJs from 3 larvae; *trol*: 37.28 ± 2.510, 6 NMJs from 3 larvae, p<0.001. (**C**) Representative images of muscle 4 NMJs in control (CS, left panel) and *trol*^{null} (*trol*^{null}*/y;+;+*) larvae stained for α-Spectrin (yellow) and Hrp (cyan). (**D**) Quantification of mean fluorescence intensity of α-Spectrin signal from control and intact *trol* muscle 4 NMJs at abdominal segment A3 or A4. Each point represents the mean intensity at one NMJ, with mean intensity indicated with the solid black line. Quantification of fluorescence intensity: control: 52.78 ± 6.049, 6 NMJs from 3 larvae; *trol*: 60.99 ± 5.047, 5 NMJs from 3 larvae, p = 0.3367. (**E**) Representative images of muscle 4 NMJs in control (*+;+;UPS-α–Spectrin/+*, left panel), *trol* (*trol*^{null}*/y;+;+*, middle panel), and *trol, α-Spec* (*trol*^{null}*/y;+;UPS-α-Spectrin/+*, right panel) larvae stained for Cpx (magenta) and Dlg (yellow). Images indicate retracted synapses despite ubiquitous overexpression of α-Spectrin in the *trol* genetic background. (**F**) Quantification of Dlg+ Ib bouton number from control, *trol,* and *trol, α-Spec* muscle 4 NMJs from abdominal segment A4. Each point represents the number of boutons at one NMJ, with mean bouton number indicated with the solid black line. Quantification of bouton number: control: 26.5 ± 1.778, 10 NMJs from 5 larvae; *trol*: 13.61 ± 1.977, 18 NMJs from 9 larvae, p<0.001; *trol, α-Spec*: 12.64 ± 2.352, 11 NMJs from 6 larvae; p<0.001 compared to control; p = 0.9403 compared to *trol*. (**G**) Representative images of muscle 4 NMJs in control (*+;+;UAS-β-Spectrin/+*, left panel), *trol* (*trol*^{null}*,vGlut-Gal4/y;+;+*, middle panel), and *trol, β-Spec* (*trol*^{null}*, vGlut-Gal4/y;+;UAS-β-Spectrin/+*, right panel) larvae stained for Cpx (magenta) and Dlg (yellow). Images indicated retracted synapses despite overexpression of β-Spectrin in MNs in the *trol* genetic background. (**H**) Representative images of muscle 4 NMJs in control (*+;+;UAS-dLIMK1/+*, left panel), *trol* (*trol*^{null}*,vGlut-Gal4/y;+;+*, middle panel), and *trol, LIMK1* (*trol*^{null}*, vGlut-Gal4/y;+;UAS-dLIMK1/+*, right panel) larvae stained for Cpx (magenta) and Dlg (yellow). Images indicated retracted synapses despite overexpression of dLIMK1 in MNs in the *trol* genetic background. (**I**) Quantification of Dlg+ Ib bouton number from control, *trol,* and *trol, LIMK1*

muscle 4 NMJs from abdominal segment A4. Each point represents the number of boutons at one NMJ, with mean bouton number indicated with the solid black line. Quantification of bouton number: control: 24.21 ± 1.651, 14 NMJs from 7 larvae; *trol*: 9.750 ± 1.564, 16 NMJs from 9 larvae, $p<0.0001$; *trol, LIMK1*: 6.737 ± 1.693, 19 NMJs from 10 larvae; $p<0.0001$ compared to control; $p = 0.4713$ compared to *trol*. All scale bars in (**A**), (**C**), (**E**), (**G**), and (**H**) are 5 μm.

Figure 2

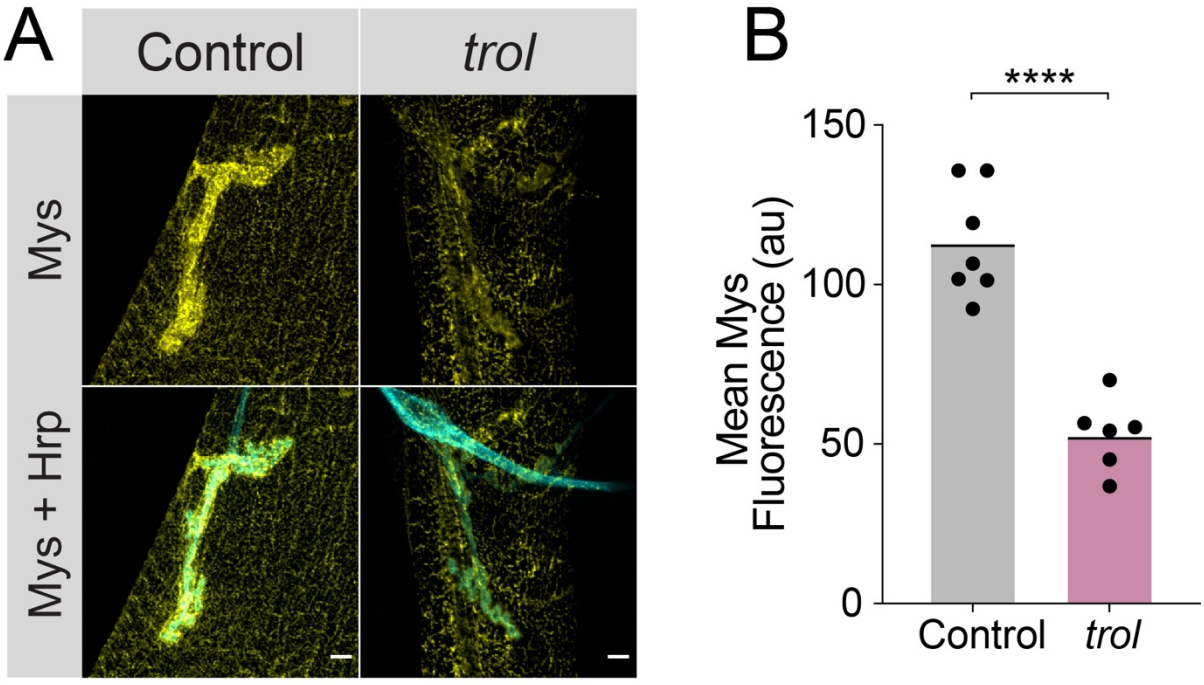
A
Control
trol
Mys
Mys + Hrp
B
****
Mean Mys Fluorescence (au)
150
100
50
0
Control
trol

Figure 2. The β-Integrin Myospheroid is reduced in *trol*^{null} synapses.

(**A**) Representative images of muscle 4 NMJs in control (CS, left panel) and *trol*^{null} (*trol*^{null}*/y;+;+*) larvae stained for Myospheroid (yellow) and Hrp (cyan). Scale bars are 5 μm. (**B**) Quantification of mean fluorescence intensity of Myospheroid signal from control and intact *trol* muscle 4 NMJs at abdominal segment A3 or A4. Each point represents the mean intensity at one NMJ, with mean intensity indicated with the solid black line. Quantification of fluorescence intensity: control: 113.6 ± 6.581, 7 NMJs from 3 larvae; *trol*: 52.99 ± 4.594, 6 NMJs from 3 larvae, $p<0.0001$.

References

Arikawa-Hirasawa, E., Le, A.H., Nishino, I., Nonaka, I., Ho, N.C., Francomano, C.A., Govindraj, P., Hassell, J.R., Devaney, J.M., Spranger, J., Stevenson, R.E., Iannaccone, S., Dalakas, M.C., Yamada, Y., 2002. Structural and functional mutations of the perlecan gene cause Schwartz-Jampel syndrome, with myotonic myopathy and chondrodysplasia. Am. J. Hum. Genet. 70, 1368–1375. doi:10.1086/340390

Arikawa-Hirasawa, E., Wilcox, W.R., Le, A.H., Silverman, N., Govindraj, P., Hassell, J.R., Yamada, Y., 2001a. Dyssegmental dysplasia, Silverman-Handmaker type, is caused by functional null mutations of the perlecan gene. Nat. Genet. 27, 431–434. doi:10.1038/86941

Arikawa-Hirasawa, E., Wilcox, W.R., Yamada, Y., 2001b. Dyssegmental dysplasia, Silverman-Handmaker type: unexpected role of perlecan in cartilage development. Am. J. Med. Genet. 106, 254–257. doi:10.1002/ajmg.10229

Bangratz, M., Sarrazin, N., Devaux, J., Zambroni, D., Echaniz-Laguna, A., René, F., Boërio, D., Davoine, C.-S., Fontaine, B., Feltri, M.L., Benoit, E., Nicole, S., 2012. A mouse model of Schwartz-Jampel syndrome reveals myelinating Schwann cell dysfunction with persistent axonal depolarization in vitro and distal peripheral nerve hyperexcitability when perlecan is lacking. Am. J. Pathol. 180, 2040–2055. doi:10.1016/j.ajpath.2012.01.035

Bishop, J.R., Schuksz, M., Esko, J.D., 2007. Heparan sulphate proteoglycans fine-tune mammalian physiology. Nature 446, 1030–1037. doi:10.1038/nature05817

Bittern, J., Pogodalla, N., Ohm, H., Brüser, L., Kottmeier, R., Schirmeier, S., Klämbt, C., 2021. Neuron-glia interaction in the Drosophila nervous system. Dev. Neurobiol. 81, 438–452. doi:10.1002/dneu.22737

Bonche, R., Chessel, A., Boisivon, S., Smolen, P., Thérond, P., Pizette, S., 2021. Two different sources of Perlecan cooperate for its function in the basement membrane of the Drosophila wing imaginal disc. Dev. Dyn. 250, 542–561. doi:10.1002/dvdy.274

Brink, D.L., Gilbert, M., Xie, X., Petley-Ragan, L., Auld, V.J., 2012. Glial processes at the Drosophila larval neuromuscular junction match synaptic growth. PLoS One 7, e37876. doi:10.1371/journal.pone.0037876

Brown, N.H., 1994. Null mutations in the alpha PS2 and beta PS integrin subunit genes have distinct phenotypes. Development 120, 1221–1231. doi:10.1242/dev.120.5.1221

Byers, T.J., Husain-Chishti, A., Dubreuil, R.R., Branton, D., Goldstein, L.S., 1989. Sequence similarity of the amino-terminal domain of Drosophila beta spectrin to alpha actinin and dystrophin. J. Cell Biol. 109, 1633–1641. doi:10.1083/jcb.109.4.1633

Cho, J.Y., Chak, K., Andreone, B.J., Wooley, J.R., Kolodkin, A.L., 2012. The extracellular matrix proteoglycan perlecan facilitates transmembrane semaphorin-mediated repulsive guidance. Genes Dev. 26, 2222–2235. doi:10.1101/gad.193136.112

Coleman, M.P., Höke, A., 2020. Programmed axon degeneration: from mouse to mechanism to medicine. Nat. Rev. Neurosci. 21, 183–196. doi:10.1038/s41583-020-0269-3

Condomitti, G., de Wit, J., 2018. Heparan sulfate proteoglycans as emerging players in synaptic specificity. Front. Mol. Neurosci. 11, 14. doi:10.3389/fnmol.2018.00014

Conforti, L., Gilley, J., Coleman, M.P., 2014. Wallerian degeneration: an emerging axon death pathway linking injury and disease. Nat. Rev. Neurosci. 15, 394–409. doi:10.1038/nrn3680

Costell, M., Gustafsson, E., Aszódi, A., Mörgelin, M., Bloch, W., Hunziker, E., Addicks, K., Timpl, R., Fässler, R., 1999. Perlecan maintains the integrity of cartilage and some basement membranes. J. Cell Biol. 147, 1109–1122. doi:10.1083/jcb.147.5.1109

Datta, S., 1995. Control of proliferation activation in quiescent neuroblasts of the Drosophila central nervous system. Development 121, 1173–1182. doi:10.1242/dev.121.4.1173

Datta, S., Kankel, D.R., 1992. l(1)trol and l(1)devl, loci affecting the development of the adult central nervous system in Drosophila melanogaster. Genetics 130, 523–537.

Díaz-Torres, A., Rosales-Nieves, A.E., Pearson, J.R., Santa-Cruz Mateos, C., Marín-Menguiano, M., Marshall, O.J., Brand, A.H., González-Reyes, A., 2021. Stem cell niche organization in the Drosophila ovary requires the ECM component Perlecan. Curr. Biol. 31, 1744–1753.e5. doi:10.1016/j.cub.2021.01.071

Dreyfuss, J.L., Regatieri, C.V., Jarrouge, T.R., Cavalheiro, R.P., Sampaio, L.O., Nader, H.B., 2009. Heparan sulfate proteoglycans: structure, protein interactions and cell signaling. An. Acad. Bras. Cienc. 81, 409–429. doi:10.1590/s0001-37652009000300007

Eaton, B.A., Davis, G.W., 2005. LIM Kinase1 controls synaptic stability downstream of the type II BMP receptor. Neuron 47, 695–708. doi:10.1016/j.neuron.2005.08.010

Eaton, B.A., Fetter, R.D., Davis, G.W., 2002. Dynactin is necessary for synapse stabilization. Neuron 34, 729–741. doi:10.1016/s0896-6273(02)00721-3

Edwards, J.S., Swales, L.S., Bate, M., 1993. The differentiation between neuroglia and connective tissue sheath in insect ganglia revisited: the neural lamella and perineurial sheath cells are absent in a mesodermless mutant of Drosophila. J. Comp. Neurol. 333, 301–308. doi:10.1002/cne.903330214

Fan, A., Joy, M.S.H., Saif, T., 2019. A connected cytoskeleton network generates axonal tension in embryonic Drosophila. Lab Chip 19, 3133–3139. doi:10.1039/c9lc00243j

Fan, A., Tofangchi, A., Kandel, M., Popescu, G., Saif, T., 2017. Coupled circumferential and axial tension driven by actin and myosin influences in vivo axon diameter. Sci. Rep. 7, 14188. doi:10.1038/s41598-017-13830-1

Farach-Carson, M.C., Warren, C.R., Harrington, D.A., Carson, D.D., 2014. Border patrol: insights into the unique role of perlecan/heparan sulfate proteoglycan 2 at cell and tissue borders. Matrix Biol 34, 64–79. doi:10.1016/j.matbio.2013.08.004

Friedrich, M.V., Schneider, M., Timpl, R., Baumgartner, S., 2000. Perlecan domain V of Drosophila melanogaster. Sequence, recombinant analysis and tissue expression. Eur. J. Biochem. 267, 3149–3159. doi:10.1046/j.1432-1327.2000.01337.x

Girós, A., Morante, J., Gil-Sanz, C., Fairén, A., Costell, M., 2007. Perlecan controls neurogenesis in the developing telencephalon. BMC Dev. Biol. 7, 29. doi:10.1186/1471-213X-7-29

Graf, E.R., Heerssen, H.M., Wright, C.M., Davis, G.W., DiAntonio, A., 2011. Stathmin is required for stability of the Drosophila neuromuscular junction. J. Neurosci. 31, 15026–15034. doi:10.1523/JNEUROSCI.2024-11.2011

Gubbiotti, M.A., Neill, T., Iozzo, R.V., 2017. A current view of perlecan in physiology and pathology: A mosaic of functions. Matrix Biol 57–58, 285–298. doi:10.1016/j.matbio.2016.09.003

Hakim-Mishnaevski, K., Flint-Brodsly, N., Shklyar, B., Levy-Adam, F., Kurant, E., 2019. Glial phagocytic receptors promote neuronal loss in adult drosophila brain. Cell Rep. 29, 1438–1448.e3. doi:10.1016/j.celrep.2019.09.086

Hunter, A.C., Petley-Ragan, L.M., Das, M., Auld, V.J., 2020. Basigin Associates with Integrin in

Order to Regulate Perineurial Glia and Drosophila Nervous System Morphology. J. Neurosci. 40, 3360–3373. doi:10.1523/JNEUROSCI.1397-19.2020
Huntwork, S., Littleton, J.T., 2007. A complexin fusion clamp regulates spontaneous neurotransmitter release and synaptic growth. Nat. Neurosci. 10, 1235–1237. doi:10.1038/nn1980
Isabella, A.J., Horne-Badovinac, S., 2015. Building from the Ground up: Basement Membranes in Drosophila Development. Curr Top Membr 76, 305–336. doi:10.1016/bs.ctm.2015.07.001
Kamimura, K., Ueno, K., Nakagawa, J., Hamada, R., Saitoe, M., Maeda, N., 2013. Perlecan regulates bidirectional Wnt signaling at the Drosophila neuromuscular junction. J. Cell Biol. 200, 219–233. doi:10.1083/jcb.201207036
Kerever, A., Mercier, F., Nonaka, R., de Vega, S., Oda, Y., Zalc, B., Okada, Y., Hattori, N., Yamada, Y., Arikawa-Hirasawa, E., 2014. Perlecan is required for FGF-2 signaling in the neural stem cell niche. Stem Cell Res. 12, 492–505. doi:10.1016/j.scr.2013.12.009
Koch, I., Schwarz, H., Beuchle, D., Goellner, B., Langegger, M., Aberle, H., 2008. Drosophila ankyrin 2 is required for synaptic stability. Neuron 58, 210–222. doi:10.1016/j.neuron.2008.03.019
Lincoln, B.L., Alabsi, S.H., Frendo, N., Freund, R., Keller, L.C., 2015. Drosophila neuronal injury follows a temporal sequence of cellular events leading to degeneration at the neuromuscular junction. J. Exp. Neurosci. 9, 1–9. doi:10.4137/JEN.S25516
Lincoln, B.L., Keller, L.C., 2016. Drosophila neuronal injury model allows for temporal dissection of neurodegenerative events. Neural Regen. Res. 11, 416–417. doi:10.4103/1673-5374.179046
Lindner, J.R., Hillman, P.R., Barrett, A.L., Jackson, M.C., Perry, T.L., Park, Y., Datta, S., 2007. The Drosophila Perlecan gene trol regulates multiple signaling pathways in different developmental contexts. BMC Dev. Biol. 7, 121. doi:10.1186/1471-213X-7-121
Llobet Rosell, A., Neukomm, L.J., 2019. Axon death signalling in Wallerian degeneration among species and in disease. Open Biol 9, 190118. doi:10.1098/rsob.190118
Lu, T.-Y., MacDonald, J.M., Neukomm, L.J., Sheehan, A.E., Bradshaw, R., Logan, M.A., Freeman, M.R., 2017. Axon degeneration induces glial responses through Draper-TRAF4-JNK signalling. Nat. Commun. 8, 14355. doi:10.1038/ncomms14355
MacDonald, J.M., Beach, M.G., Porpiglia, E., Sheehan, A.E., Watts, R.J., Freeman, M.R., 2006. The Drosophila cell corpse engulfment receptor Draper mediates glial clearance of severed axons. Neuron 50, 869–881. doi:10.1016/j.neuron.2006.04.028
Mashayekhi, F., Sadeghi, M., Rajaei, F., 2011. Induction of perlecan expression and neural cell proliferation by FGF-2 in the developing cerebral cortex: an in vivo study. J. Mol. Neurosci. 45, 87–93. doi:10.1007/s12031-010-9393-2
Massaro, C.M., Pielage, J., Davis, G.W., 2009. Molecular mechanisms that enhance synapse stability despite persistent disruption of the spectrin/ankyrin/microtubule cytoskeleton. J. Cell Biol. 187, 101–117. doi:10.1083/jcb.200903166
Matsubayashi, Y., Louani, A., Dragu, A., Sánchez-Sánchez, B.J., Serna-Morales, E., Yolland, L., Gyoergy, A., Vizcay, G., Fleck, R.A., Heddleston, J.M., Chew, T.-L., Siekhaus, D.E., Stramer, B.M., 2017. A moving source of matrix components is essential for de novo basement membrane formation. Curr. Biol. 27, 3526–3534.e4. doi:10.1016/j.cub.2017.10.001
Matzat, T., Sieglitz, F., Kottmeier, R., Babatz, F., Engelen, D., Klämbt, C., 2015. Axonal

wrapping in the Drosophila PNS is controlled by glia-derived neuregulin homolog Vein. Development 142, 1336–1345. doi:10.1242/dev.116616
Meyer, S., Schmidt, I., Klämbt, C., 2014. Glia ECM interactions are required to shape the Drosophila nervous system. Mech. Dev. 133, 105–116. doi:10.1016/j.mod.2014.05.003
Montana, E.S., Littleton, J.T., 2004. Characterization of a hypercontraction-induced myopathy in Drosophila caused by mutations in Mhc. J. Cell Biol. 164, 1045–1054. doi:10.1083/jcb.200308158
Montana, E.S., Littleton, J.T., 2006. Expression profiling of a hypercontraction-induced myopathy in Drosophila suggests a compensatory cytoskeletal remodeling response. J. Biol. Chem. 281, 8100–8109. doi:10.1074/jbc.M512468200
Muha, V., Müller, H.-A.J., 2013. Functions and Mechanisms of Fibroblast Growth Factor (FGF) Signalling in Drosophila melanogaster. Int. J. Mol. Sci. 14, 5920–5937. doi:10.3390/ijms14035920
Nicole, S., Davoine, C.S., Topaloglu, H., Cattolico, L., Barral, D., Beighton, P., Hamida, C.B., Hammouda, H., Cruaud, C., White, P.S., Samson, D., Urtizberea, J.A., Lehmann-Horn, F., Weissenbach, J., Hentati, F., Fontaine, B., 2000. Perlecan, the major proteoglycan of basement membranes, is altered in patients with Schwartz-Jampel syndrome (chondrodystrophic myotonia). Nat. Genet. 26, 480–483. doi:10.1038/82638
Olofsson, B., Page, D.T., 2005. Condensation of the central nervous system in embryonic Drosophila is inhibited by blocking hemocyte migration or neural activity. Dev. Biol. 279, 233–243. doi:10.1016/j.ydbio.2004.12.020
Page, D.T., Olofsson, B., 2008. Multiple roles for apoptosis facilitating condensation of the Drosophila ventral nerve cord. Genesis 46, 61–68. doi:10.1002/dvg.20365
Park, Y., Fujioka, M., Jaynes, J.B., Datta, S., 1998. Drosophila homeobox geneeve enhancestrol, an activator of neuroblast proliferation in the larval CNS. Dev. Genet. 23, 247–257. doi:10.1002/(SICI)1520-6408(1998)23:3<247::AID-DVG9>3.0.CO;2-I
Park, Y., Ng, C., Datta, S., 2003a. Induction of string rescues the neuroblast proliferation defect in trol mutant animals. Genesis 36, 187–195. doi:10.1002/gene.10216
Park, Y., Rangel, C., Reynolds, M.M., Caldwell, M.C., Johns, M., Nayak, M., Welsh, C.J.R., McDermott, S., Datta, S., 2003b. Drosophila perlecan modulates FGF and hedgehog signals to activate neural stem cell division. Dev. Biol. 253, 247–257. doi:10.1016/s0012-1606(02)00019-2
Pastor-Pareja, J.C., Xu, T., 2011. Shaping cells and organs in Drosophila by opposing roles of fat body-secreted Collagen IV and perlecan. Dev. Cell 21, 245–256. doi:10.1016/j.devcel.2011.06.026
Perrimon, N., Engstrom, L., Mahowald, A.P., 1989. Zygotic lethals with specific maternal effect phenotypes in Drosophila melanogaster. I. Loci on the X chromosome. Genetics 121, 333–352. doi:10.1093/genetics/121.2.333
Pielage, J., Bulat, V., Zuchero, J.B., Fetter, R.D., Davis, G.W., 2011. Hts/Adducin controls synaptic elaboration and elimination. Neuron 69, 1114–1131. doi:10.1016/j.neuron.2011.02.007
Pielage, J., Cheng, L., Fetter, R.D., Carlton, P.M., Sedat, J.W., Davis, G.W., 2008. A presynaptic giant ankyrin stabilizes the NMJ through regulation of presynaptic microtubules and transsynaptic cell adhesion. Neuron 58, 195–209. doi:10.1016/j.neuron.2008.02.017
Pielage, J., Fetter, R.D., Davis, G.W., 2005. Presynaptic spectrin is essential for synapse stabilization. Curr. Biol. 15, 918–928. doi:10.1016/j.cub.2005.04.030

Pöschl, E., Schlötzer-Schrehardt, U., Brachvogel, B., Saito, K., Ninomiya, Y., Mayer, U., 2004. Collagen IV is essential for basement membrane stability but dispensable for initiation of its assembly during early development. Development 131, 1619–1628. doi:10.1242/dev.01037

Purice, M.D., Ray, A., Münzel, E.J., Pope, B.J., Park, D.J., Speese, S.D., Logan, M.A., 2017. A novel Drosophila injury model reveals severed axons are cleared through a Draper/MMP-1 signaling cascade. Elife 6. doi:10.7554/eLife.23611

Purice, M.D., Speese, S.D., Logan, M.A., 2016. Delayed glial clearance of degenerating axons in aged Drosophila is due to reduced PI3K/Draper activity. Nat. Commun. 7, 12871. doi:10.1038/ncomms12871

Qin, J., Liang, J., Ding, M., 2014. Perlecan antagonizes collagen IV and ADAMTS9/GON-1 in restricting the growth of presynaptic boutons. J. Neurosci. 34, 10311–10324. doi:10.1523/JNEUROSCI.5128-13.2014

Ramos-Lewis, W., Page-McCaw, A., 2019. Basement membrane mechanics shape development: Lessons from the fly. Matrix Biol 75–76, 72–81. doi:10.1016/j.matbio.2018.04.004

Restrepo, L.J., DePew, A.T., Moese, E.R., Tymanskyj, S.R., Parisi, M.J., Aimino, M.A., Duhart, J.C., Fei, H., Mosca, T.J., 2022. γ-secretase promotes Drosophila postsynaptic development through the cleavage of a Wnt receptor. Dev. Cell 57, 1643–1660.e7. doi:10.1016/j.devcel.2022.05.006

Rogalski, T.M., Gilchrist, E.J., Mullen, G.P., Moerman, D.G., 1995. Mutations in the unc-52 gene responsible for body wall muscle defects in adult Caenorhabditis elegans are located in alternatively spliced exons. Genetics 139, 159–169. doi:10.1093/genetics/139.1.159

Rogalski, T.M., Mullen, G.P., Bush, J.A., Gilchrist, E.J., Moerman, D.G., 2001. UNC-52/perlecan isoform diversity and function in Caenorhabditis elegans. Biochem. Soc. Trans. 29, 171–176. doi:10.1042/0300-5127:0290171

Sarrazin, S., Lamanna, W.C., Esko, J.D., 2011. Heparan sulfate proteoglycans. Cold Spring Harb. Perspect. Biol. 3. doi:10.1101/cshperspect.a004952

Schlessinger, J., Plotnikov, A.N., Ibrahimi, O.A., Eliseenkova, A.V., Yeh, B.K., Yayon, A., Linhardt, R.J., Mohammadi, M., 2000. Crystal structure of a ternary FGF-FGFR-heparin complex reveals a dual role for heparin in FGFR binding and dimerization. Mol. Cell 6, 743–750. doi:10.1016/s1097-2765(00)00073-3

Siechen, S., Yang, S., Chiba, A., Saif, T., 2009. Mechanical tension contributes to clustering of neurotransmitter vesicles at presynaptic terminals. Proc. Natl. Acad. Sci. USA 106, 12611–12616. doi:10.1073/pnas.0901867106

Skeath, J.B., Wilson, B.A., Romero, S.E., Snee, M.J., Zhu, Y., Lacin, H., 2017. The extracellular metalloprotease AdamTS-A anchors neural lineages in place within and preserves the architecture of the central nervous system. Development 144, 3102–3113. doi:10.1242/dev.145854

Stork, T., Engelen, D., Krudewig, A., Silies, M., Bainton, R.J., Klämbt, C., 2008. Organization and function of the blood-brain barrier in Drosophila. J. Neurosci. 28, 587–597. doi:10.1523/JNEUROSCI.4367-07.2008

Tofangchi, A., Fan, A., Saif, M.T.A., 2016. Mechanism of axonal contractility in embryonic drosophila motor neurons in vivo. Biophys. J. 111, 1519–1527. doi:10.1016/j.bpj.2016.08.024

Töpfer, U., Guerra Santillán, K.Y., Fischer-Friedrich, E., Dahmann, C., 2022. Distinct contributions of ECM proteins to basement membrane mechanical properties in

Drosophila. Development 149. doi:10.1242/dev.200456
Trisnadi, N., Stathopoulos, A., 2014. Ectopic expression screen identifies genes affecting Drosophila mesoderm development including the HSPG Trol. G3 (Bethesda) 5, 301–313. doi:10.1534/g3.114.015891
Voigt, A., Pflanz, R., Schäfer, U., Jäckle, H., 2002. Perlecan participates in proliferation activation of quiescent Drosophila neuroblasts. Dev. Dyn. 224, 403–412. doi:10.1002/dvdy.10120
Waller, A., 1850. Experiments on the section of the glossopharyngeal and hypoglossal nerves of the frog, and observations of the alterations produced thereby in the structure of their primitive fibres. Philosophical Transactions of the Royal Society of London 140, 423–429. doi:10.1098/rstl.1850.0021
Wang, J.T., Medress, Z.A., Barres, B.A., 2012. Axon degeneration: molecular mechanisms of a self-destruction pathway. J. Cell Biol. 196, 7–18. doi:10.1083/jcb.201108111
Xie, X., Auld, V.J., 2011. Integrins are necessary for the development and maintenance of the glial layers in the Drosophila peripheral nerve. Development 138, 3813–3822. doi:10.1242/dev.064816
You, J., Zhang, Y., Li, Z., Lou, Z., Jin, L., Lin, X., 2014. Drosophila perlecan regulates intestinal stem cell activity via cell-matrix attachment. Stem Cell Rep. 2, 761–769. doi:10.1016/j.stemcr.2014.04.007
Yurchenco, P.D., 2011. Basement membranes: cell scaffoldings and signaling platforms. Cold Spring Harb. Perspect. Biol. 3, a004911. doi:10.1101/cshperspect.a004911